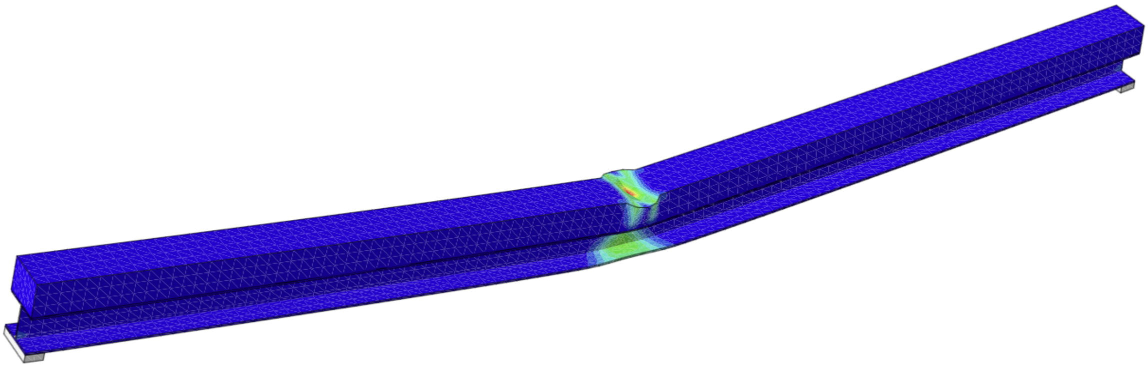

Steel-Timber Composite Beams as an Alternative to Conventional Steel and Glulam

A Structural and Sustainability Assessment

Master's thesis in Structural Engineering and Building Technology

DIMITRIOS CHRISTOS KARYDAS
RASHID MOHSEN

DEPARTMENT OF ARCHITECTURE AND CIVIL ENGINEERING
CHALMERS UNIVERSITY OF TECHNOLOGY
Gothenburg, Sweden 2026
www.chalmers.se

Master's thesis 2026

Steel-Timber Composite Beams as an Alternative to Conventional Steel and Glulam

A Structural and Sustainability Assessment

DIMITRIOS CHRISTOS KARYDAS
RASHID MOHSEN

Department of Architecture and Civil Engineering
Division of Structural Engineering
Steel and Timber Structures Research Area
Chalmers University of Technology
Gothenburg, Sweden 2026

Steel-Timber Composite Beams as an Alternative to Conventional Steel and Glulam
A Structural and Sustainability Assessment
DIMITRIOS CHRISTOS KARYDAS
RASHID MOHSEN

Supervisor: Yutaka Goto, Department of Architecture and Civil Engineering
Examiner: Mahbube Subhani, Department of Architecture and Civil Engineering

Master's Thesis 2026
Department of Architecture and Civil Engineering
Division of Structural Engineering
Steel and Timber Structures Research Area
Chalmers University of Technology
SE-412 96 Gothenburg
Telephone +46 31 772 1000

Cover: Deformed mesh and plastic strain distribution of a steel-timber composite beam at failure, from nonlinear finite element analysis.

Typeset in LaTeX
Printed by Chalmers Reproservice
Gothenburg, Sweden 2026

Steel-Timber Composite Beams as an Alternative to Conventional Steel and Glulam
A Structural and Sustainability Assessment
DIMITRIOS CHRISTOS KARYDAS
RASHID MOHSEN
Department of Architecture and Civil Engineering
Chalmers University of Technology

Abstract

Steel and timber can be combined into hybrid structural elements known as steel-timber composite (STC) beams, offering improved structural performance while reducing embodied carbon and cost compared to conventional alternatives. Despite their potential, no dedicated Eurocode provisions currently exist for STC beam design, limiting their adoption in practice and motivating the need for further research.

This study investigates two STC configurations: STC-1, consisting of a steel HEA section with a glulam element positioned above the top flange, and STC-2, a glulam beam reinforced with a steel plate on its bottom surface. Both configurations are designed using Newmark's partial-interaction theory and optimized through a parameter sweep in MATLAB, in which Life Cycle Assessment(LCA) and Life Cycle Cost (LCC) analyses are performed on the candidate configurations to obtain their CO_2 emission and cost performance, with a Marginal Abatement Cost (MAC) framework subsequently applied as the selection criterion. The optimized STC configurations are then compared against pure steel and pure glulam reference beams. LCA and LCC analyses are conducted across span lengths ranging from 3 m to 12 m, with nonlinear finite element simulations in Abaqus being performed for two representative spans of 7 m and 12 m under office and shopping mall load cases.

Results show that STC beams can offer environmental and economic advantages beyond a threshold span length, with STC-1 achieving CO_2 reductions of up to 20% relative to the steel reference beyond approximately 5 m, while STC-2 reduces cost up to 30% compared to the glulam reference beyond approximately 9 m. Finite element analysis confirms that both configurations exhibit ductile behavior governed by steel yielding, with failure modes and load-displacement responses varying between configurations and span lengths. These findings demonstrate that Newmark's partial-interaction theory provides a viable design basis for STC beams in the absence of dedicated Eurocodes.

Keywords: Steel-timber composites (STC), Partial interaction, Newmark method, Life cycle assessment (LCA), Life cycle cost (LCC), Marginal Abatement Cost (MAC), Eurocode, Finite element analysis (FEA).

Stål-trä-kompositbalkar som ett alternativ till konventionellt stål och limträ
En strukturell och hållbarhetsmässig utvärdering
DIMITRIOS CHRISTOS KARYDAS
RASHID MOHSEN
Institutionen för arkitektur och samhällsbyggnadsteknik
Chalmers tekniska högskola

Sammanfattning

Stål och trä kan kombineras till hybrida bärande element, kända som stål-trä-kompositbalkar (STC), vilket ger förbättrad strukturell prestanda samtidigt som inbäddat koldioxidavtryck och kostnad minskar jämfört med konventionella alternativ. Trots denna potential saknas i dagsläget specifika Eurokod-bestämmelser för dimensionering av STC-balkar, vilket begränsar deras användning i praktiken och motiverar behovet av vidare forskning.

Denna studie undersöker två STC-konfigurationer: STC-1, som består av en stål-HEA-profil med ett limträelement placerat ovanför den övre flänsen, och STC-2, en limträbalk förstärkt med en stålplåt på dess undersida. Båda konfigurationerna dimensioneras med hjälp av Newmarks teori för partiell samverkan och optimeras genom en parametersvep i MATLAB, där livscykelanalys (LCA) och livscykelkostnadsanalys (LCC) utförs på de framtagna konfigurationerna för att erhålla deras koldioxidutsläpp och kostnadsprestanda, varpå ett ramverk för marginell utsläppsminskningskostnad (MAC) därefter tillämpas som urvalskriterium. De optimerade STC-konfigurationerna jämförs sedan mot referensbalkar av rent stål och rent limträ. LCA- och LCC-analyser utförs över spannlängder från 3 m till 12 m, med olinjära finita-elementsimuleringar i Abaqus utförda för två representativa spannlängder, 7 m och 12 m, under lastfallen kontor och köpcentrum.

Resultaten visar att STC-balkar kan erbjuda miljömässiga och ekonomiska fördelar bortom en viss tröskelspannlängd, där STC-1 uppnår koldioxidminskningar på upp till 20 % relativt stålreferensen bortom cirka 5 m, medan STC-2 minskar kostnaden med upp till 30 % jämfört med limträreferensen bortom cirka 9 m. Finita-elementanalysen bekräftar att båda konfigurationerna uppvisar ett segt beteende styrt av stålets plasticering, där brottmoder och last-förskjutningssamband varierar mellan konfigurationerna och spannlängderna. Dessa resultat visar att Newmarks teori för partiell samverkan utgör en användbar dimensioneringsgrund för STC-balkar i avsaknad av specifika Eurokoder.

Nyckelord: Stål-trä-kompositer (STC), Partiell samverkan, Newmarks metod, Livscykelanalys (LCA), Livscykelkostnad (LCC), Marginell utsläppsminskningskostnad (MAC), Eurokod, Finita elementmetoden (FEA)

Acknowledgements

This master's thesis was conducted at Chalmers University of Technology during the spring semester of 2026 and comprises 30 credits. The report is written at the Department of Architecture and Civil Engineering and investigates how steel and timber can be combined to form composite beam elements, evaluating their mechanical, environmental, and economic performance.

We would like to deeply thank our supervisor, Yutaka Goto, and our examiner, Mahbube Subhani, for their tremendous support and guidance throughout this project. Their expertise has been essential to the completion of this thesis.

Dimitrios Christos Karydas & Rashid Mohsen, Gothenburg, June 2026

List of Acronyms

Below is the list of acronyms that have been used throughout this thesis listed in alphabetical order:

CLT	Cross-Laminated Timber
EPD	Environmental Product Declaration
FEA	Finite Element Analysis
GA	Genetic Algorithm
GWP	Global Warming Potential
LCA	Life Cycle Assessment
LCC	Life Cycle Cost
LCCA	Life Cycle Cost Analysis
LCI	Life Cycle Inventory
LTB	Lateral Torsional Buckling
MAC	Marginal Abatement Cost
PUR	Polyurethane
STC	Steel-Timber Composite

Nomenclature

Below is the nomenclature of indices, sets, parameters, and variables that have been used throughout this thesis.

Roman letters — uppercase

A_s	Cross-sectional area of steel beam
A_t	Cross-sectional area of timber element
C	Total cost
C_{inv}	Initial investment cost
C_{mat}	Material procurement cost
C_{fab}	Fabrication cost
C_{trans}	Transportation cost
C_{const}	Construction and installation cost
E	Total embodied carbon
E_s	Elastic modulus of steel
E_t	Elastic modulus of timber
E_1, E_2, E_3	Direction-dependent elastic moduli of glulam
EI	Full-interaction flexural stiffness of composite section
ΣEI	Sum of individual flexural stiffnesses
EA	Composite axial stiffness
F_{shr}	Longitudinal shear force
$F_{v,Rd}$	Design shear resistance of a single connector
G_{12}, G_{13}, G_{23}	Shear moduli of glulam
I_s	Second moment of area of steel beam
I_{eff}	Effective second moment of area
K_b	Connector stiffness per unit length
K_{ser}	Slip modulus at serviceability limit state

K_u	Slip modulus at ultimate limit state
L	Beam span length
L_s	Connector spacing
M	Total bending moment
M_1, M_2	Bending moments in steel and timber elements
N_1, N_2	Axial forces in steel and timber elements
$P^L_{j,t}$	Active power of load demand
$V_{l,full}$	Longitudinal shear force at full interaction

Roman letters — lowercase

a_0	Unit longitudinal flexibility of shear connection
a_1	Passive slip strain coefficient
a_2	Active slip strain coefficient
a_4	Unit slip curvature
b_f	Flange width of steel section
b_t	Timber width
f_{cd}	Design compressive strength of timber
f_{md}	Design bending strength of timber
f_{yd}	Design yield strength of steel
h_1, h_2	Distances from element centroids to interface
h_s	Total height of steel section
h_t	Timber depth
n	Modular ratio (E_s/E_t)
$n_{pr,min}$	Minimum number of connectors per row
n_{rows}	Number of connector rows
q	Uniformly distributed load
s	Interface slip
v	Deflection
y_{NA}	Elastic neutral axis position
z_s	CO_2 emission factor for steel
z_t	CO_2 emission factor for glulam

Greek letters — uppercase

Δt	Time discretization step

Greek letters — lowercase

ε_1, ε_2	Interface strains in steel and timber elements
ε_{slp}	Slip strain
η	Degree of shear connection
γ	Partial interaction factor
κ	Curvature
λ	Characteristic slip parameter
ν_{12}, ν_{13}, ν_{23}	Poisson's ratios of glulam
ρ_t	Characteristic density of timber
ρ_s	Characteristic density of steel
$\sigma_{s,Ed}$	Design bending stress in steel
$\sigma_{t,Ed}$	Design bending stress in timber

Contents

List of Acronyms **ix**

Nomenclature **xi**

List of Figures **xix**

List of Tables **xxi**

1 Introduction **1**
1.1 Background . . . 1
1.2 Aim . . . 3
1.3 Scope of the Study . . . 3
1.4 Use of Generative AI . . . 4

2 Literature Review **5**
2.1 Material Properties . . . 5
2.1.1 Timber . . . 5
2.1.2 Steel . . . 7
2.2 Configurations of Steel-Timber Members . . . 8
2.2.1 Integration Levels . . . 8
2.2.2 Characteristics of Cross-Sectional Configurations . . . 9
2.3 Connection Methods . . . 10
2.3.1 Mechanical Fasteners . . . 10
2.3.2 Design of Dowel-Type Connections . . . 12
2.3.3 Adhesive Connections . . . 13
2.3.4 Hybrid Connections . . . 13
2.4 Composite Action . . . 14
2.4.1 Slip Modulus . . . 14
2.4.2 Types of Composite Action . . . 15
2.4.3 Shear Connection and Shear Interaction . . . 16
2.4.4 Partial-Interaction Theory for Composite Beams . . . 17
2.5 Genetic Algorithm . . . 19
2.5.1 Principle of a Genetic Algorithm . . . 19
2.5.2 Types of Optimization Problems . . . 20
2.5.3 Constraint Handling with Penalty Functions . . . 21
2.6 Life Cycle Assessment (LCA) . . . 21
2.7 Life Cycle Costing (LCC) . . . 23

2.7.1 Marginal Abatement Cost 24

3 Methodology **27**
3.1 Methodological Framework 27
3.2 Design Phase 28
3.2.1 Steel-Timber Composite Configurations 28
3.2.2 Load Cases 30
3.2.3 Application of Newmark's method for Composite Systems . . 30
3.2.3.1 Equilibrium Relationships 30
3.2.3.2 Curvature Compatibility 31
3.2.3.3 Partial-Interaction Shear Force 32
3.2.3.4 Deflection 32
3.2.4 Validation of Analytical Method Using Abaqus FEA 33
3.2.4.1 Material Properties 34
3.2.4.2 Contact Property 34
3.2.4.3 Boundary Conditions and Meshing 34
3.2.4.4 Model Simulation 35
3.3 Optimization Phase 36
3.3.1 Genetic Algorithm 36
3.3.1.1 Input File: Section Properties 36
3.3.1.2 Step 1: Structural Filter (Full Interaction) 37
3.3.1.3 Step 2: Connection Design (Partial Interaction) . . . 37
3.3.1.4 Step 3: MAC Ranking and Recommended Design . . 38
3.3.2 Assumptions Made for STC-1 39
3.3.3 Assumptions Made for STC-2 40
3.3.4 LCA System Boundary 41
3.3.5 LCC System Boundary 42
3.4 Numerical Analysis Phase 43
3.4.1 Abaqus FEA 43
3.4.1.1 Material Properties 43
3.4.1.2 Model Simulation 44

4 Results **45**
4.1 Validation and Accuracy of Newmark Partial Interaction Theory . . . 45
4.2 LCA for Varying Span Lengths 46
4.2.1 Absolute Values 47
4.2.2 Normalized Values 47
4.3 LCC for Varying Span Lengths 48
4.3.1 Absolute Values 49
4.3.2 Normalized Values 49
4.4 Load-Displacement 51
4.4.1 7m Span: Office Load 51
4.4.2 12m Span: Office Load 52
4.4.3 7m Span: Shopping Mall Load 53
4.4.4 12m Span: Shopping Mall Load 54
4.4.5 Effective Bending Stiffness 55
4.5 Slip 56

4.5.1 7m and 12m Span: Office Load 57
4.5.2 7m and 12m Span: Shopping Mall Load 57
4.6 Stress Distribution 58
4.6.1 Stress Distribution of STC-1 58
4.6.2 Stress Distribution of STC-2 59
4.6.3 Stress Distribution Summary 60
4.7 Failure Modes 62
4.7.1 Failure Modes of STC-1 62
4.7.2 Failure Modes of STC-2 62

5 Discussion 65
5.1 Summary of Findings 65
5.2 Answers to Research Questions 66
5.2.1 Applicability of Newmark's Partial-Interaction Beam Theory . 66
5.2.2 Comparative Environmental and Economic Performance for Varying Span 67
5.2.2.1 LCA Results 68
5.2.2.2 LCC Results 68
5.2.3 Structural Behavior (Load-Displacement,Stress, Slip, Failure Modes) 69
5.2.4 Methodological Constraints Affecting the Results 71

6 Conclusion 73
6.1 Recommendations for Future Work 73

Bibliography 75

A Appendix: Calculations of Beam I

B Appendix: Calculations of Connection XLIII

C Appendix: Figures of Results LXI

List of Figures

1.1 Total greenhouse gas emissions from the construction and real estate sector by sub-sector, 2008–2022 [3]. 1

2.1 Stress-strain relationship under compression and tension parallel to grain [18]. 6
2.2 Stress-strain relationship for steel [21]. 7
2.3 Overview of possible cross-sectional configurations for STC beams [10]. 9
2.4 Typical screw shear connection in a STC beam [33]. 11
2.5 Typical bolt shear connection in a STC beam [33] 12
2.6 Typical shear connection configuration in STC beams [29]. 12
2.7 Strain distribution for varying degrees of composite action in a beam [43]. 15

3.1 Flowchart of the methodological framework, outlining the three study phases. 28
3.2 Selected composite beam configurations: (a) STC-1 and (b) STC-2. . 29
3.3 Applied load cases for the selected beam configurations. 30
3.4 Representative mesh convergence study for a 7 m span configuration. 35
3.5 Complete three-step procedure used in the optimization sweep. 39
3.6 Covered modules of LCA, source: Moelven 41

4.1 STC-1: Analytical vs numerical calculations for (a) vertical deflection and (b) axial stress 46
4.2 STC-2: Analytical vs numerical calculations for (a) vertical deflection and (b) axial stress 46
4.3 Absolute CO_2 emissions for different span lengths: (a) office load and (b) shopping mall load. 47
4.4 Normalized CO_2 emissions for different span lengths: (a) office load and (b) shopping mall load. 48
4.5 Absolute cost for different span lengths: (a) office load and (b) shopping mall load 49
4.6 Normalized cost for different span lengths: (a) office load and (b) shopping mall load. 50
4.7 Load-displacement response for 7 m span under office load. 52
4.8 Load-displacement response for 7 m span under office load. 53
4.9 Load-displacement response for 7 m span under shopping mall load. . 54
4.10 Load-displacement response for 12 m span under shopping mall load. 55

4.11 Effective bending stiffness for all configurations. 56
4.12 Load-slip response of STC-1 and STC-2 under office load, at (a) 7 m and (b) 12 m span. 57
4.13 Load-slip response of STC-1 and STC-2 under shopping mall load, at (a) 7 m and (b) 12 m span. 58
4.14 Stress distribution of STC-1 at 7 m span under office load. 59
4.15 Stress distribution of STC-2 at 7 m span under office load. 60
4.16 Summary of bending stress prior to yielding vs corresponding yield load of STC-1. 61
4.17 Summary of bending stress prior to yielding vs corresponding yield load of STC-2. 61
4.18 Failure mode of STC-1 at 7 m span under office load. 62
4.19 Failure mode of STC-2 at 7 m span under office load. 63
4.20 Failure mode of STC-2 at 12 m span under office load. 64

C.1 Stress distribution of STC-1 at 12 m span under office load. LXI
C.2 Stress distribution of STC-2 at 12 m span under office load. LXII
C.3 Stress distribution of STC-1 at 7 m span under shopping mall load. . LXII
C.4 Stress distribution of STC-2 at 7 m span under shopping mall load. . LXIII
C.5 Stress distribution of STC-1 at 12 m span under shopping mall load. LXIII
C.6 Stress distribution of STC-2 at 12 m span under shopping mall load. LXIV
C.7 Failure mode of STC-1 at 12 m span under office load. LXIV
C.8 Failure mode of STC-1 at 7 m span under shopping mall load. LXV
C.9 Failure mode of STC-2 at 7 m span under shopping mall load. LXV
C.10 Failure mode of STC-1 at 12 m span under shopping mall load. . . . LXVI
C.11 Failure mode of STC-2 at 12 m span under shopping mall load. . . . LXVI

List of Tables

3.1 Linear material properties for steel and timber. 34
3.2 Boundary conditions of numerical model. 35
3.3 Nonlinear material properties for steel and timber. 44
3.4 Inputs for Hill's yield criterion. 44

4.1 Effective bending stiffness and gamma coefficient for all configurations. 56

1
Introduction

1.1 Background

The construction sector is a major driver of global greenhouse gas emissions, accounting for approximately 38% of the global total and around 40% of global energy consumption [1]. This has placed the industry under increasing pressure from international agreements such as the Paris Agreement and the Kyoto Protocol [2]. In 2022, the Swedish National Board of Housing, Building and Planning (Boverket) reported total emissions from the sector of 17.7 million tonnes of CO_2 equivalents, including imported materials, while domestic construction and real estate activities accounted for 10.8 million tonnes (22.1% of Sweden's total emissions). As illustrated in Figure 1.1, these emissions arise from new construction, renovation, real estate management and building heating [3].

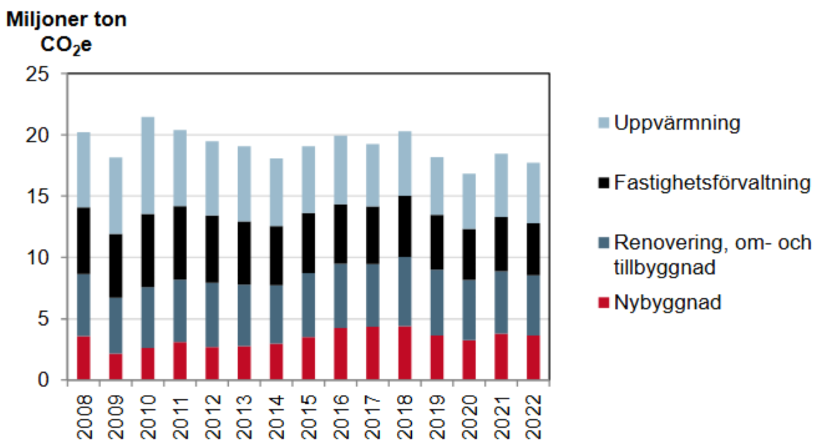

Figure 1.1: Total greenhouse gas emissions from the construction and real estate sector by sub-sector, 2008–2022 [3].

A significant share of the impact is linked to concrete, the world's most widely used construction material, whose footprint is largely driven by cement production, an energy intensive process that emits substantial CO_2 through both fuel combustion and chemical calcination. In a Swedish context, cement production plays a central role in these emissions. In 2020, 2.8 million tonnes of cement were produced in Sweden, resulting in approximately 1.9 million tonnes of CO_2 emissions from the country's two cement plants. Around 90% of the cement used domestically is produced within Sweden, while the remaining share is imported from nearby European countries [4].

Reducing reliance on conventional concrete is a central challenge for the industry, especially given Sweden's climate targets. The Swedish Environmental Protection Agency (Naturvårdsverket) mandates that the nation reach net-zero emissions by 2045, followed by negative emissions [2]. However, current trends show that reductions are not happening fast enough [5]. This gap underscores the need for transformative shifts in construction practices rather than minor adjustments, requiring new materials and methods that align with national sustainability goals [2].

In response to these challenges, engineered wood products such as glued laminated timber (glulam) and cross-laminated timber (CLT) have gained considerable attention over the recent decades, enabling the construction of multi-story timber buildings to increase [6]. Timber is a renewable material, has low embodied energy, and stores carbon throughout its lifecycle, allowing timber structures to achieve significantly lower carbon footprints than steel or reinforced concrete [7]. Despite these advantages, timber also exhibits inherent limitations arising from its natural characteristics. As an anisotropic material, timber generally possesses lower stiffness, strength and durability compared with conventional structural materials. Consequently, its application in structural components requiring long service lives, high load-bearing capacities, or strict deflection control is often restricted [8].

To overcome these structural restrictions while maintaining sustainability objectives, steel-timber composite (STC) systems have gained increasing attention in recent years. By combining the high strength and stiffness of steel with the low embodied carbon and high strength-to-weight ratio of timber, STC systems can exploit the complementary properties of both materials [9]. This composite approach offers the potential to reduce material consumption and greenhouse gas emissions while maintaining high structural efficiency. However, achieving this potential requires careful design and detailing, as the overall performance of STC systems is strongly influenced by the distinct material properties of steel and timber, the characteristics of their connections, and long-term durability considerations [10].

Another restriction is the lack of a unified Eurocode framework for STC systems. Unlike steel-concrete composites, which have been used and codified for decades, STC systems are relatively new, and the complex behavior of their connections makes the standardization difficult. This lack of design standards creates uncertainty and makes it harder for STC systems to be widely used in practice [10]. Therefore, alternative analytical methods need to be applied to design these composite beams. One such method is the Newmark partial interaction theory, first proposed by Newmark et al. [11] in 1951 for steel-concrete composite beams. This method accounts for the composite action between two materials, capturing the relative displacement that occurs at their interface. Given the absence of a dedicated design standard for STC systems, the applicability of this theory is of particular interest.

Ultimately, the suitability of a structural system cannot be judged on mechanical performance alone. A design that is structurally sound and low-carbon may still be impractical if it is cost prohibitive, and in many cases, systems designed to reduce environmental impact are associated with higher financial costs [7]. Thus, there is a need for a systematic evaluation that accounts for structural, environmental, and economic performance simultaneously. By comparing various STC configurations against conventional solutions using a genetic algorithm-based approach, this thesis aims to identify the specific conditions under which these systems can effectively reduce the carbon footprint while remaining economically feasible.

1.2 Aim

This research aims to evaluate steel-timber composite elements based on mechanical performance, environmental impact, and cost-effectiveness, while identifying the factors that influence their suitability for structural applications.

The research questions developed to achieve this aim are:

- Can existing generic mathematical theories, particularly the Newmark partial interaction method, be used to model and design steel–timber composite beam configurations in the absence of Eurocode guidance?
- How do steel–timber composite beam configurations compare with pure steel and timber beams in terms of cost and CO_2 emissions under varying spans and load combinations, and what are the actual configuration designs to benefit environmentally and economically?
- How do the load–displacement, stress distribution, and load–slip responses of the designed steel–timber composite beams compare with conventional beams under office and retail loading at selected spans, and what failure modes govern each configuration?

1.3 Scope of the Study

This study focuses on two selected steel-timber composite beam systems, whose structural efficiency is evaluated under short-term loading conditions only. Long-term phenomena, such as creep and moisture-dependent effects in timber, as well as relaxation and fatigue in steel, are not considered in the structural analysis.

In addition, the scope of this study is limited to numerical simulations performed using Abaqus FEA, as no physical laboratory experiments were conducted. This applies to both the validation of the Newmark partial interaction theory and the detailed finite element analysis. Furthermore, the finite element analysis is considers only simply supported beams subjected to two load combinations and two span lengths, allowing for a clearer comparison of how these parameters influence the overall structural behavior of the composite systems.

It should be noted that societal and ethical considerations fall outside the scope of this study, as the research focuses primarily on numerical analysis and empirical data. Instead, the investigation emphasized the ecological dimension, specifically the LCA of the different systems, to evaluate and substantiate their potential to reduce emissions.

In this study, the Life Cycle Assessment (LCA) follows the EN 15804 standard but addresses only specific stages: modules A1–A3 (Product Stage), C3 (Waste Processing), and D (Benefits and Loads Beyond the System Boundary) [12]).

The remaining stages are excluded from the system boundary based on specific methodological choices. Transport and construction stages (A4–A5), as well as deconstruction and end-of-life transport (C1–C2), are omitted because they depend heavily on project-specific locations and logistics. Excluding them avoids introducing highly uncertain variables into the component-level structural optimization. Furthermore, the use stage (B1–B7) is excluded because structural elements function as passive components that require no routine maintenance or operational resources. Trying to predict these activities decades into the future is highly difficult and would only introduce unnecessary, uncertain factors into the study.

For environmental indicators, only Global Warming Potential (GWP) is evaluated. While this targets carbon emissions directly, it is a known limitation because it misses potential trade-offs in other environmental areas, such as acidification or eutrophication.

To maintain consistency, the Life Cycle Costing (LCC) boundaries are harmonized with the LCA scope. The economic optimization evaluates only the initial investment costs (A1–A3) and excludes speculative future costs during the use or demolition phases. This ensures that both environmental and financial indicators are optimized using identical, high-certainty data boundaries.

1.4 Use of Generative AI

ChatGPT was used to assist with grammar correction and sentence structuring. Claude AI was also used to support the development of the genetic algorithm code in MATLAB.

2

Literature Review

This chapter presents the literature review that forms the foundation of the thesis implementation. It begins with a brief overview of the mechanical properties of timber and steel, followed by a discussion of various configurations for combining these materials in composite systems. The chapter then examines different connection methods used to achieve composite action, as well as approaches for evaluating the interaction between the materials. Because the number of possible combinations of beam designs is large, a systematic optimization method is required. Thus, the fundamental principles of genetic algorithms are introduced. The chapter concludes with descriptions of life cycle assessment (LCA) and life cycle cost assessment (LCCA).

2.1 Material Properties

Timber and steel are two materials widely used in construction, each offering distinct characteristics. Timber has a high strength-to-weight ratio and allows for short construction times, making it an efficient structural material [13], [14]. Steel also exhibits very high strength and is widely used in structural applications due to its high ductility and stiffness, which allow it to support large spans [15]. By combining steel and timber, the advantages of both materials can be utilized, enabling them to act synergistically and achieve higher mechanical performance than components made solely of timber or steel [14].

2.1.1 Timber

Timber is a material with significant potential to reduce the environmental impact and energy demand of buildings. It is a renewable resource, possesses lower embodied energy than most conventional construction materials, and is capable of storing carbon, thereby contributing positively to the overall carbon footprint of a building [7]. In addition, timber is lightweight and well suited for prefabrication, enabling efficient manufacturing and assembly processes. In recent years, timber has gained increasing attention and wider application in the construction industry, largely driven by global efforts toward carbon neutrality and more sustainable building practices [16].

Nevertheless, timber presents several challenges due to its anisotropic nature. This means that its mechanical properties vary depending on the direction of loading, as shown in Figure 2.1. As a result, the application of timber can be limited in situations requiring strict deflection criteria, high load-bearing capacity, or long service life [8]. These limitations stem from the material's relatively low modulus of elasticity, strength, and durability compared to steel or concrete. This consequently exhibits a low stiffness and a greater susceptibility to excessive deflection [17].

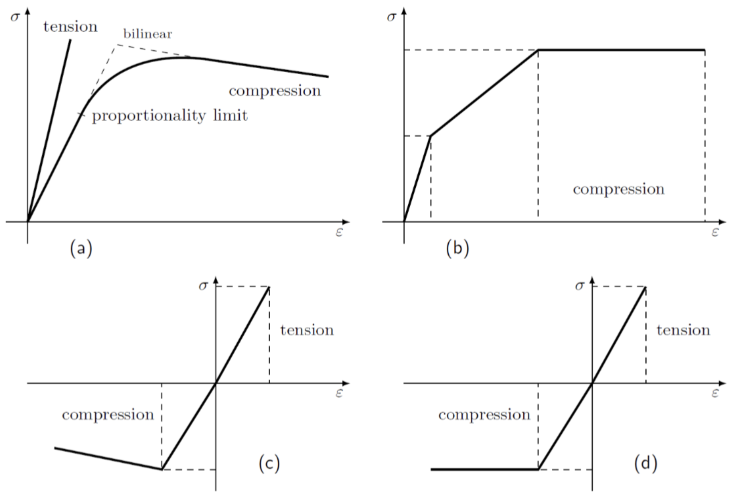

Figure 2.1: Stress-strain relationship under compression and tension parallel to grain [18].

Despite these limitations, timber beams are increasingly being utilized in modern structures with larger spans. One of the primary challenges associated with long-span timber beams is satisfying the serviceability limit state (SLS), particularly in terms of deflection and vibration performance. Beams with spans greater than 6 m are generally classified as long-span beams and are often governed by SLS criteria rather than ultimate strength capacity. Thus, controlling deflections becomes a key consideration in the design of efficient and functional timber structural systems [17].

To address the inherent limitations of timber, several reinforcement techniques have been developed to enhance its structural performance. It has been shown that such reinforcement methods can provide significant benefits. Harrach et al. [19] investigated the effect of applying carbon fiber reinforced polymer (CFRP) to the tension side of timber beams and evaluated its influence on the overall structural behavior. The results demonstrated that the use of a material with high tensile strength can significantly improve beam performance by transferring tensile stresses away from the timber, thereby allowing the compression zone of the beam to yield more effectively.

Another reinforcement approach involves the use of internal steel rods, placed on the tension side of the timber beam in a similar manner to steel reinforcement in concrete structures. This technique limits crack propagation and local rupture, and has been shown to increase both stiffness and strength, depending on the reinforcement ratio. Steel plates, inserted either vertically or horizontally within the timber cross-section, represent a further reinforcement option. Compared to unreinforced timber beams, which typically exhibit brittle failure, steel-plated beams demonstrated a more ductile failure behavior, with no observed delamination between the timber and steel [20].

2.1.2 Steel

Steel is a manufactured alloy of iron and carbon that has been widely used as a construction material in structures such as bridges and buildings. It offers an exceptionally high strength-to-weight ratio and significant ductility, enabling lightweight, transparent and elegant structures with spatial flexibility and large openings. Unlike timber, steel is an isotropic material, meaning its mechanical properties are uniform in all directions, which makes its structural behavior highly predictable and simplifies design. These properties make steel particularly well-suited to relatively long-span applications, where its high tensile strength and elastic modulus allow large spans to be achieved with slender, efficient members [16][21].

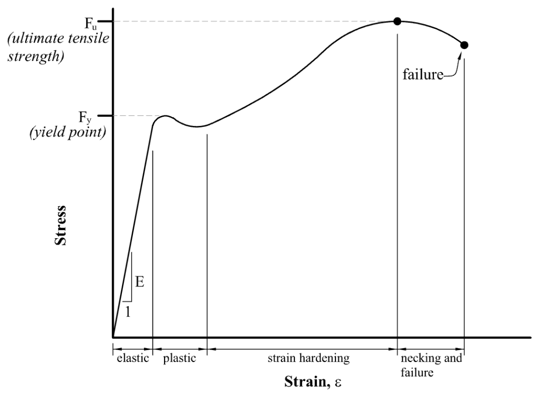

Figure 2.2: Stress-strain relationship for steel [21].

However, one of the main challenges associated with steel is their susceptibility to lateral torsional buckling (LTB), particularly in long-span beams and slender members, where it often governs the design. Hassan & Johansson [22] investigated the lateral torsional buckling behavior of steel beams and concluded that the resistance to LTB decreases significantly with increasing span length, making longer beams more vulnerable to this failure mode. Numerous studies have examined different types of steel members, consistently identifying LTB as a common yet complex stability problem that must be carefully considered in structural design [23].

To mitigate lateral torsional buckling in steel beams, timber can be incorporated effectively to provide lateral restraint and enhance the overall structural stability. Yang et al. [8] studied the effectiveness of combining steel beams with timber and concluded that timber can efficiently limit buckling in steel and improve the structural stability depending on the configuration. However, the interface between the two materials must be carefully designed, as the significant difference in stiffness between steel and timber can lead to interface damage in composite elements if connections are inadequate.

2.2 Configurations of Steel-Timber Members

Steel-timber composite members can be configured in several distinct ways, yet research on their structural performance and possible applications remains limited compared to timber-concrete and timber-timber systems [24]. More broadly, steel-timber composites can be categorized into three principal configurations: timber-encased steel sections, steel-encased timber sections, and adaptable multilayer steel-timber systems [10]. This section outlines the principal configurations of steel-timber composite members.

2.2.1 Integration Levels

Before the development of steel-timber composites at the element level, the two materials were primarily combined at the system level. In such systems, steel and timber are not mechanically connected to act compositely, instead, they function independently while complementing each other to ensure structural safety and improve overall performance. This approach proved particularly effective in addressing common design challenges, such as long spans and significant vertical loads. Today, typical steel-timber hybrid systems consist of timber walls and floor assemblies combined with steel load-bearing elements [25].

Another motivation for combining materials at the system level is to overcome height limitations, which are often associated with timber structures. By integrating steel and timber in a hybrid configuration, it becomes possible to achieve greater building heights in an efficient manner. Consequently, the design of these structures remains inherently conservative. This rigorous caution is largely due to the face that hybrid systems do not yet benefit from the same clear, universal design guidelines that govern single-material construction. While hybrid structures at the system level have proven effective in utilizing the complementary properties of steel and timber, the full potential of steel-timber systems is realized when the materials are integrated at the element level to act compositely [16].

In the past decade, increasing emphasis has been placed on replacing less sustainable construction methods in response to the urgent need to reduce environmental impact [10]. Among the proposed alternatives are steel-timber composites at the element level, which offer significant potential for lowering the carbon footprint compared to conventional construction systems. Numerous configurations of beams and columns have been proposed and investigated through experimental studies and numerical simulations. For steel and timber, the cross-section is commonly formed by combining timber elements with steel H-sections or T-sections, although a wide variety of configurations can be considered in the design [16]. Some possible component-level configurations are illustrated in Figure 2.3.

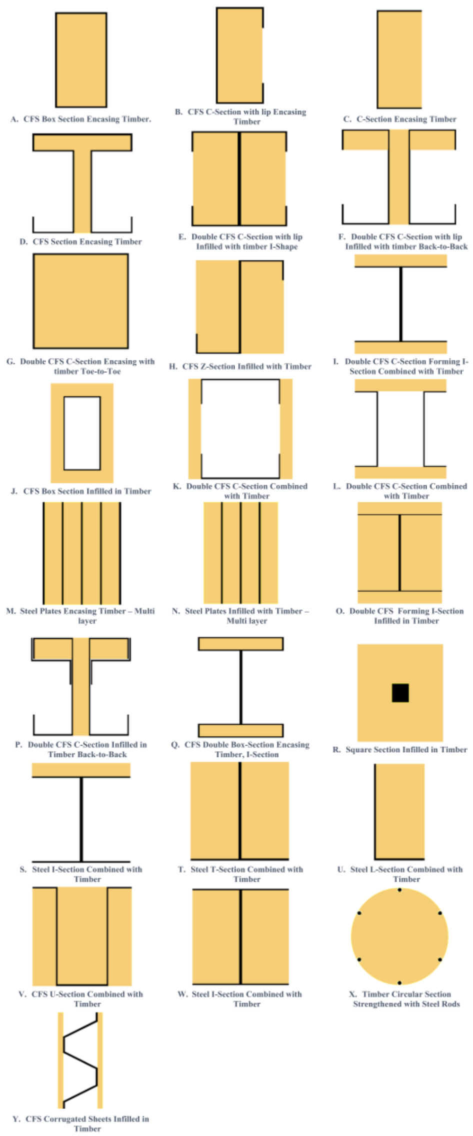

Figure 2.3: Overview of possible cross-sectional configurations for STC beams [10].

2.2.2 Characteristics of Cross-Sectional Configurations

A major challenge associated with these composite systems is the significant difference in the mechanical and physical properties of the two materials. Steel is a manufactured material with predictable properties and can be fully recycled after use. In contrast, wood is a natural and renewable material whose stiffness and strength vary depending on the direction of the grain. Therefore, these factors are crucial in the design process and must be carefully considered and controlled when developing composite systems that combine these two materials [15].

Among the beneficial characteristics of timber-encased steel systems, Eldeib et al. [10] identified improved buckling resistance, since steel elements are generally susceptible to buckling instability. However, it should be noted that most existing research on these configurations has primarily focused on columns rather than beam applications. Steel-encased timber configurations, on the other hand, have demonstrated increased load-bearing capacity in beams. In these systems, the timber restrains the steel element, thereby enhancing torsional stiffness and reducing the risk of local steel buckling.

Nabati et al. [26] found that adaptable multilayer steel-timber systems can considerably enhance the structural integrity of the system. When properly configured, these systems can improve the ultimate deflection capacity, increase ductility and stiffness, and reduce the risk of tensile rupture in the wood fibers through the reinforcement effect of the steel components. Ultimately, the durability of steel-timber systems largely depends on the quality of the design, construction practices, and material selection, as both steel and timber can achieve excellent durability when properly designed and constructed [10].

Despite their promise and the encouraging results reported in literature, the practical implementation of steel-timber composite systems remains limited. This is largely due to the current lack of comprehensive design codes and the relatively low number of real-world applications, which constrains the development of technical expertise in this field [27].

2.3 Connection Methods

Steel and timber can be connected to form composite members using two main types of connection systems: mechanical fasteners, such as bolts and screws, or adhesive bonding through chemical means [28]. As in all composite systems, the connection between the two materials is crucial for ensuring effective interaction. A well-designed connection enhances both the load-carrying capacity and the stiffness of the beam compared to beams made solely of steel or timber [10]. The choice of connection method must therefore be carefully matched to the requirements of the specific composite system.

2.3.1 Mechanical Fasteners

Mechanical fasteners are widely used in timber engineering because they effectively bridge longer beam spans and facilitate the development of larger joist cross-sections [30]. Moreover, they are adhesive-free, cost-efficient, and enable the use of low-grade timber that would otherwise be structurally insufficient on its own, contributing to more sustainable and resource-efficient systems. By combining the advantageous properties of both materials, mechanically fastened steel-timber composites can achieve improved structural performance compared with timber-timber sections, with load-carrying capacity increasing by 3 to 4 times and stiffness by 3 to 6 times on average [31].

Screws are widely used for connecting materials due to their high strength, ease of installation, and practical applicability. They typically consist of threaded shafts of varying sizes and lengths, which provide resistance to withdrawal forces. The effectiveness of the withdrawal resistance depends on several factors, and studies have shown that it increases with greater screw-driven depth and with an optimal pilot hole diameter [32]. Furthermore, Yang et al. [8] found that when screws are used as shear connectors, the stiffness of the composite beam can exceed that achieved with bolts. This improvement is attributed to reduced slip at the interface, as well as enhanced confinement between the connected materials.

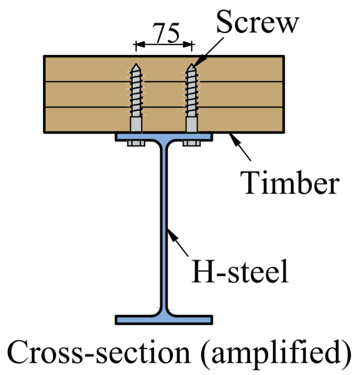

Figure 2.4: Typical screw shear connection in a STC beam [33].

Bolts are metallic connectors widely used in composite structures, as they provide reliable connections and contribute to enhanced structural ductility. Unlike screws, which transfer loads through thread engagement along their embedded length, the load transfer and bearing capacity of bolts primarily depend on the bolt diameter and the thickness of the connected members. An increase in either bolt diameter or specimen thickness generally results in a higher bearing capacity [34]. In addition, bolted connections facilitate disassembly, allowing for material recycling and potential reuse without damaging the structural elements responsible to safety, strength, and functionality. Such characteristics make bolted systems advantageous in the context of circular construction, promoting improved sustainability resource efficiency, and design flexibility [35].

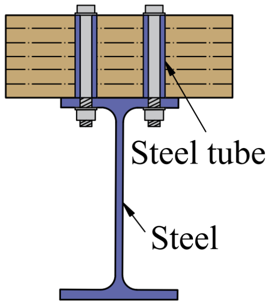

Figure 2.5: Typical bolt shear connection in a STC beam [33]

In addition to fastener type, the arrangement of shear connectors can also be defined in multiple ways. One such configuration is presented in Figure 2.6. Yang et al. [8] investigated the influence of connector spacing in steel-timber composite beams, particularly with respect to bending performance. The findings indicate that closer spacing between connectors can enhance load-carrying capacity, as the shear transfer is improved when the connectors act more effectively in combination. Conversely, increasing the spacing between connectors does not lead to a significant improvement in load-carrying capacity. Overall, however, the influence of connector spacing is relatively limited and should not be regarded as a governing factor in the overall capacity of the beam [16].

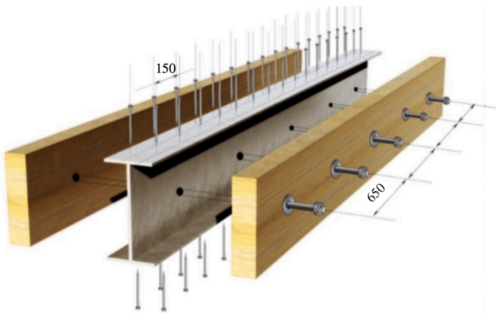

Figure 2.6: Typical shear connection configuration in STC beams [29].

2.3.2 Design of Dowel-Type Connections

Mechanically fastened connections are typically designed according to Eurocode 5 (EN 1995-1-1), which treats timber-to-timber and steel-to-timber connections differently. Additionally, the number of shear planes per fastener is a critical parameter in the design process. Johansen's yield theory is used to calculate the load-carrying capacity of the connector, depending on the number of shear planes and whether the steel plate is considered thin or thick. This theory covers all metal dowel-type fasteners, including bolts, dowels, nails, staples, and screws [46].

Eurocode 5 (EN 1995-1-1) specifies minimum spacing requirements, as well as end and edge distances, depending on the type of fastener used. These requirements depend mainly on the fastener diameter and the angle between the force and the grain direction. Other parameters are also considered when designing dowel-type connections according to Eurocode 5, such as the withdrawal capacity, the density of the timber, and the penetrations depth of the fastener. Once these parameters are accounted for, the load-carrying capacity of a single fastener can be determined, and subsequently the number of fasteners required to resist the shear force acting on the connection [46].

2.3.3 Adhesive Connections

Adhesive bonding is a connection method that includes using chemical means to connect the two different members, which can simplify the construction assembly work. This technique is an advanced and modern approach used in the manufacturing process in the engineered wood products [8]. Common structural adhesives used for steel-timber connections are epoxy and polyurethane (PUR), as they provide a strong bond between the materials and enhance the overall composite action. Epoxy adhesives offer high strength but exhibit brittle behavior, while PUR adhesives provide greater ductility, allowing for some load distribution before failure [36].

Gilbert et al. [9] reported that adhesive bonding can significantly enhance composite action, approaching near-full interaction between the connected materials. This is beneficial, as steel-timber composite beams with near-full composite action can achieve larger span-to-depth ratios due to the substantial improvements in strength, stiffness, and overall robustness under high loads. This is supported by shear tests conducted by Haase et al. [28], who investigated a connection consisting of a steel plate sandwiched within a glulam element using structural adhesive. Their results demonstrated that both stiffness and strength were superior to those of other connection configurations consisting of screws, with failure occurring in the timber rather than at the adhesive interface.

However, the performance of adhesive connections is affected by moisture and temperature variations and need to be used with caution. When adhesively bonded systems are exposed to long-term climatic conditions, the environmental factors can cause the timber to expand or contract in volume, potentially leading to failure in the binder due to the high stresses that occur at the interface of the bonded elements. This results in decreased structural stability and is difficult to repair, as the adhesive layer is not easily accessible once the beam is assembled [8].

2.3.4 Hybrid Connections

Beyond conventional mechanical and adhesive connections, new configurations have been developed to enhance the shear performance at the connection interface. One such approach involves combining screws with adhesives to improve both the bending capacity of the composite beam and the shear stiffness of the connection interface [33]. Hassanieh et al. [37] investigated this configuration through push-out tests on steel-timber composite beams connected using structural epoxy adhesive and coach screws, with the aim of evaluating failure modes and load-slip behavior. The results indicated that near-full composite action can be achieved, and that the combination of adhesive and mechanical fasteners promotes a more ductile response of the connection.

Lin et al. [38] investigated shear connections using hybrid bonding, consisting of both shear studs and epoxy mortar, in steel-concrete composite beams. The study concluded that the interaction between the shear studs and the epoxy mortar provides a higher shear capacity than that of traditional connections using only stud connectors. This improvement is attributed to the ability of the adhesive layer to sustain shear loads prior to reaching the ultimate capacity of the specimen, as well as its role in reducing stress concentrations in the studs by distributing stresses more uniformly.

2.4 Composite Action

To achieve adequate structural integrity and performance in conventional composite beams, the shear connection must be designed to ensure effective interaction between the components. The shear connection provides the necessary linkage that enables the materials to act compositely rather than independently, thereby enhancing the overall stiffness and load-carrying capacity of the system [39]. Consequently, the degree of composite action, which describes the extent to which the components behave as a single unit, is a key factor governing the overall efficiency of the structure [35].

2.4.1 Slip Modulus

Slip between two connected components is a phenomenon which occurs when a semi-rigid system is laterally loaded, causing the connectors to deform and leading to displacements of the overall structure. Research into this phenomenon dates back to the 1950s, when early studies examined how connector deformation influences the interaction between connected elements and governs slip behavior. These approaches were generally founded on equilibrium analysis of an infinitesimal beam segment. Despite differences in formulation, they led to comparable results, as they were all based on the concept of partial interaction and assumed linear behavior of the connectors [40].

Since the interaction and overall stiffness of a composite system are governed by the stiffness of its connectors, the structural response is largely defined by the load-slip relationship. In the initial stage, this relationship can be approximated as linear, where the slope represents the slip modulus. Design provisions, such as those in Eurocode 5 (EN 1995-1-1), are therefore based on this linear assumption when evaluating the stiffness of mechanically jointed beams. Within this framework, two slip modulus values are defined: K_{ser} for serviceability limit state calculations and K_u for ultimate limit state calculations. Both parameters depend on factors such as wood density and fastener diameter, and are typically determined for loading parallel to the grain [40].

The slip modulus can also be determined using numerical and empirical approaches that capture the inherently non-linear behavior of connectors. One common experimental method is the push-out test, from which empirical expressions for the load-slip relationship can be derived [41]. In a push-out test, two slabs are connected to a steel beam using mechanical fasteners and subjected to a compressive load. This setup is designed to evaluate the performance of the connectors, which are primarily subjected to direct shear forces. The test results provide valuable data for quantifying the load-displacement relationship at the interface between the connected materials [42].

Ultimately, the slip modulus is influenced not only by the stiffness properties of the steel and wood, but also by the geometric characteristics of the connection, such as the diameter of the fastener. The behavior of the connectors therefore plays a crucial role in governing the distribution of internal forces between the components, including shear forces and overall structural displacements. Consequently, an accurate determination of the slip modulus is essential in the analysis of composite beams. If it is not evaluated correctly, the resulting predictions of structural behavior may be unreliable and lead to inefficient of unsafe designs [40].

2.4.2 Types of Composite Action

Composite systems are generally classified into three categories based on their structural behavior: full composite action, partial composite action, and non-composite action. These categories describe the degree to which the interconnected components act together as a single unit. Figure 2.7 shows how the strain distribution across the beam cross-section changes with varying degrees of composite action, ranging from a fully discontinuous profile under non-composite action to a continuous linear profile under full composite action.

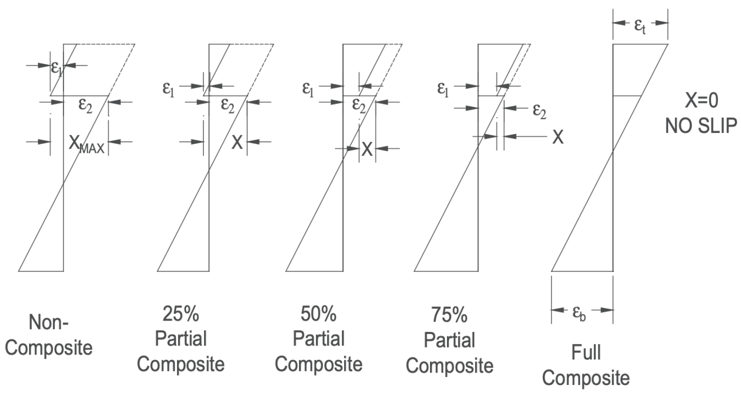

Figure 2.7: Strain distribution for varying degrees of composite action in a beam [43].

A system is said to exhibit full composite action when the structural components are connected by a sufficient number of adequately stiff shear connectors, such that the system behaves essentially monolithically with negligible relative slip at the interface [39]. Under this condition, the materials are utilized close to their maximum structural capacity, and the failure mode is typically governed by the moment resistance of the composite section rather than by the shear connection.

Partial composite action occurs when the shear connectors provided at the interface are either insufficient in number or inadequate in stiffness to fully transfer the longitudinal shear forces. In this state, measurable relative slip develops between the components, and they no longer act as a single monolithic unit. The failure of such systems is typically initiated by the shear connection reaching its limited load-carrying capacity before the full bending resistance of the composite section can be mobilized [39].

When two structural components are simply placed in contact without any mechanical shear connectors, no reliable shear transfer occurs across the interface. Under applied loading, the components act as independent elements and experience significant relative slip. This condition is termed non-composite action (or zero composite action) [39]. Although minimal shear transfer may occur through friction, this contribution is unreliable and is conservatively neglected in design.

2.4.3 Shear Connection and Shear Interaction

To properly understand the categories of composite action, it is essential to distinguish between two related but conceptually distinct terms: shear connection and shear interaction. Shear connection refers to the physical provision of fasteners and is associated with the strength of the longitudinal shear connection [39]. The degree of shear connection, denoted η, is defined as the ratio of the number of shear connectors provided to the number required to achieve full composite action [33]. A system with $\eta \geq 1.0$ is said to have full shear connection, whereas $0 \leq \eta < 1.0$ corresponds to partial shear connection.

Shear interaction describes the resulting mechanical behavior at the interface and is associated with the stiffness of the connection. Full shear interaction implies the complete elimination of interfacial slip. This is an idealized condition that is physically impossible due to connectors having finite stiffness and inherent flexibility, resulting in some longitudinal slip at the interface as well as deformation of the connectors themselves [39] [44]. Although shear connection and shear interaction are governed by different parameters, both contribute to the overall degree of composite action achieved in a beam.

2.4.4 Partial-Interaction Theory for Composite Beams

The absence of a dedicated Eurocode design framework for steel–timber composite beams presents challenges during the preliminary design stage. In particular, the interaction behaviour between the steel beam and timber slab cannot be accurately represented using conventional full-interaction beam theory, as relative slip occurs at the interface between the connected elements. Full-interaction theory provides an upper bound estimate of the stiffness and strength of composite beams. However, in order to determine the actual structural response, it is necessary to account for the slip behaviour of the shear connectors and the resulting partial interaction between the connected elements [45].

Several analytical methods have been proposed for partial interaction analysis of composite beams, including the Gamma method (γ-method), Timoshenko-based formulations, and Newmark's theory. All three share the same fundamental principle of modelling longitudinal slip at the interface between connected elements, differing primarily in their kinematic assumptions and scope of application. The Gamma method is codified in Annex B of Eurocode 5 for timber–timber systems, while Timoshenko-based formulations incorporate shear deformation within each layer, an effect that becomes negligible for members with high span-to-depth ratios, where both methods converge to the same result [46],[47]. Newmark's theory, based on Euler–Bernoulli beam kinematics, provides closed-form solutions and is not restricted to a specific material combination, requiring only the elastic moduli, cross-sectional properties, and connector stiffness of the two components, making it directly applicable to two-material composite systems beyond timber–timber configurations, including steel–timber members [45]. Newmark's theory is therefore adopted in this study, as the Gamma method is limited to timber–timber systems and Timoshenko-based formulations offer no practical advantage over Newmark's theory for the slender beam proportions investigated.

A partial-interaction formulation based on Newmark's linear-elastic composite beam theory was therefore adopted, further developed using the generalized derivation presented by Wu et al. [45] for composite beam-column members. The method accounts for the influence of connector slip on the structural response, capturing the reduction in composite action caused by partial interaction and providing a more realistic prediction of longitudinal shear transfer, interface slip, effective flexural stiffness, and beam deflection compared with conventional full-interaction theory. Although originally developed for steel–concrete composite systems, the theory is generic and may be applied to steel–timber composite beams provided that the connection behaviour can be represented using distributed elastic shear connectors. Its applicability to the configurations investigated in this study is verified numerically in Section 3.2.4.

The partial-interaction theory adopted in this study is based on the following assumptions [45]:

1. **All constituent materials behave linearly elastically.**

The interface strain in each element is given by:

$$\varepsilon_1 = \frac{M_1 h_1}{(EI)_1}, \qquad \varepsilon_2 = -\frac{M_2 h_2}{(EI)_2} \tag{2.1}$$

2. **The cross-section is uniform along the member length.**
   All stiffness quantities meaning $(EI)_i$, $(EA)_i$ and also the height h_i are constant along the member, yielding a governing differential equation with constant coefficients and a closed-form solution.

3. **Bernoulli's hypothesis applies independently to each element.**
   Strain varies linearly within each element. The curvature of each element is:

$$\kappa = \frac{M_1}{(EI)_1} = \frac{M_2}{(EI)_2} \tag{2.2}$$

   The strain profiles need not be continuous across the interface, which gives rise to the slip strain ε_{slp}.

4. **Shear connectors are continuously and uniformly distributed.**
   The slip at any section is related to the longitudinal shear force by:

$$s = \frac{L_s}{K_b}\frac{\mathrm{d}F_{\text{shr}}}{\mathrm{d}x} = a_0\frac{\mathrm{d}F_{\text{shr}}}{\mathrm{d}x} \tag{2.3}$$

   where $a_0 = L_s/K_b$ is the unit longitudinal flexibility of the connection.

5. **No transverse separation occurs at the interface.**
   Both elements share the same curvature at every section. The slip strain is therefore purely longitudinal:

$$\varepsilon_{\text{slp}} = \varepsilon_1 - \varepsilon_2 = -\frac{\mathrm{d}s}{\mathrm{d}x} \tag{2.4}$$

These assumptions allow the composite beam to be represented using a continuous partial-interaction model, where the degree of composite action is governed by the longitudinal slip occurring at the interface between the steel and timber components. Based on the assumptions above, Wu et al. [45] derive the following differential equations for the longitudinal shear force and deflection.
The governing equation for the Longitudinal Shear Force F_{shr} is:

$$a_0\frac{\mathrm{d}^2F_{\text{shr}}}{\mathrm{d}x^2} - a_1F_{\text{shr}} + a_2M(x) = 0 \tag{2.5}$$

The governing equation for the lateral deflection v is:

$$\frac{\mathrm{d}^2v}{\mathrm{d}x^2} = a_4a_0\frac{\mathrm{d}^2F_{\text{shr}}}{\mathrm{d}x^2} - \frac{M(x)}{EI} \tag{2.6}$$

The four constants appearing in these equations are defined as follows:

$$a_0 = \frac{L_s}{K_b} \qquad \text{unit longitudinal flexibility of the shear connection} \tag{2.7}$$

$$a_1 = \frac{EI}{EA \cdot \Sigma EI} \qquad \text{passive slip strain coefficient} \tag{2.8}$$

$$a_2 = \frac{h_1 + h_2}{\Sigma EI} \qquad \text{active slip strain coefficient} \tag{2.9}$$

$$a_4 = \frac{(h_1 + h_2)\, EA}{EI} \qquad \text{unit slip curvature} \tag{2.10}$$

where the composite stiffness quantities are:

$$\Sigma EI = (EI)_1 + (EI)_2 \tag{2.11}$$

$$\frac{1}{EA} = \frac{1}{(EA)_1} + \frac{1}{(EA)_2} \tag{2.12}$$

$$EI = \Sigma EI + EA\,(h_1 + h_2)^2 \tag{2.13}$$

Here EI is the full-interaction flexural stiffness of the composite cross-section.

2.5 Genetic Algorithm

Optimization is a widely used concept that can be applied across many different fields to solve complex problems and identify efficient or innovative solutions. In engineering applications, optimization techniques are particularly valuable due to the large and complex search spaces that often characterize design problems. Thus, evolutionary algorithms have become some of the most commonly used and preferred optimization methods. Among these evolutionary algorithms, genetic algorithms account for more than half of the reported applications, demonstrating their significant popularity and continued relevance despite the emergence of newer optimization techniques [48].

2.5.1 Principle of a Genetic Algorithm

Genetic algorithms are computational models inspired by the principles of natural evolution and selection. They are developed to solve specific problems by generating and evaluating different combinations of possible solutions while retaining and refining beneficial information throughout the optimization process. Although genetic algorithms can be applied to a wide range of problem types, they are most commonly used as optimization tools for identifying optimal or near-optimal solutions to complex functions and design problems [49].

Genetic algorithms operate using a chromosome-like data structure, where a set of candidate solutions forms an initial population. The initial population can be generated using several different approaches, however, in many applications, a randomly generated population is considered the most appropriate and effective method [50]. The algorithm then evaluates these chromosomes to identify the most suitable candidates, which are subsequently selected for reproduction and further evaluation [49]. Through this iterative process, new generations of solutions are created and progressively improved.

Once the initial population has been generated, the algorithm selects two chromosomes to serve as parent solutions. These parent chromosomes are then combined to reproduce and generate new candidate solutions, commonly referred to as children. The selection of parent chromosomes can be performed randomly or through various selection strategies, such as rank selection, tournament selection, or roulette wheel selection. The choice of selection method depends on the objective of the algorithm, as some techniques prioritize chromosome with high fitness values in order to increase the likelihood of producing superior children [50].

Ultimately, candidate solutions with the highest potential are assigned a greater probability of reproducing than less suitable chromosomes. Through this evolutionary process, the population gradually converges toward an optimal solution, as the best-adapted chromosome are more likely to survive and pass on their characteristics to subsequent generations. To distinguish strong solutions from weaker ones, chromosomes are typically evaluated and compared against the reference population. In general, genetic algorithms are particularly effective for solving complex optimization problems characterized by large, vague, or poorly defined search spaces [49] [51].

2.5.2 Types of Optimization Problems

Optimization problems are generally categorized intro three types: single-objective optimization, multi-objective optimization and weighted multi-objective optimization [1]. The main distinction between these categories lies in the number of competing objectives considered. Single-objective optimization involves only one objective function, whereas multi-objective optimization considers two or more conflicting objectives. In this context, conflicting objectives refer to the condition where improving one objective typically comes at the expense of another [2]. Weighted multi-objective optimization, on the other hand, is a form of multi-objective optimization in which the different objectives are combined into a single objective function through the application of weighting factors [48].

In engineering applications, multi-objective optimization is among the most commonly used approaches, as it provides a broader understanding of the design space and facilities informed decision-making. This approach is particularly advantageous when dealing with complex or large design variables. Compared with weighted multi-objective optimization, standard multi-objective optimization does not require predefined weighting factors between the objectives. This is beneficial because selecting appropriate weights with sufficient accuracy can be highly challenging and may significantly influence the resulting optimal solution [48].

However, it is important to recognize that these optimization approaches are also associated with computational costs and large sample sizes [52]. In real-world engineering problems, such as the design of composite structures, the design space may contain thousands of possible variable combinations and potential solutions. This complexity often leads to multiple local optima within the search space, thereby increasing the computational effort required for the optimization process [48]. Consequently, it is necessary to carefully assess the design workflow and determine whether a single-objective optimization approach is sufficient or whether a multi-objective optimization method provides a more effective solution for the problem under consideration [52].

2.5.3 Constraint Handling with Penalty Functions

Since the solution space in optimization can be extremely large, constraint functions are introduced to reduce the number of feasible solutions. Their purpose is to eliminate solutions that are not applicable by imposing limitations based on logical restrictions, material properties, and other design requirements. In this sense, constraint functions serve to distinguish feasible solutions from feasible ones, as certain outcomes may be unrealistic, physically impossible, or even cause the simulation model to fail [53].

A common approach for handling infeasible solutions is the use of penalty functions. The purpose of these functions is to reduce the fitness of solutions that violate imposed constraints, thereby decreasing their likelihood of being selected for reproduction. Typically, the magnitude of the penalty is determined based on the degree of constraint violation, with the penalty factor chosen by the designer. Solutions associated with larger violations receive more severe penalties, resulting in significantly lower fitness values. Since there are no universally applicable guidelines for selecting an appropriate penalty factor, its definition generally depends on the specific characteristics and requirements of the optimization problem under consideration [53].

2.6 Life Cycle Assessment (LCA)

Life Cycle Assessment (LCA) is a standardized, quantitative method for evaluating the environmental impact of a product across its entire life cycle, from raw material extraction, through the use phase, to end of life [54]. The defining characteristic of LCA is its systems perspective, which captures impacts across all life cycle stages and helps prevent problem shifting—the risk that reducing an environmental burden at one stage creates or worsens it elsewhere [55].

According to Hauschild et al. [55], LCA is grounded in the principle of mass and energy balance. All physical flows, such as materials, energy, and emissions associated with a product system, are traced and quantified in the Life Cycle Inventory

(LCI). These flows are then converted into environmental impact scores using different characterization models. The model most relevant for this thesis is related to climate change, namely Global Warming Potential (GWP), developed by the IPCC. GWP expresses the cumulative radiative forcing of a greenhouse gas relative to CO_2 over a 100-year time horizon, with the result expressed in kg CO_2-equivalents.

In practice, LCA studies are populated using primary manufacturer data together with verified background databases, for example those provided by the Swedish National Board of Housing, Building and Planning (Boverket). These sources provide specific or generic Environmental Product Declarations (EPDs), which are standardized and third-party-verified documents reporting the environmental performance of a specific product.

The life cycle of a construction product is divided into standardized modules as defined in EN 15978 and EN 15804. These modules span four main stages, covering the entire life cycle from raw material extraction to end-of-life processing.

A1–A3 | Product stage (cradle to gate). This stage includes raw material extraction (A1), transport to the manufacturer (A2), and manufacturing processes (A3). These modules represent the embodied carbon of a material at the factory gate and are typically the dominant contributors to the life cycle Global Warming Potential (GWP) of structural materials. This is the system boundary applied in the present thesis.

A4–A5 | Construction process stage. This stage covers the transport of products from the factory to the construction site (A4), as well as on-site installation and construction processes, including the generation and management of construction waste (A5).

B1–B7 | Use stage. The use stage represents the operational life of the structure and includes processes such as maintenance (B2), repair (B3), replacement of components (B4), and refurbishment (B5), as well as operational energy and water use (B6–B7). For passive structural elements such as beams, direct emissions during the use stage are generally negligible.

C1–C4 | End-of-life stage. This stage includes deconstruction or demolition (C1), transport of waste to processing facilities (C2), waste processing such as sorting or crushing (C3), and final disposal (C4). The treatment of materials at the end of life can significantly influence the overall environmental impact profile of a building component.

Module D | Beyond the system boundary. Module D accounts for potential benefits from the reuse, recovery, and recycling of materials beyond the defined system boundary. For structural steel, this module is particularly important, as its high recyclability means that recovered scrap at the end of life can offset a substantial portion of the production-stage GWP. Module D is reported separately and is not aggregated into the total results for stages A1–C, since it represents potential future benefits rather than impacts directly attributable to the current product system (Salokangas, 2013).

The goal of LCA is to provide a rigorous and comparable basis for evaluating the environmental consequences of design and material choices, thereby making sustainability quantifiable and explicit. Without a life cycle perspective, optimizing for structural performance or cost risks overlooking significant environmental burdens embedded in material production [56].

2.7 Life Cycle Costing (LCC)

Life Cycle Costing (LCC) is an economic analysis method used to evaluate all relevant costs of a project over a specific period of time. This method considers both initial capital costs and future operational expenditures, providing a complete economic assessment by looking at all projected cash flows. For large infrastructure projects like bridges or highways, these costs are typically divided into three categories: agency costs, user costs, and society costs [57].

Agency costs include all expenses paid directly by the owner, such as planning, design, initial construction, routine maintenance, and operations. User costs are the indirect economic impacts experienced by the public due to construction or maintenance delays; for example, when a structure undergoes repair, traffic disruptions cause users to lose valuable time or working hours. Lastly, society costs cover broader impacts on the general public, including accidents, environmental damage, and potential functional failures [57]. This total infrastructure cost framework can be expressed as:

$$LCC_{\text{total}} = LCC_{\text{agency}} + LCC_{\text{user}} + LCC_{\text{society}} \tag{2.14}$$

Within established life cycle costing frameworks, the total cost handled directly by the managing organization—the agency cost (LCC_{agency})—is split into three primary parts based on when they occur and their associated risk [57]:

$$LCC_{\text{agency}} = LCC_{\text{acquisition}} + LCC_{\text{MR\&R}} + LCC_{\text{consequence}} \tag{2.15}$$

Where $LCC_{\text{acquisition}}$ represents the upfront investment (programming, detailed design, and construction), $LCC_{\text{MR\&R}}$ denotes the ongoing costs for maintenance, repair, and rehabilitation over the lifecycle, and $LCC_{\text{consequence}}$ accounts for future costs from potential structural failures or performance issues [57].

For simple, individual structural components, such as the beam elements optimized in this study, the large-scale user and society costs are omitted, leaving agency costs as the primary economic metric. Furthermore, because these specific components are protected inside a building's stable interior environment, they do not require active operational energy or routine maintenance, meaning that both ongoing maintenance costs and risk-associated consequence costs are negligible ($LCC_{\text{MR\&R}} = 0$ and $LCC_{\text{consequence}} = 0$).

As a result, the economic evaluation isolates the upfront investment phase ($LCC_{\text{acquisition}}$) as the solitary design metric [57]. This investment cost (C_{inv}) covers the entire physical realization of the structural component and is evaluated using the following breakdown:

$$LCC_{\text{acquisition}} = C_{\text{inv}} = C_{\text{mat}} + C_{\text{fab}} + C_{\text{trans}} + C_{\text{const}} \tag{2.16}$$

Where:

- C_{mat} is the material procurement cost (the base costs for timber, steel, and connectors).
- C_{fab} is the manufacturing and fabrication cost (including plant processing, cutting, and gluing).
- C_{trans} is the transportation cost of getting the components to the construction site.
- C_{const} represents the onsite assembly and installation costs.

2.7.1 Marginal Abatement Cost

Life cycle assessment (LCA) and life cycle costing (LCC) are the two most established frameworks for evaluating the environmental and economic performance of structural systems across their full service life. LCA quantifies embodied carbon from cradle to grave, while LCC captures the monetary costs distributed across the same lifecycle stages. Individually, each tool provides a clear and consistent picture, but the conflict arises when both must be used together to guide a decision. Since no standard exists to integrate LCA and LCC, comparing their outputs, kg CO_2-equivalent against a net present monetary value, leaves the decision-maker without a common basis for judgement [58].

While several approaches exist to bridge the gap between economic and environmental metrics, the Marginal Abatement Cost Curve (MAC) offers a particularly direct solution. It unifies both dimensions into a single objective parameter, expressed as a unit cost per mass of avoided emissions (£/kg CO_2), allowing financial investment and carbon reduction to be evaluated within a single framework [59].

The core logic of the method is expressed as:

$$\text{MAC} = \frac{\Delta C}{\Delta E} \tag{2.17}$$

where ΔC is the change in cost relative to a reference case (£), and ΔE is the corresponding change in greenhouse gas emissions (kg CO_2eq). A negative MAC indicates that a strategy both reduces emissions and saves money, while a positive value reflects a net cost for achieving the abatement.

The MAC approach was first widely popularised by McKinsey & Company [60] to map the costs of reducing greenhouse gas emissions across different industries, and was later adopted in UK policy to guide carbon pricing and evaluate sector-specific reduction targets. However, because traditional MACs omitted material efficiency strategies, such as reducing structural material quantities in construction, Dunant et al. [59] expanded the methodology. Their framework incorporates detailed engineering cost profiles, accounts for cost uncertainties, and handles the interactions between different design strategies.

3 Methodology

3.1 Methodological Framework

This study employs a methodology that can be divided into three main parts, each corresponding to one of the defined research questions. The process begins by establishing the load cases and span lengths to be investigated. A case study is then developed in which the loading conditions are defined in accordance with Eurocode EN 1991-1-1 [61]. In this study, the selected imposed loads represent office and retail load.

The reference beams are designed using linear-elastic analysis, with the selected cross-sections chosen to satisfy the strength requirements while maximizing material utilization and minimizing material volume. Since no dedicated Eurocode standard currently exists for steel-timber composite members, their design relies on analytical procedures that account for partial interaction between the steel and timber components. The Newmark partial interaction theory is therefore used to evaluate the composite action and determine the structural response of the beams. To verify the applicability of this approach, an assumed composite cross-section is numerically modelled, and the analytical predictions are compared with the numerical simulations to assess the accuracy of the method.

Subsequently, a life cycle assessment (LCA) and life cycle cost analysis (LCCA) are performed for all span lengths between 3 m and 12 m. The objective is to identify the span lengths and loading scenarios for which steel-timber composite systems provide environmental and economical advantages compared to the reference beam solutions. Due to the large number of possible STC configurations, a genetic algorithm implemented in MATLAB is used to identify only the feasible design solutions that satisfy the predefined design constraints. However, even after filtering for feasibility, a substantial number of candidate solutions remain. Therefore, a selection procedure is required to identify the most suitable composite beam configuration. For this purpose, the Marginal Abatement Cost (MAC) approach is employed. The optimal solutions is defined as the beam configuration that provides the greatest cost savings per unit increase in CO_2 emissions, expressed in SEK per kgCO_2e.

After completing the LCA and LCCA for span lengths ranging from 3 m to 12 m, the study proceeds with a detailed numerical investigation in Abaqus. This analysis focuses on two selected long-span cases: 7 m and 12 m, using the same load cases as previously defined. These span lengths are chosen to represent long-span behavior and to enable a comparison of how structural performance evolves with increasing span. The numerical study begins with a linear elastic analysis, followed by a linear buckling analysis and a nonlinear analysis to capture the realistic response of the beams under increasing load. From the nonlinear simulations, key results such as load-displacement behavior, load-slip responses, stress distributions, and failure modes are extracted for all configurations, and compared with the reference beams.

To provide an overview of the methodological framework, a flowchart is presented in Figure 3.1. It illustrates how the three parts of the study are structured and interconnected, each corresponding to one of the three research questions.

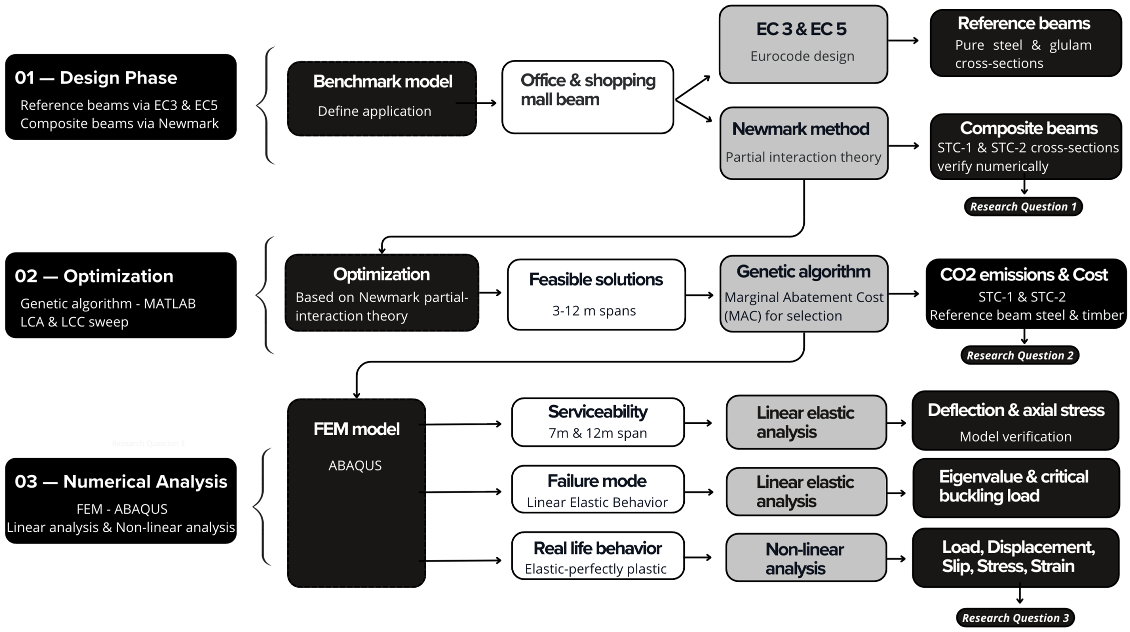

Figure 3.1: Flowchart of the methodological framework, outlining the three study phases.

3.2 Design Phase

In the design phase, the cross-sections of the reference beams and the steel-timber composite beams are established, along with the governing load cases, based on a conceptual case study. The reference beams are designed in accordance with Eurocode EN 1993-1-1 [62] and Eurocode EN 1995-1-1 [46], while the composite beams are designed using the Newmark partial interaction theory, with relevant design provisions adapted from Eurocode EN 1994-1-1 [63] for steel-concrete composite structures.

3.2.1 Steel-Timber Composite Configurations

As the thesis focuses on steel and timber, the reference beams in the building are defined using each material separately. One analysis considers the structure with only steel beams, in order to determine the required steel section for the given load combinations and spans, as well as to identify the governing failure mode. A corresponding analysis is carried out for timber beams, where the required glulam sections and their governing failure modes are established under the same conditions. The steel beams are selected from a range of HEA sections, while the timber beams are chosen from the GL30c strength class.

The investigated STC solutions consist of two principal concepts. The first configuration, referred to as STC-1, consists of a steel HEA beam with a timber element positioned above the top flange. The second configuration, referred to as STC-2, consists of a timber beam reinforced with a steel plate attached to its underside. The timber element in STC-1 aims to prevent lateral-torsional buckling, while the steel plate in STC-2 aims to increase stiffness and ductility, thereby reducing deflections. These improvements are particularly important because lateral-torsional buckling commonly governs the design of steel beams, whereas deflection limits often govern the design of timber beams. The configurations of the two composite beams are illustrated in Figure 3.2.

(a) **(b)**

Figure 3.2: Selected composite beam configurations: (a) STC-1 and (b) STC-2.

Limiting the study to these two configurations allows a direct comparison between a steel-governed and a timber-governed composite strategy, isolating the effects of each governing mechanism. Other configurations from Section 2.2.1, such as side-by-side or fully encased arrangements, were excluded because they do not target a single dominant failure mode as clearly, and add geometric and connection complexity without a clear gain in LTB resistance or deflection control. This keeps the parameter sweep, optimization, and FEA validation manageable within the project timeline, while still covering the two configurations most representative of practical steel-timber composite use.

3.2.2 Load Cases

The load cases are based on a conceptual case study of a multi-storey building with floors of varying occupancy. The floors are designed for either office use or retail use, resulting in two load cases that differ in the magnitude of the imposed load. The structural behavior and load performance are assessed based on load combinations specified in Eurocode EN 1991-1-1, with imposed and permanent loads defined according to the function and location of each beam within the building. In all cases, the beams are assumed to be simply supported. This allows for a comparison of how the imposed load magnitude influences the structural behavior, LCA, and LCC of the analyzed beams. The load configuration for each case is illustrated in Figure 3.3.

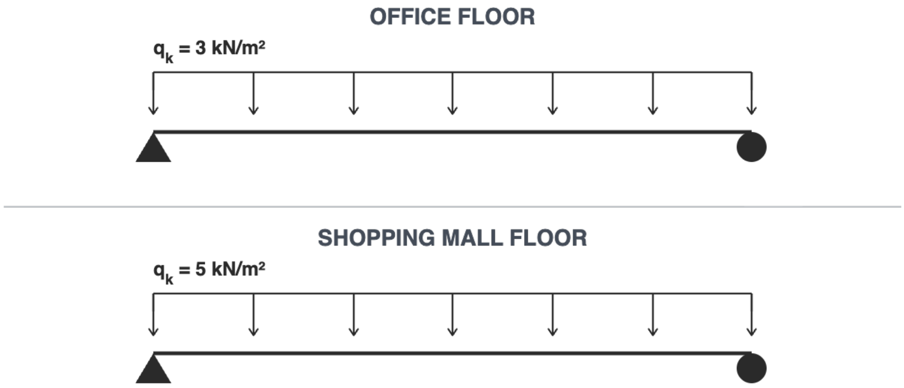

Figure 3.3: Applied load cases for the selected beam configurations.

3.2.3 Application of Newmark's method for Composite Systems

The analytical formulation adopted in this study is based on the partial interaction theory developed by Wu et al. [45]. The derivation is based on equilibrium, compatibility, and constitutive relationships for a two-element composite beam connected through distributed elastic shear connectors.

The composite member consists of two structural elements connected along a common interface:

- Element 1: steel beam
- Element 2: timber slab

The longitudinal coordinate is denoted by x, and the relative longitudinal displacement between the two elements is represented by the interface slip $s(x)$.

3.2.3.1 Equilibrium Relationships

The longitudinal shear force transferred through the interface is denoted by $F_{shr}(x)$. This quantity represents the cumulative longitudinal interaction force transferred between the steel beam and timber slab through the distributed shear connectors. For the case without externally applied axial loading, equilibrium of axial forces gives

$$N_1 = -F_{shr} \tag{3.1}$$

$$N_2 = F_{shr} \tag{3.2}$$

where:
- N_1 is the axial force in the steel beam,
- N_2 is the axial force in the timber slab.

The total bending moment acting on the composite section is resisted through:
1. direct bending moments within the individual elements,
2. the axial force couple generated by the interface interaction force.

Moment equilibrium therefore gives

$$M(x) = M_1 + M_2 + F_{shr}(h_1 + h_2) \tag{3.3}$$

where:
- M_1 is the bending moment carried by the steel beam,
- M_2 is the bending moment carried by the timber slab,
- h_1 and h_2 are the distances from the centroids of the individual elements to the connection interface.

The term $F_{shr}(h_1 + h_2)$ represents the moment contribution generated by the axial force couple acting between the two elements.

3.2.3.2 Curvature Compatibility

Since no transverse separation occurs at the interface, both elements experience identical curvature at the same longitudinal position. According to Euler–Bernoulli beam theory,

$$\kappa_1 = \kappa_2 \tag{3.4}$$

which gives

$$\frac{M_1}{E_1 I_1} = \frac{M_2}{E_2 I_2} \tag{3.5}$$

Rearranging Equation 3.5 together with Equation 3.3 gives

$$M_1 = \frac{E_1 I_1}{E_1 I_1 + E_2 I_2} \left[M(x) - F_{shr}(h_1 + h_2) \right] \tag{3.6}$$

$$M_2 = \frac{E_2 I_2}{E_1 I_1 + E_2 I_2} \left[M(x) - F_{shr}(h_1 + h_2) \right] \tag{3.7}$$

3.2.3.3 Partial-Interaction Shear Force

The longitudinal shear force $F_{\text{shr}}(x)$ is governed by

$$a_0\, F''_{\text{shr}} - a_1\, F_{\text{shr}} + a_2\, M(x) = 0, \qquad M(x) = \tfrac{q}{2}(Lx - x^2) \tag{3.8}$$

whose general solution is

$$F_{\text{shr}}(x) = C_1 e^{\lambda x} + C_2 e^{-\lambda x} + \frac{a_2 q}{a_1}\left(\frac{Lx}{2} - \frac{x^2}{2} - \frac{a_0}{a_1}\right), \qquad \lambda = \sqrt{\frac{a_1}{a_0}} \tag{3.9}$$

The longitudinal shear flow $q_{\text{shr}} = dF_{\text{shr}}/dx$ is proportional to the vertical shear force, which is linear under UDL. Therefore F_{shr}, as the integral of a linear function, is parabolic, zero at both supports and maximum at mid-span. The boundary conditions are accordingly:

$$\text{BC1: } F_{\text{shr}}(0) = 0 \qquad \Rightarrow \quad C_1 + C_2 = \frac{a_2\, q\, a_0}{a_1^2} \tag{3.10}$$

$$\text{BC2: } F_{\text{shr}}(L) = 0 \qquad \Rightarrow \quad C_1\, e^{\lambda L} + C_2\, e^{-\lambda L} = \frac{a_2\, q\, a_0}{a_1^2} \tag{3.11}$$

Subtracting equation (3.10) from equation (3.11):

$$C_1\left(e^{\lambda L} - 1\right) - C_2\left(1 - e^{-\lambda L}\right) = 0 \quad \Rightarrow \quad C_1\left(e^{\lambda L} - 1\right) = C_2\left(1 - e^{-\lambda L}\right) \tag{3.12}$$

Noting that $1 - e^{-\lambda L} = e^{-\lambda L}(e^{\lambda L} - 1)$:

$$C_1 = C_2\, e^{-\lambda L} \tag{3.13}$$

Substituting back into BC1:

$$C_2\, e^{-\lambda L} + C_2 = \frac{a_2\, q\, a_0}{a_1^2} \quad \Rightarrow \quad C_2 = \frac{a_2\, q\, a_0}{a_1^2} \cdot \frac{e^{\lambda L}}{e^{\lambda L} + 1} \tag{3.14}$$

giving the integration constants:

$$\boxed{C_1 = \frac{a_2\, q\, a_0}{a_1^2} \cdot \frac{1}{e^{\lambda L} + 1}} \qquad \boxed{C_2 = \frac{a_2\, q\, a_0}{a_1^2} \cdot \frac{e^{\lambda L}}{e^{\lambda L} + 1}} \tag{3.15}$$

The maximum longitudinal shear force occurs at midspan $x = L/2$ and is evaluated as:

$$F_{\text{shr,max}} = C_1\, e^{\lambda L/2} + C_2\, e^{-\lambda L/2} + \frac{a_2\, q}{a_1}\left(\frac{L^2}{4} - \frac{L^2}{8} - \frac{a_0}{a_1}\right) \tag{3.16}$$

3.2.3.4 Deflection

The deflection $v(x)$ is obtained from the curvature relation $v'' = \kappa = M_1/(E_1 I_1)$, which after substituting the moment expression and connector flexibility yields

$$-\frac{d^2 v}{dx^2} - a_4\, a_0\, \frac{d^2 F_{\text{shr}}}{dx^2} + \frac{M(x)}{b} = 0 \tag{3.17}$$

where $b = (E_1 I_1 + E_2 I_2) + a(h_1 + h_2)^2$ is the full-composite flexural stiffness and $a_4 = (h_1 + h_2)\, a/b$. Integrating twice with boundary conditions $v(0) = 0$ and $v(L) = 0$, and noting that $F_{\text{shr}}(0) = 0$ and $F_{\text{shr}}(L) = 0$ (from the shear force boundary conditions), the integration constants vanish and the total deflection is

$$v(x) = v_{\text{full}}(x) + v_{\text{slip}}(x) \tag{3.18}$$

where the full-interaction contribution is

$$v_{\text{full}}(x) = \frac{q}{24\, b}\, x\Big(L^3 - 2Lx^2 + x^3\Big) \tag{3.19}$$

and the slip contribution is

$$v_{\text{slip}}(x) = a_4\, a_0\, F_{\text{shr}}(x) \tag{3.20}$$

The total deflection at any section is therefore

$$v(x) = \frac{q}{24\, b}\, x\Big(L^3 - 2Lx^2 + x^3\Big) + a_4\, a_0\, F_{\text{shr}}(x) \tag{3.21}$$

where $F_{\text{shr}}(x)$ is given by equation (3.16). Since F_{shr} is parabolic with maximum at mid-span, the slip contribution v_{slip} is also maximum at mid-span, giving the maximum total deflection as

$$\boxed{v_{\max} = v\Big(\tfrac{L}{2}\Big) = \frac{5\, q\, L^4}{384\, b} + a_4\, a_0\, F_{\text{shr}}\Big(\tfrac{L}{2}\Big)} \tag{3.22}$$

where $F_{\text{shr}}(L/2)$ is evaluated from equation (3.16).

3.2.4 Validation of Analytical Method Using Abaqus FEA

The analytical model is derived based on equilibrium, compatibility, and constitutive relationships, and must be validated before it can be used for further analysis. Therefore, a three-dimensional finite element model is developed in Abaqus FEA to assess the accuracy of the analytical results. This is carried out for both STC-1 and STC-2, with the deflection and axial stresses of the two models compared to evaluate their agreement. The beam configurations follow those defined in Section 3.2.1, with the load cases and boundary conditions from Section 3.2.2.

The model consists of three separate parts that are subsequently assembled: the steel beam, the timber beam, and additional steel support plates. The support plates are introduced to reduce the large stress concentrations that typically develop near the beam supports due to the imposed boundary conditions. By distributing the reaction forces over a larger area, the plates mitigate excessive stress concentrations in the region close to the beam ends.

3.2.4.1 Material Properties

The timber material is defined using the *Engineering Constants* formulation in order to account for its orthotropic behavior, including direction-dependent elastic and shear moduli. The material properties correspond to the GL30c strength class and are obtained from the *Glulam Handbook, Volume 1.* On the other hand, the steel and support plates are modelled as *Isotropic* materials, with structural steel grade S355 adopted for the analysis. The mechanical properties of the materials are summarized in Table 3.1.

Table 3.1: Linear material properties for steel and timber.

Glulam GL30c								
E_1 [MPa]	E_2 [MPa]	E_3 [MPa]	ν_{12} [-]	ν_{13} [-]	ν_{23} [-]	G_{12} [MPa]	G_{13} [MPa]	G_{23} [MPa]
13000	300	300	0.3	0.3	0.4	650	650	77
Steel S355								
E [GPa]				ν [-]				
210				0.3				

3.2.4.2 Contact Property

The interaction between the steel and timber components is modeled using a surface-to-surface contact formulation with a *Hard contact* normal behavior and *Frictionless* tangential behavior. A frictionless interface is adopted to ensure consistency with the analytical calculations, which are likewise based on the assumptions of no friction. This enables a more direct and fair comparison between the analytical and numerical results. The shear connectors, consisting of either bolts or screws, are modeled as *Point-based* fasteners using the *Cartesian* connector formulation. Within this connector type, the connector stiffness can be explicitly defined. For the analyses, the slip modulus values K_{ser} and K_u are assigned for the serviceability limit state and ultimate limit state, respectively. These stiffness parameters are based on elastic theory and are obtained from Eurocode 5 EN 1995-1-1.

3.2.4.3 Boundary Conditions and Meshing

The load is applied as a uniformly distributed pressure load. Boundary conditions are assigned to a reference point located at the center of the bottom surface of the support plate. This reference point is coupled to the surface using a distributing *Coupling* constraint. Since the beam is modeled as simply supported, one end is defined with a roller support and the opposite end with a pinned support. The applied boundary conditions are shown in Table 3.2. The finite element mesh consists of 8-node linear brick elements with incompatible modes (C3D8I).

Table 3.2: Boundary conditions of numerical model.

Boundary conditions			
	U1	U2	U3
Roller support	*Fixed*	*Fixed*	*Free*
Pinned support	*Fixed*	*Fixed*	*Fixed*

The element size is determined based on a mesh convergence study performed for each composite beam configuration, using the average deflection along the beam length as the convergence parameter. For each configuration, the mesh progressively refined from a coarse mesh of 130 mm down to approximately 10 mm. The exact fine mesh size is adjusted slightly between configurations so that an even number of elements fits across the beam width. Convergence is achieved once the mid-span deflection falls within 2% of the value from the finest mesh. Based on this criterion, the converged element size varies between 20 mm and 45 mm across the eight STC configurations, and these element sizes are adopted for the subsequent analyses. The procedure is illustrated in Figure 3.4 for a representative 7 m span configuration.

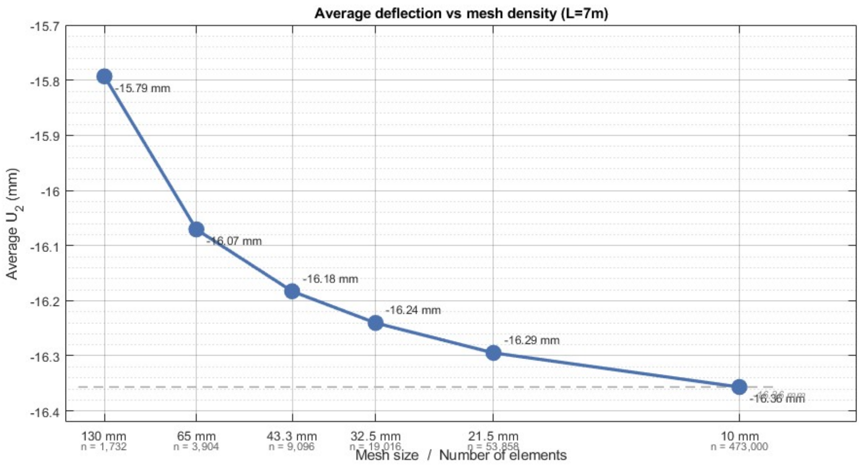

Figure 3.4: Representative mesh convergence study for a 7 m span configuration.

3.2.4.4 Model Simulation

Linear elastic analysis is carried out using the *Static, General* procedure in Abaqus. Since the degree of partial interaction in the analytical model is governed by the connector type and number, the simulation of the numerical model must adopt the same assumptions to enable a valid comparison. However, as the connector type and number have not yet been determined at this stage, full composite action is assumed in both models, meaning perfect bonding at the interface with no relative slip permitted. In Abaqus, this is achieved using a *Tie constraint* between the steel and timber parts, with a frictionless interface to remain consistent with the analytical assumptions. This approach allows the numerical and analytical models to be directly compared under identical conditions, independent of any connector properties.

To subsequently validate Newmark's partial interaction theory, the *Tie constraint* is removed and replaced with discrete mechanical fasteners representing the shear connection between the steel and timber parts. The connector stiffness is assigned according to the selected slip modulus values, allowing relative slip to occur at the interface and thereby reproducing partial composite action in the numerical model. This enables the partial-interaction analytical results to be directly compared against the corresponding numerical predictions.

3.3 Optimization Phase

In the second phase of the methodological framework, an optimization is performed to identify the most favorable composite beam configuration for each beam span length between 3 m and 12 m. Since numerous composite beam configurations and dimensions are possible, a genetic algorithm is developed to identify feasible solutions. For each proposed configuration within a given beam span, an LCA and LCCA are performed to obtain its CO_2 emissions and cost performance. These results are then used to carry out a Marginal Abatement Cost (MAC) evaluation, which is implemented as the selection criterion to ensure a consistent basis for comparing and selecting among the numerous feasible configurations. The environmental and economic performance of the selected configurations is subsequently compared against that of the corresponding reference beam for the same beam span.

3.3.1 Genetic Algorithm

The design and optimization of the steel-timber composite beam was performed through an exhaustive parameter sweep implemented in MATLAB. The procedure consists of two components: an input file defining the steel section properties, and an optimization script that evaluates all feasible configurations in three sequential steps.

3.3.1.1 Input File: Section Properties

Prior to the sweep, two input files `HEA_properties.m` and `GL30c_properties.m`, were written containing the geometric and cross-sectional properties of all standard HEA sections from HEA 100 to HEA 800, as well as all standard GL30c sections from the Glulam Handbook. For each steel section, the file provides the cross-sectional area A_s, second moment of area I_s, flange width b_f, and total section height h_s. A total of 22 sections are defined, covering the full range of commercially available HEA profiles. For each glulam section, the file provides the height h_s and width b_f corresponding to the standard manufacturing range of glulam beams produced in Sweden. A total of 133 different sections are defined, covering the full range of commercially manufactured glulam dimensions.

3.3.1.2 Step 1: Structural Filter (Full Interaction)

The first step performs a structural feasibility check under the assumption of full composite interaction. For STC-1, every combination of HEA section and glulam depth h_t is evaluated, where h_t is swept from 50 mm to 500 mm in increments of 10 mm, subject to the geometric constraints $h_t \leq h_s$ and $h_s + h_t \leq 1.2$ m. For STC-2, every combination of GL30c section and steel depth h_s is evaluated, where h_s is swept from 10 mm to 100 mm in increments of 5 mm, subject to the geometric constraints $h_s \leq h_t$ and $h_s + h_t \leq 1.2$ m. For each combination, the transformed cross-section is computed using the modular ratio $n = E_s/E_t$, yielding the elastic neutral axis position y_{NA} and the effective second moment of area I_{eff}.
Two utilisation ratios are then evaluated:

$$U_{v,\text{FI}} = \frac{v_{\text{full}}}{L/300} \leq 1.0 \tag{3.23}$$

$$U_{m,\text{FI}} = \max\left(\frac{\sigma_{s,\text{Ed}}}{f_{yd}},\ \frac{\sigma_{t,\text{Ed}}}{f_{md}}\right) \leq 1.0 \tag{3.24}$$

where v_{full} is the mid-span deflection under full interaction, $\sigma_{s,\text{Ed}}$ and $\sigma_{t,\text{Ed}}$ are the design stresses in the steel and timber, and f_{yd}, f_{md} are the design strengths. Only combinations satisfying both criteria pass to Step 2. No cost or environmental objective is applied at this stage; the filter is purely structural.

3.3.1.3 Step 2: Connection Design (Partial Interaction)

For each section passing Step 1, the connection layout is determined following the design standards in Eurocode 5. Johansen's yield theory is applied to calculate the load-carrying capacity of the connectors. In both composite beams, the steel plates are considered thick and the connections consist of a single shear plane. For STC-1, bolts are selected as the connector type, since they are well suited for connections through the steel flange. Diameters of $d = 12$, 16, 20, and 24 mm are considered, with 2 or 4 rows of connectors across the flange. For STC-2, self-tapping screws are selected, as they are well suited for inclined insertion into the timber cross-section. These are inserted at an angle of 45 degrees, with diameters of $d = 6$, 8, 10, and 12 mm considered, using 2 rows of connectors across the width of the beam.
The bolt spacing L_s is determined directly from the full shear connection requirement $\eta = 1.0$. The minimum number of connectors per row, $n_{\text{pr,min}}$, is first computed from:

$$n_{\text{pr,min}} = \left\lceil \frac{\eta \cdot V_{l,\text{full}}}{n_{\text{rows}} \cdot F_{v,\text{Rd}}} \right\rceil \tag{3.25}$$

where $V_{l,\text{full}}$ is the longitudinal shear force at full interaction and $F_{v,\text{Rd}}$ is the design shear resistance of a single connector. The spacing is then set to the maximum value satisfying EC5 geometric constraints and the depth limit $L_s \leq h_t$:

$$L_s = \max\left(\left\lfloor \frac{L_{\text{avail}}}{n_{\text{pr,min}} - 1} \right\rfloor_{5\,\text{mm}},\ L_{s,\text{min}}\right) \tag{3.26}$$

The γ-factor (EC5 Annex B) is subsequently computed as an outcome of the spacing rather than a design target:

$$\gamma = \frac{1}{1 + \dfrac{\pi^2 E_t A_t L_s}{K_{\text{ser,eff}}\, L^2}} \tag{3.27}$$

Newmark's partial interaction theory is then applied to verify the SLS deflection and ULS bending utilisation under the actual connector layout, as described in Section 3.2.3. An η tolerance of $\pm 15\%$ is applied to avoid over-connected configurations. Configurations failing any structural check are rejected. Of the feasible configurations for each section, the one yielding the minimum total embodied carbon, beam and connectors combined, is retained as an output.

3.3.1.4 Step 3: MAC Ranking and Recommended Design

For each retained configuration, a Life Cycle Assessment (LCA) and Life Cycle Cost Analysis (LCCA) are first performed to obtain its total embodied carbon (E) and total cost (C), respectively, within the previously defined system boundary. These values are then used to evaluate and rank all retained configurations using the Marginal Abatement Cost framework following Dunant et al. [59], as described in Section 2.7.1:

$$\text{MAC} = \frac{C_{\text{composite}} - C_{\text{reference}}}{E_{\text{reference}} - E_{\text{composite}}} \quad \left[\frac{\text{SEK}}{\text{kgCO}_2\text{eq}}\right] \tag{3.28}$$

where C denotes total cost and E denotes total embodied carbon, both including beam material and connectors within the A1–A3 + C3 + D system boundary per section 2.6.

Configurations where the total composite carbon exceeds the reference, yielding a negative denominator in Equation (3.28), are retained rather than excluded. While such configurations do not represent a net carbon abatement, they are still reported because at shorter spans the composite systems may not yet achieve a reduction relative to the reference beam, and excluding them would leave no feasible configuration to report at all. Highlighting these cases is therefore important, as it shows the span range over which the composite systems become both economically and environmentally favorable, rather than masking the spans where they do not.

Because ΔC and ΔE can each independently be positive or negative, the sign of MAC alone does not indicate whether a configuration is favorable: a positive or negative MAC can each correspond to either a beneficial or an unfavorable outcome, depending on the underlying signs of cost and carbon change. The recommended design for each load case is therefore double-checked manually, using the MAC value together with the underlying cost and carbon changes to identify the most favorable, or least unfavorable, configuration available for that span. A configuration with a higher MAC that still achieves a cost saving or a carbon saving relative to the reference is considered preferable to one with a lower MAC that results in both a higher cost and higher carbon emissions.

The complete three-step procedure is summarized in Figure 3.5.

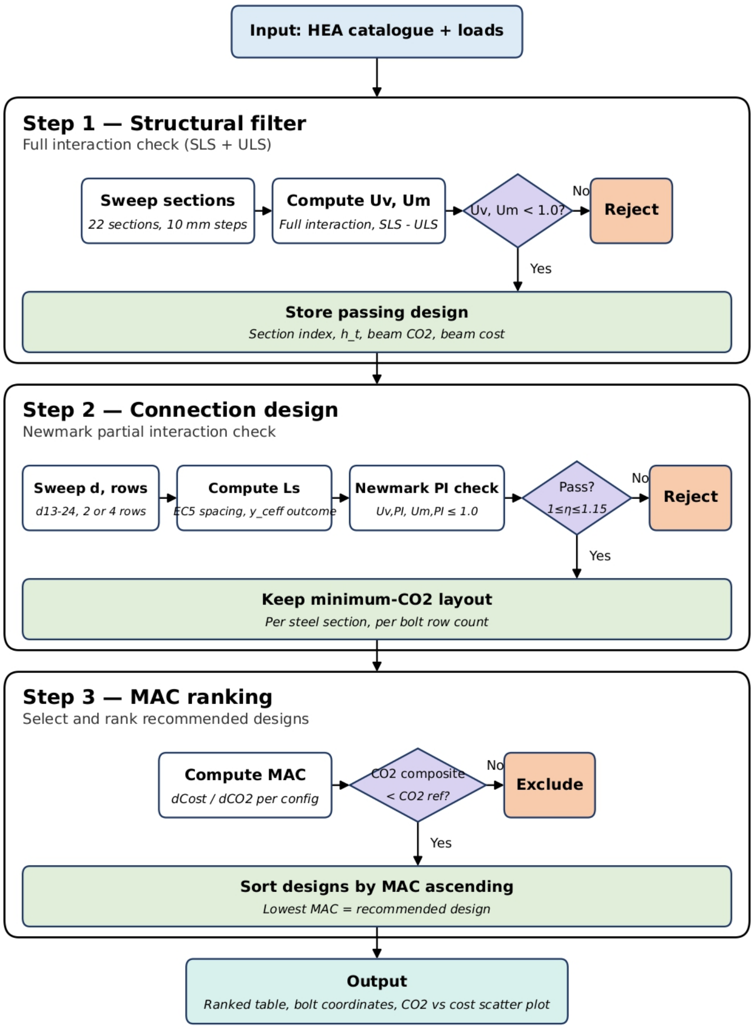

Figure 3.5: Complete three-step procedure used in the optimization sweep.

3.3.2 Assumptions Made for STC-1

The beam is designed in accordance with the Newmark's partial interaction theory and connection design procedure described in Sections 2.4.4 and 2.3.2. The following assumptions are specific to the STC-1 cross-section geometry and are enforced directly in the optimisation code:

- The glulam width cannot exceed the steel flange width: $b_t = b_f$
- The timber depth is bounded by the steel section depth: $h_t \leq h_s$
- The total composite depth is limited to:

$$h_s + h_t \leq h_{\text{ref,glulam}} \tag{3.29}$$

- The full shear connection longitudinal force is governed by the weaker material:

$$V_{l,\text{full}} = \min(b_t \cdot h_t \cdot f_{cd}, \quad A_s \cdot f_{yd}) \tag{3.30}$$

- An η tolerance of $\pm 15\%$ is applied ($1.0 \leq \eta \leq 1.15$) to avoid over-connected configurations arising from discrete bolt spacing
- No creep or long-term deformation is considered — the SLS check is based on instantaneous elastic deflection only

These assumptions reflect both structural and practical constraints. The width and depth limits ($b_t = b_f$ and $h_t \leq h_s$) keep the glulam flush within the steel flange and web, preventing an eccentric overhang that would introduce out-of-plane bending and complicate the connector layout. The total depth limit ($h_s + h_t \leq h_{\text{ref,glulam}}$) keeps STC-1 comparable in size to the glulam reference, avoiding an oversized hybrid section. The expression for $V_{l,\text{full}}$ follows from equilibrium, as the connection cannot transfer more shear than the weaker material, timber in compression or steel in tension, can resist. The η tolerance of $\pm 15\%$ accounts for the discrete nature of bolt spacing under the EC5 spacing rules. Without this tolerance, near-optimal designs would be rejected due to fastener discretisation rather than an actual structural deficiency. Finally, creep and long-term deformation are excluded so that the SLS check reflects the short-term structural comparison only, a simplification acknowledged as a limitation of the analytical model.

3.3.3 Assumptions Made for STC-2

Unlike for STC-1, where the rolled steel section sets the governing width and depth, for STC-2 the glulam section sets them. The following assumptions are enforced directly in the optimisation code for STC-2, in a similar way to STC-1:

- The steel plate width cannot exceed the glulam width: $b_s \leq b_t$
- The steel plate depth is bounded by the glulam section depth: $h_s \leq h_t$
- The total composite depth is limited to:

$$h_s + h_t \leq h_{\text{ref,glulam}} \tag{3.31}$$

- The full shear connection longitudinal force is governed by the weaker material:

$$V_{l,\text{full}} = \min(b_t \cdot h_t \cdot f_{cd}, \quad b_s \cdot h_s \cdot f_{yd}) \tag{3.32}$$

These assumptions mirror the STC-1 constraints but with the governing material reversed. The width and depth limits ($b_s \leq b_t$ and $h_s \leq h_t$) keep the steel plate fully embedded within the glulam footprint, preventing an exposed or overhanging plate that would complicate fastening and leave the connection unevenly loaded. The total depth limit ($h_s + h_t \leq h_{\text{ref,glulam}}$) keeps STC-2 comparable in size to the glulam reference, for the same reason as in STC-1: an oversized hybrid section would distort the structural and environmental comparison. The expression for $V_{l,\text{full}}$ again follows from equilibrium, but with the governing area now defined by the steel plate rather than the full steel section, since the plate is the load-bearing steel element in this configuration.

3.3.4 LCA System Boundary

The life cycle assessment implemented in this study covers modules A1–A3 (raw material extraction and manufacturing), C3 (waste processing), and D (reuse and recovery potential) per section 2.6, providing the total embodied carbon (E) used in the Marginal Abatement Cost (MAC) evaluation. Transport (A4–A5), the use phase (B1–B7), and demolition (C1–C2) are excluded. This system boundary is selected to cover the carbon storage of timber and the reuse advantages of steel, which gives the study a fair environmental comparison.

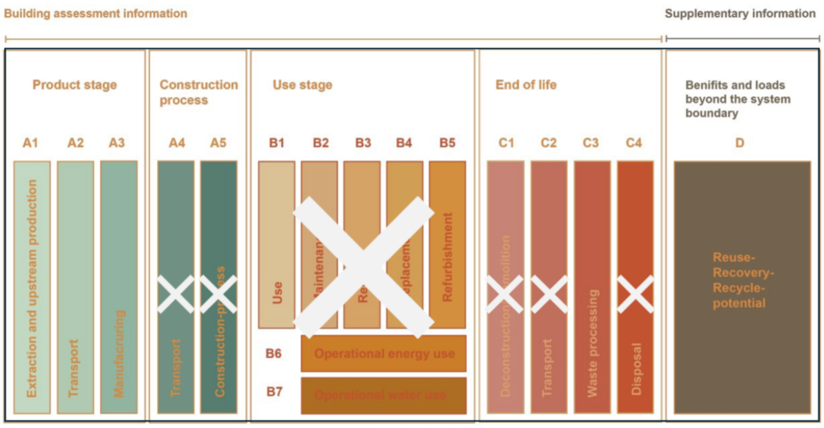

Figure 3.6: Covered modules of LCA, source: Moelven

Environmental product declarations (EPDs) were obtained directly from two manufacturers through personal communication: Moelven for the GL30c glulam timber and Stålgrossisten AB for the HEA steel sections. Each EPD reports emissions across multiple environmental impact categories, including global warming potential, eutrophication, acidification, and resource depletion. The EPDs served as the primary data source for the life cycle inventory, ensuring manufacturer-specific and product-specific emission factors were applied rather than generic database values.

This study uses only the Global Warming Potential (GWP) from each EPD, expressed in kgCO_2eq. This is the most widely used indicator in structural engineering practice and is the parameter that the Swedish National Board of Housing (Boverket) demands in the climate declaration of new buildings [56]. However, focusing on GWP alone means that trade-offs in other impact categories are not captured. A design optimised for minimum GWP might, for example, use more timber, which reduces fossil carbon emissions but may increase eutrophication due to fertiliser use in forestry. Conversely, selecting a smaller steel section reduces steel production emissions but may not improve performance in categories such as resource depletion. This is a known limitation of single-indicator optimisation and the results should be interpreted accordingly [55].

The emission factors used in this study are derived from the GWP values reported in each EPD. For steel, the XCarb EPD from Stålgrossisten declares emissions per tonne of finished section, giving:

$$z_s = \frac{333 + 1.6 + 214}{1000} = 0.549 \quad \text{kgCO}_2\text{eq/kg} \tag{3.33}$$

across modules A1-A3, C3 and D respectively. For glulam, the Moelven EPD reports GWP-total values of $-674\,\text{kgCO}_2\text{eq/m}^3$ (A1-A3), $+751\,\text{kgCO}_2\text{eq/m}^3$ (C3) and $+102\,\text{kgCO}_2\text{eq/m}^3$ (D), giving a net of $179\,\text{kgCO}_2\text{eq/m}^3$. Divided by the characteristic density $\rho_t = 390\,\text{kg/m}^3$ this yields:

$$z_t = \frac{179}{390} = 0.459 \quad \text{kgCO}_2\text{eq/kg} \tag{3.34}$$

The large negative value in A1-A3 reflects biogenic carbon storage during tree growth, which is released again at end of life in C3, the two terms largely cancel, and the resulting emission factor reflects primarily the fossil fuel consumption during glulam processing.

3.3.5 LCC System Boundary

To evaluate the economic sustainability of the optimized structural configurations, a simplified Life Cycle Cost Analysis (LCCA) is conducted, providing the total cost (C) used in the Marginal Abatement Cost (MAC) evaluation. The general life cycle cost framework can be expressed as:

$$LCC = C_{\text{inv}} + C_{\text{MR\&R}} + C_{\text{user}} \tag{3.35}$$

where C_{inv} represents the initial investment cost, $C_{\text{MR\&R}}$ the maintenance, repair, and rehabilitation costs, and C_{user} indirect user-related costs.
In this study, the compared structural alternatives have identical building functions, geometries, and operational conditions. Therefore, user-related costs are assumed equal for all alternatives and are excluded from the analysis.
Furthermore, both the environmental and economic assessments are limited to a cradle-to-gate perspective (modules A1–A3), focusing only on the material production and procurement stage. Long-term maintenance and future rehabilitation costs are excluded due to uncertainties related to future material prices, technological development, discount rates, and end-of-life scenarios.
As a result, the comparison is simplified to the initial investment cost:

$$LCC_{\text{simplified}} = C_{\text{inv}} = \sum_i (V_i \cdot U_{c,i}) \tag{3.36}$$

where V_i represents the volume or mass of material component i, and $U_{c,i}$ is the corresponding unit cost.

The material costs used in the analysis were obtained through personal communication with the same manufacturers and suppliers that provided the Environmental Product Declarations (EPDs). Unit prices for the GL30c glulam were provided by Moelven, and unit prices for the structural steel HEA sections were provided by Stålgrossisten AB. This ensures consistency between the environmental and economic data sources, as both the carbon emission factors and the material costs reflect the same products from the same supply chain. For structural steel sections, the following approximate costs were provided by Stålgrossisten AB:

- HEA100–HEA240: 12 500 SEK/ton
- HEA260–HEA340: 12 900 SEK/ton
- HEA360–HEA500: 13 100 SEK/ton

For glulam timber, an approximate cost of 11 500 SEK/m^3 was provided by Moelven.

3.4 Numerical Analysis Phase

The last part of the methodological framework consists of a numerical analysis to simulate the structural behavior of the selected beam configurations at span lengths of 7 m and 12 m. The load cases remain the same as in the previous phases. The analysis begins with a linear elastic analysis, where the mid-span deflections and axial stresses are compared against analytical calculations to verify the accuracy of the model, including shear connectors. Subsequently, a linear buckling analysis is performed, followed by a nonlinear analysis to obtain the critical buckling load and failure modes of each beam. From the nonlinear analysis, the structural response under increasing load is captured, and the resulting displacements, slip, stresses, and strains are extracted and presented in tables and figures for further evaluation.

3.4.1 Abaqus FEA

Abaqus was once again used in order to perform the nonlinear analyses, building on the same finite element model described in Section 3.2.4. Abaqus was selected due to its ability to accurately model nonlinear material behavior and complex contact interactions, making it particularly well suited for the simulation of steel-timber composite beams beyond the linear elastic range. The geometry, mesh, and boundary conditions setup remain unchanged from Section 3.2.4, while the material properties, contact properties, and connector modeling ar extended to capture nonlinear behavior, as described in the following subsections.

3.4.1.1 Material Properties

In the nonlinear analysis, the steel behavior is assumed to be elastic-perfectly plastic, meaning that strain hardening beyond the yield point is neglected to simplify the modelling. The inelastic behavior of timber is represented using Hill's yield criterion to account for its orthotropic and complex nonlinear response. This is achieved by partitioning the glulam element at its neutral axis, where the compression side is assigned the compressive strength with a ductile material failure, and the tension side the tensile strength with brittle material failure, in the longitudinal direction. The neutral axis position is determined based on full composite action, since the resulting partial.interaction stress distribution is not known prior to the analysis. The nonlinear material properties and corresponding failure behavior for each material are summarized in Table 3.3. The R-values from Hill's yield criterion, representing the strength ratios in the longitudinal, tangential, and radial directions, are assigned according to the values presented in Table 3.4.

Table 3.3: Nonlinear material properties for steel and timber.

Material	**Stress [MPa]**	**Strain [-]**
Steel S355	355	0
	355	0.2
Timber GL30c (Compression)	24.5	0
	24.5	0.2
Timber GL30c (Tension)	19.5	0
	0.001	0.0001

Table 3.4: Inputs for Hill's yield criterion.

Hill's yield criterion					
R_{11}	R_{22}	R_{33}	R_{12}	R_{13}	R_{23}
1	0.104	0.104	0.146	0.146	0.042

3.4.1.2 Model Simulation

An initial linear elastic analysis is carried out using the *Static, General* procedure in Abaqus to assess the elastic response of the beams. Since a nonlinear analysis is subsequently performed to investigate the nonlinear response and overall structural integrity of the composite system, an initial linear buckling analysis is first carried out using the *Linear Perturbation, Buckle* procedure. This analysis provides the eigenvalue corresponding to the critical buckling load of the system. Once the buckling behavior has been identified, the nonlinear response is analyzed using the *Static, Riks* procedure together with nonlinear material properties, as relative slip occurs at the interface between the connected elements.

4

Results

This chapter presents the results obtained to address the three research questions formulated in the previous chapters. It begins by evaluating the validity and accuracy of the Newmark partial interaction theory for the composite beam configurations through comparisons with numerical models developed in Abaqus. Since the reference beams are designed in accordance with dedicated Eurocode provisions, no validation is required for these configurations. The chapter then presents the life cycle assessment and life cycle cost results for the beam configurations selected using the MAC ranking, where the configuration with the lowest cost per saved CO_2 emissions is selected, for all reference beams and composite beam systems with span lengths ranging from 3 m to 12 m, as defined in Section 3.3, enabling a direct comparison of CO_2 emissions and cost between the reference and composite systems. Finally, the structural behavior of the designed composite beams for 7 m and 12 m spans are presented, including load-displacement response, slip behavior, stress distribution, and failure modes.

4.1 Validation and Accuracy of Newmark Partial Interaction Theory

This section presents the validation results obtained using the finite element model described in Section 3.2.4, comparing the linear elastic analysis performed in Abaqus and analytical hand calculations using the Newmark's partial-interaction theory.

Figure 4.1 presents the comparison between the analytical predictions obtained using Newmark's partial-interaction theory and the numerical results from the linear elastic analysis in Abaqus for the STC-1 configuration. For deflection, the differences range from 0.3% to 6.9%, with three of the four cases remaining below 2%. For axial stress, the differences range from 4.6% to 9.2%. In both cases, the largest deviations are observed for the 12 m span configurations.

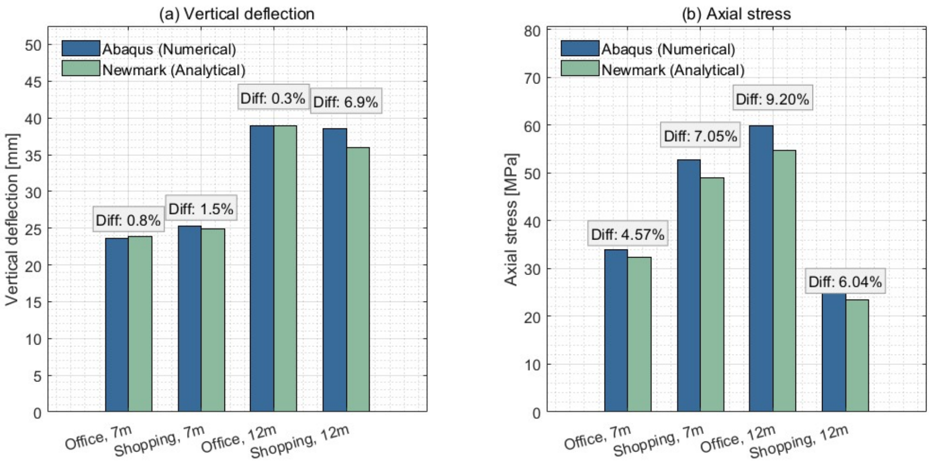

Figure 4.1: STC-1: Analytical vs numerical calculations for (a) vertical deflection and (b) axial stress

Figure 4.2 presents the analytical versus numerical comparison for the STC-2 configuration. For deflection, the differences range from 6.5% to 15.2%, with the largest deviation observed for the 7 m span under shopping mall loading. For axial stress, the differences range from 2.4% to 10.2%, with the 12 m shopping mall case exhibiting the largest deviation. In both cases, the largest deviations are observed for the shopping mall load cases. Overall, STC-2 shows larger discrepancies compared to STC-1.

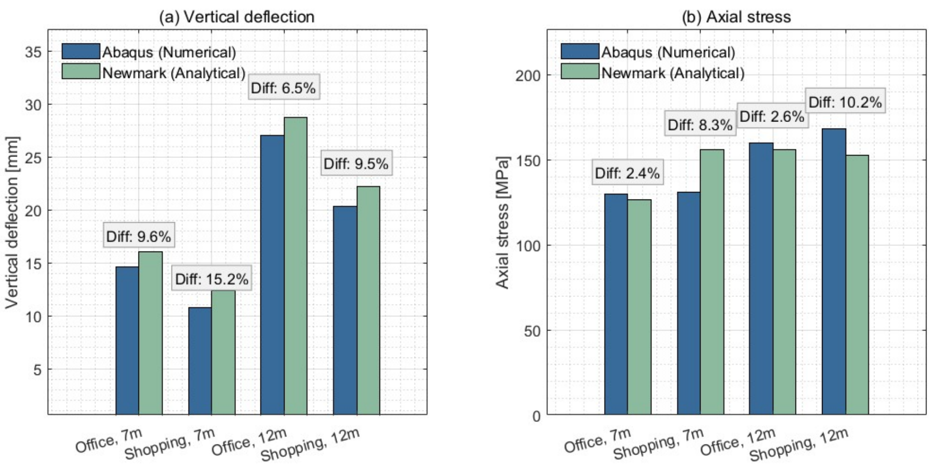

Figure 4.2: STC-2: Analytical vs numerical calculations for (a) vertical deflection and (b) axial stress

4.2 LCA for Varying Span Lengths

This section presents the life cycle assessment results for the reference beams and the composite beams STC-1 and STC-2 for span lengths between 3 m and 12 m, based on the beam configurations obtained from the optimization phase as described in Section 3.3.

Section 4.2.1 presents the absolute values of the total CO_2 emissions for each beam configuration at every span length, highlighting how the total carbon emissions of each system vary with increasing span. Section 4.2.2 presents the results in normalized form, illustrating the relative advantages or disadvantages of each composite system compared with its corresponding reference beam in percentage terms.

4.2.1 Absolute Values

Figure 4.3 shows similar trends for both load combinations. In both cases, the composite beams result in lower CO_2 emissions than the reference beams beyond a certain span length. For STC-1, this occurs at approximately 8 m for the office load and 6 m for the shopping mall load. For STC-2, the corresponding span lengths are approximately 10 m and 7 m. However, the reduction is less pronounced for STC-2, where the difference in CO_2 emissions remains relatively small across the investigated spans.

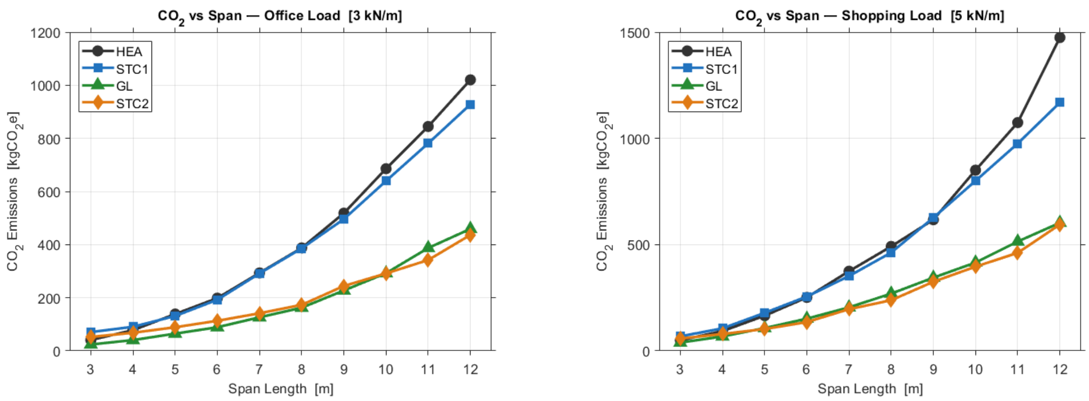

(a) (b)

Figure 4.3: Absolute CO_2 emissions for different span lengths: (a) office load and (b) shopping mall load.

4.2.2 Normalized Values

The normalized CO_2 emissions are presented relative to the corresponding reference beam, with the dashed line at 100% representing the reference level. STC-1 is normalized against the HEA reference and STC-2 against the glulam reference. Values below 100% indicate lower emissions than the reference, while values above 100% indicate higher emissions.

Figure 4.4a presents the normalized CO_2 emissions of STC-1 relative to the HEA reference beam for span lengths ranging from 3 m to 12 m under office and shopping load combinations. For short spans (3–4 m), STC-1 exhibits CO_2 emissions exceeding the HEA reference by up to 75%, indicating that the composite configuration is less environmentally efficient at shorter spans. As span length increases, emissions converge toward the reference value for both load cases. At longer spans (10–12 m), the shopping load case yields CO_2 reductions of approximately 20% relative to the HEA reference, while the office load case achieves a more modest reduction of approximately 10% at 12 m, remaining close to the reference value across most of the intermediate span range.

Figure 4.4b presents the normalized CO_2 emissions of STC-2 relative to the glulam reference beam for the same span range. For short spans (3–4 m), STC-2 exhibits CO_2 emissions exceeding the glulam reference by up to 65% under office loads and approximately 50% under shopping loads. Beyond approximately 5 m, the shopping load case falls consistently below the reference, with emissions ranging between approximately 88% and 100% of the glulam reference across the remaining span range, representing a mild but consistent reduction. The office load case decreases more gradually, approaching but not clearly crossing below the reference until 10–12 m. Neither load case achieves a substantial CO_2 reduction relative to glulam, with maximum reductions remaining below 15%.

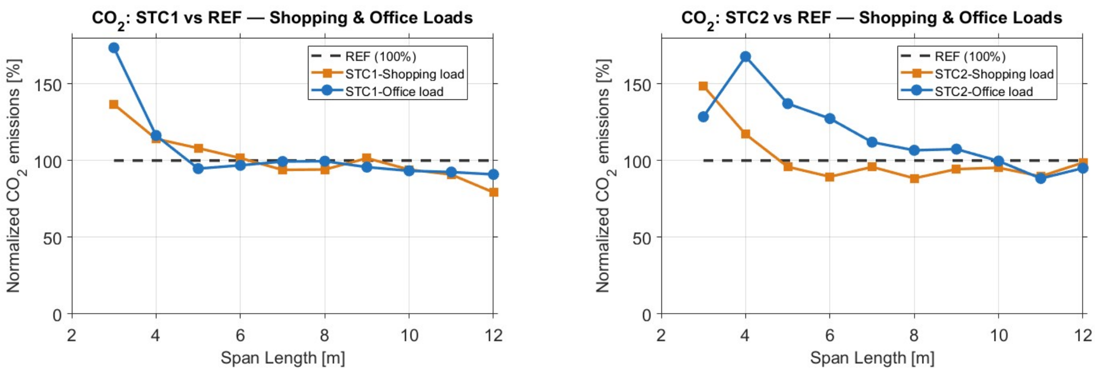

(a) **(b)**

Figure 4.4: Normalized CO_2 emissions for different span lengths: (a) office load and (b) shopping mall load.

4.3 LCC for Varying Span Lengths

This section presents the life cycle cost results for the reference beams and the composite beams STC-1 and STC-2 for span lengths between 3 m and 12 m, based on the beam configurations obtained from the optimization phase as described in Section 3.3.

Section 4.3.1 presents the absolute values of the total cost for each beam configuration at every span length, highlighting how the cost of each system vary with increasing span. Section 4.3.2 presents the results in normalized form, illustrating the relative advantages or disadvantages of each composite system compared with its corresponding reference beam in percentage terms.

4.3.1 Absolute Values

Figure 4.5 shows that the glulam reference beams and STC-1 are generally the most costly alternatives, particularly for longer span lengths, compared to the steel reference beams and STC-2 under office loading conditions. However, for the shopping mall load, the trend changes slightly, as STC-1 becomes a more cost-efficient alternative to its reference beam at lengths of approximately 12 m. Nevertheless, both load combinations indicate that pure glulam beams tend to result in higher overall costs, a trend that becomes more pronounced under higher loading conditions.

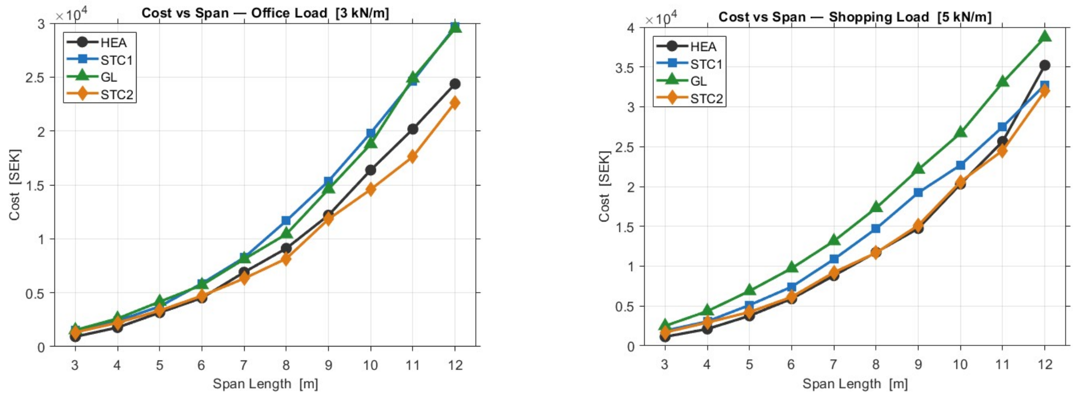

(a) **(b)**

Figure 4.5: Absolute cost for different span lengths: (a) office load and (b) shopping mall load

4.3.2 Normalized Values

The normalized costs are presented relative to the corresponding reference beam, with the dashed line at 100% representing the reference level. STC-1 is normalized against the HEA reference and STC-2 against the glulam reference. Values below 100% indicate a cost saving relative to the reference, while values above 100% indicate a cost premium.

Regarding cost, as shown in Figures 4.6a and 4.6b, STC-1 consistently exceeds the HEA reference across all studied spans. The cost premium decreases with increasing span length, from approximately 65% above the reference at 3 m to near parity at 12 m. Under shopping loads, the normalized cost falls below the HEA reference at a span of 12 m, indicating a cost advantage for STC-1 at longer spans under higher load intensities. The office load case, however, remains above the reference across all studied spans, suggesting that STC-1 does not achieve cost parity under lower load intensities within the studied span range.

The normalized cost for STC-2 is shown in Figure 4.6b, and exhibits a different trend compared to STC-1. The office load case remains consistently below the glulam reference across all studied spans, with cost reductions ranging from approximately 15% to 25%. Under shopping loads, the cost premium of approximately

20% observed at 3 m decreases with increasing span length, falling below the glulam reference beyond approximately 8 m and reaching a maximum cost reduction of approximately 30% at 11 m.

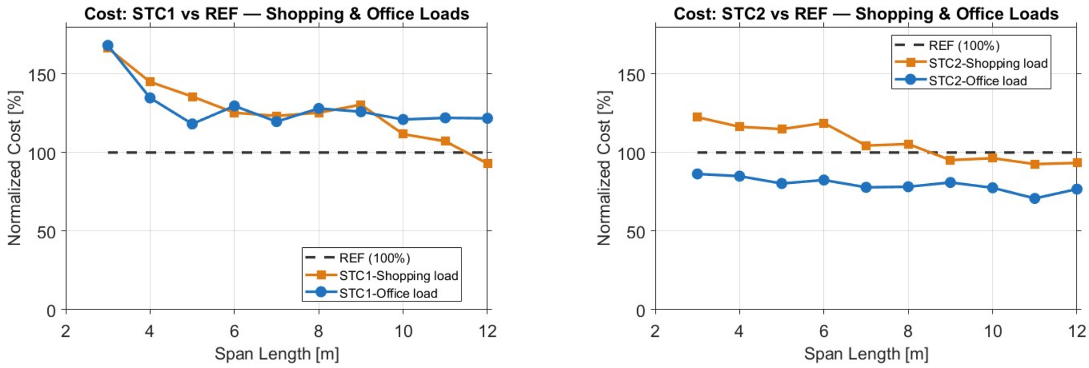

(a) **(b)**

Figure 4.6: Normalized cost for different span lengths: (a) office load and (b) shopping mall load.

4.4 Load-Displacement

Section 4.1 validated the analytical Newmark partial-interaction model against Abaqus for the optimized STC-1 and STC-2 configurations at 7 m and 12 m spans. Section 4.4 uses these same two validated geometries, not the full 3–12 m span range considered in the LCA and LCC optimization of Sections 4.2 and 4.3. A nonlinear analysis of these geometries is necessary because the analytical model assumes linear-elastic behavior and cannot capture steel yielding, timber crushing, or post-peak ductility, effects that govern the ultimate limit state. The objective of Section 4.4, and of the nonlinear investigation carried through Sections 4.4–4.7, is to determine whether the optimized sections are over- or under-designed once these effects are accounted for, and to characterize their load-displacement response, ductility, and failure mode. This also allows the failure mechanisms of the STC systems to be understood and compared against the reference beams, providing insight into how the combination of steel and timber alters the structural behavior relative to a single-material section.

The load-displacement curves presented in this section are obtained from the numerical analysis performed in Abaqus, as described in Section 3.4. The reference beams and composite beam configurations STC-1 and STC-2 are analyzed at span lengths of 7 m and 12 m, under both office and shopping mall load cases. All beam configurations are plotted within the same figure to facilitate direct comparison. The results illustrate how the ductility and maximum load capacity differ between the reference beams and the composite systems for the same span length and load case.

4.4.1 7m Span: Office Load

Figure 4.7 shows the load-displacement curves for the beam configurations at 7 m span under office loading (3 kN/m), comparing STC-1 (HEA240+GL150) and STC-2 (GL115×585+S10) against their respective reference beams, HEA280 and GL140×720. The HEA280 reference reached the highest peak load of approximately 450 kN at 70 mm displacement, followed by a ductile post-peak plateau that terminated at around 135 mm. STC-1 peaked at a lower load of approximately 390 kN, around 89% of the steel reference's capacity, but continued deforming well beyond the point of steel failure, still carrying load past 200 mm displacement. This indicates that the glulam component does not only contribute stiffness to STC-1, but extends its ductile range beyond that of the bare steel section. In contrast, the GL140x720 reference beam reached a maximum load of only 285 kN at 25 mm displacement before a brittle termination.

STC-2 reached a comparable peak load to STC-1, at approximately 390 kN, a 37% increase over the glulam reference, and failed at approximately 85 mm displacement, roughly 3.5 times the displacement capacity of the glulam alone, though still considerably less ductile than STC-1. The comparison shows that both STC configurations substantially recover the peak load capacity of their stiffer reference beam while adding ductility relative to their weaker constituent, with STC-1 retaining the greater share of that ductility due to the steel section's own post-yield behavior.

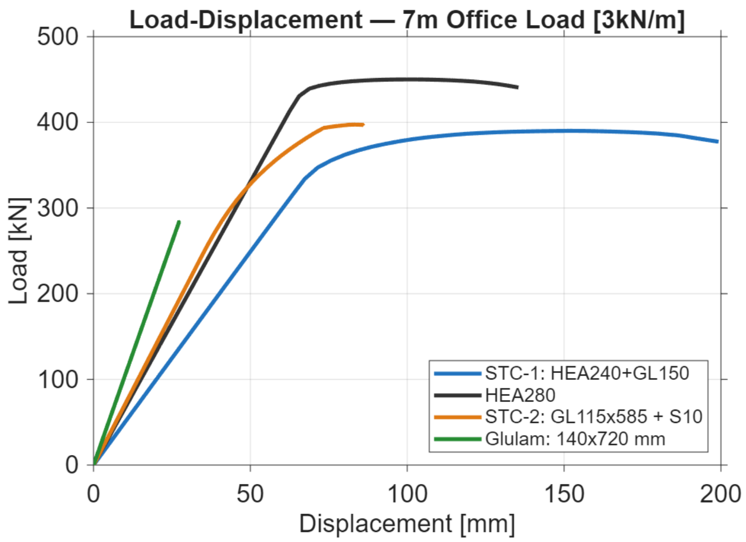

Figure 4.7: Load-displacement response for 7 m span under office load.

4.4.2 12m Span: Office Load

Figure 4.8 shows the load-displacement curves for the beam configurations at 12 m span under office loading (3 kN/m), comparing STC-1 (HEA340+GL320) and STC-2 (GL165×900+S10) against their respective reference beams, HEA500 and GL190×1125. The HEA500 reference reached the highest peak load of approximately 930 kN at around 110 mm displacement, maintaining a stable plateau out to 300 mm. STC-1 peaked at approximately 720 kN – around 77% of the steel reference's capacity – at 150 mm displacement, followed by a gradual post-peak softening back to approximately 680 kN by 300 mm. Unlike the 7 m span case, STC-1 does not outlast its steel reference here: both HEA500 and STC-1 remain responsive over a comparable displacement range, indicating that the glulam's contribution to ductility is less pronounced at this span. In contrast, the GL190x1125 reference beam reached a maximum load of approximately 535 kN at around 50 mm displacement before a brittle termination.

STC-2 reached a peak load of approximately 660 kN at 110 mm displacement, a 23% increase over the glulam reference, and continued to approximately 120 mm before failure, roughly 2.4 times the displacement capacity of the glulam alone, though with a more abrupt post-peak response than STC-1, consistent with its timber-governed failure mode. As at 7 m, both STC configurations substantially recover the peak capacity of their stiffer reference beam while adding ductility relative to their weaker constituent, though the relative gain in ductile displacement from the steel component is smaller at 12 m than at 7 m.

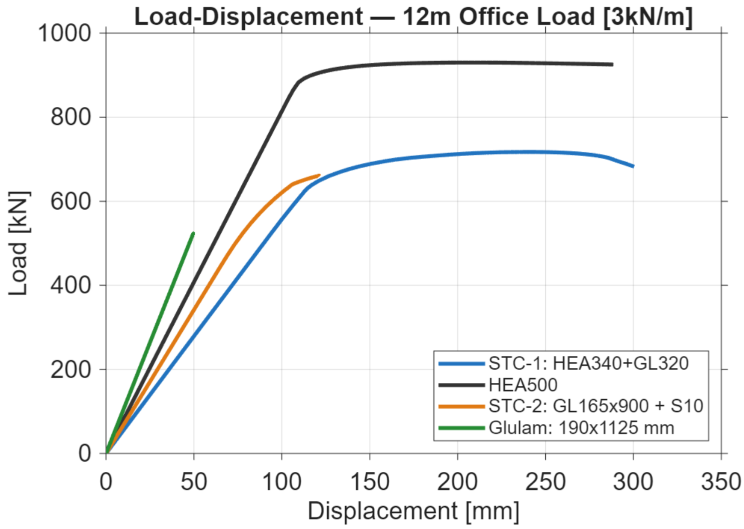

Figure 4.8: Load-displacement response for 7 m span under office load.

4.4.3 7m Span: Shopping Mall Load

Figure 4.9 shows the load-displacement curves for the beam configurations at 7 m span under shopping mall loading (5 kN/m), comparing STC-1 (HEA260+GL220) and STC-2 (GL140×720+S10) against their respective reference beams, HEA320 and GL165×810. The HEA320 reference reached the highest peak load of approximately 680 kN at around 60 mm displacement, maintaining a stable ductile plateau out to 215 mm. STC-1 peaked at approximately 550 kN, around 81% of the steel reference's capacity, at 100 mm displacement, exhibiting a gradual, ductile post-peak response inherited from the steel section, though ending slightly earlier than HEA320 at approximately 180 mm. This is the reverse of the 7 m office load case, where STC-1 outlasted its steel reference; under the heavier shopping mall load, STC-1 instead fails marginally before HEA320, suggesting that the relative ductility gain from the glulam is sensitive to load magnitude as well as span.

STC-2 reached a peak load of approximately 700 kN at 60 mm displacement, essentially matching the peak capacity of HEA320, but the two configurations diverge sharply beyond that point: while HEA320 sustains its load over a further 150 mm of displacement, STC-2 fails abruptly shortly after its peak, consistent with a timber-governed failure mode rather than the steel-governed ductility of HEA320. Compared to its own glulam reference (GL165x810, approximately 600 kN at 25 mm before brittle termination), STC-2 still represents an improvement, a 17% increase in peak load and roughly 2.4 times the displacement capacity, but it falls well short of the ductility offered by an equivalent steel section. As at 12 m, both STC configurations recover a large share of their stiffer reference beam's peak capacity, but the comparison here highlights that matching peak load is not the same as matching ductility: STC-2's steel plate raises capacity without meaningfully delaying failure, whereas STC-1's steel section delivers both.

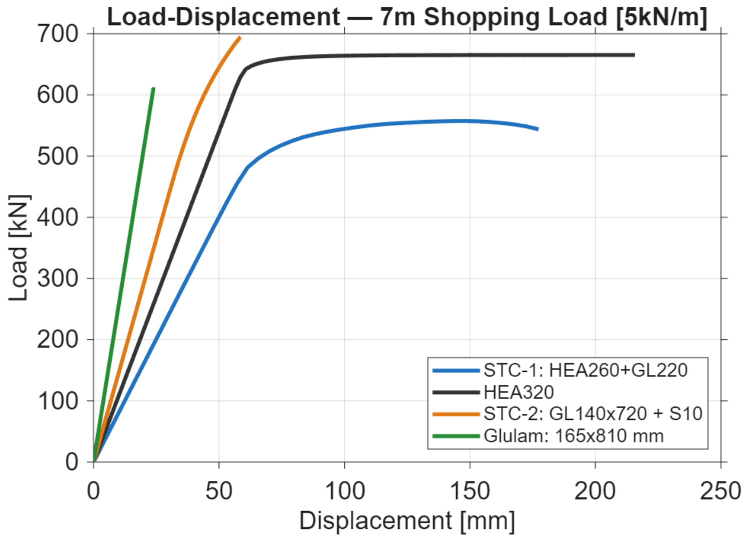

Figure 4.9: Load-displacement response for 7 m span under shopping mall load.

4.4.4 12m Span: Shopping Mall Load

Figure 4.10 shows the load-displacement curves for the beam configurations at 12 m span under shopping mall loading (5 kN/m), comparing STC-1 (HEA500+GL200) and STC-2 (GL190×1125+S10) against their respective reference beams, HEA800 and GL215×1305. STC-1 and its steel reference HEA800 reached a similar peak load of approximately 1100 kN, but their failure modes differ fundamentally. HEA800 failed abruptly at only 45 mm displacement, governed by lateral-torsional buckling rather than material yielding, a stability failure typical of slender, unrestrained steel sections at this span. STC-1 avoids this failure mode entirely: the glulam element braces the steel flange against lateral movement, suppressing buckling and allowing the section to instead exhibit a ductile post-peak plateau extending to approximately 345 mm, nearly eight times the displacement capacity of the bare steel section. This is the clearest evidence in the load-displacement results that the steel-timber combination does not simply add capacity, but can change which failure mechanism governs the design.

STC-2 reached a peak load of approximately 1200 kN at around 170 mm displacement, twice the ultimate load of its glulam reference beam, GL215x1305, which reached approximately 600 kN at a maximum displacement of 25 mm before brittle failure terminated the analysis, a nearly sevenfold increase in displacement capacity. Unlike STC-1, STC-2's improvement over its reference remains one of degree rather than of failure mechanism: both GL215x1305 and STC-2 fail in a timber-governed mode, with the steel plate delaying but not preventing that mode. Taken together, the 12 m shopping mall results show the most pronounced benefit of the STC systems observed so far, with STC-1's suppression of lateral-torsional buckling standing out as a qualitatively different, rather than merely incremental, improvement over its reference beam.

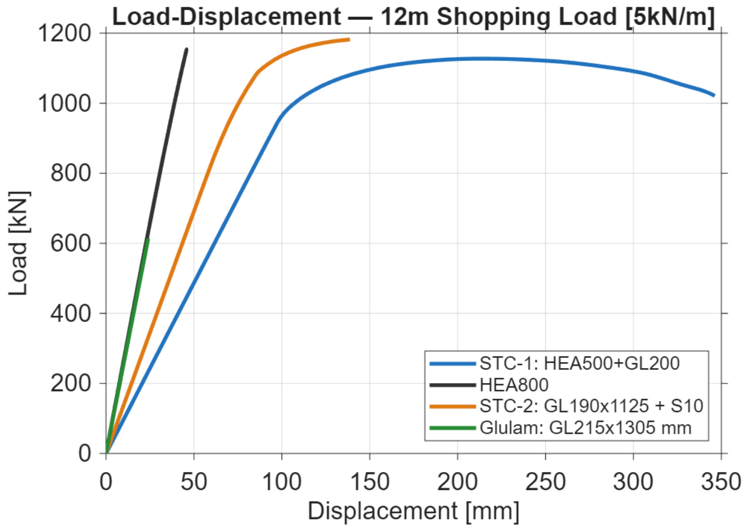

Figure 4.10: Load-displacement response for 12 m span under shopping mall load.

4.4.5 Effective Bending Stiffness

The load-displacement results presented in the preceding sections show that the glulam reference beam consistently exhibits the highest initial stiffness across all investigated cases. However, since the configurations differ in cross-sectional dimensions and degree of composite action, a direct comparison based on load-displacement response alone would not be fair, a stiffer beam may simply be larger rather than structurally more efficient. Therefore, the effective bending stiffness is calculated for each configuration using the gamma method in accordance with Eurocode 5 (EN 1995-1-1), providing a normalized basis for comparing the composite sections against the pure steel and pure glulam reference beams.

Figure 4.11 shows the effective bending stiffness for each configuration across all span lengths and load cases. In almost all cases, STC-2 achieves the highest stiffness, followed by the glulam reference beam, the steel reference beam, and STC-1 as the least stiff configuration. This ranking reveals a fundamental difference between the two composite configurations. STC-2 consistently achieves a higher effective stiffness than the glulam reference beam across all investigated cases, while STC-1 results in a lower effective stiffness than the steel reference beam in all cases.

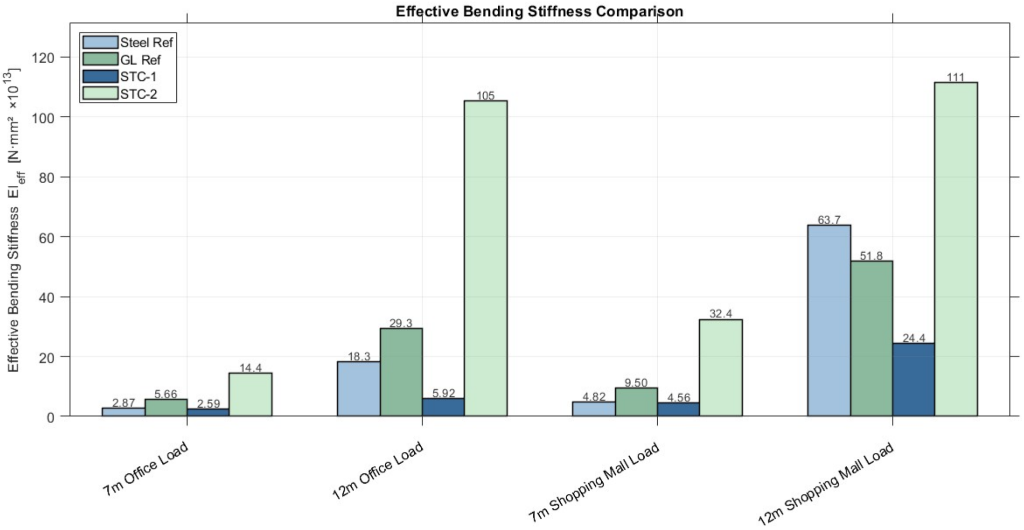

Figure 4.11: Effective bending stiffness for all configurations.

Table 4.1 presents the effective bending stiffness and the corresponding gamma coefficient for all configurations, expressed in N·mm^2. The gamma values indicate the degree of composite action achieved in each STC configuration, where a value approaching unity represents near-full composite action.

Table 4.1: Effective bending stiffness and gamma coefficient for all configurations.

Configuration	7m Office $\mathbf{EI_{eff}}$ / γ	12m Office $\mathbf{EI_{eff}}$ / γ	7m Shopping $\mathbf{EI_{eff}}$ / γ	12m Shopping $\mathbf{EI_{eff}}$ / γ
Steel Ref	2.87×10^{13} / —	1.83×10^{14} / —	4.82×10^{13} / —	6.37×10^{14} / —
GL Ref	5.66×10^{13} / —	2.93×10^{14} / —	9.50×10^{13} / —	5.18×10^{14} / —
STC-1	2.589×10^{13} / 0.568	5.92×10^{13} / 0.635	4.562×10^{13} / 0.509	2.441×10^{14} / 0.707
STC-2	1.441×10^{14} / 0.281	1.052×10^{15} / 0.304	3.24×10^{14} / 0.245	1.114×10^{15} / 0.260

4.5 Slip

The load-slip behavior at the steel-timber interface for STC-1 and STC-2 is presented in this section, obtained from the numerical analysis phase as described in Section 3.4. Since slip only occurs when two members interact through a connection, the reference beams are excluded from this analysis. The results cover span lengths of 7 m and 12 m under both office and shopping mall load cases. The load-slip response reflects the degree of composite action and connection ductility, and both configurations are plotted within the same figure to facilitate direct comparison. The initial stiffness differs between the two systems due to their different connector types and numbers, as STC-1 uses 12 mm bolts while STC-2 uses 8 mm screws.

4.5.1 7m and 12m Span: Office Load

Figure 4.12 presents the load-slip behavior of both composite beams at 7 m and 12 m span under office loading. At 7 m, STC-2 exhibits a higher initial stiffness than STC-1, evidenced by the steeper slope of its load-slip curve at low slip values. Both systems reach approximately the same ultimate load of nearly 400 kN, but STC-1 demonstrates a larger slip prior to failure, approximately 3.5 mm, compared to approximately 2.7 mm for STC-2. The same stiffness trend holds at 12 m: STC-2 again shows the steeper initial slope and here also reaches a higher ultimate load, approximately 650 kN compared to approximately 600 kN for STC-1. STC-1 nonetheless retains its ductility advantage, with a slip at failure of approximately 3.9 mm against approximately 2.6 mm for STC-2. The consistent stiffness and ductility difference across both spans indicates that this behaviour is governed primarily by the connection detail itself, STC-1's 12 mm bolts versus STC-2's 8 mm screws rather than by span, though the gap in ultimate load capacity between the two systems widens somewhat at the longer span.

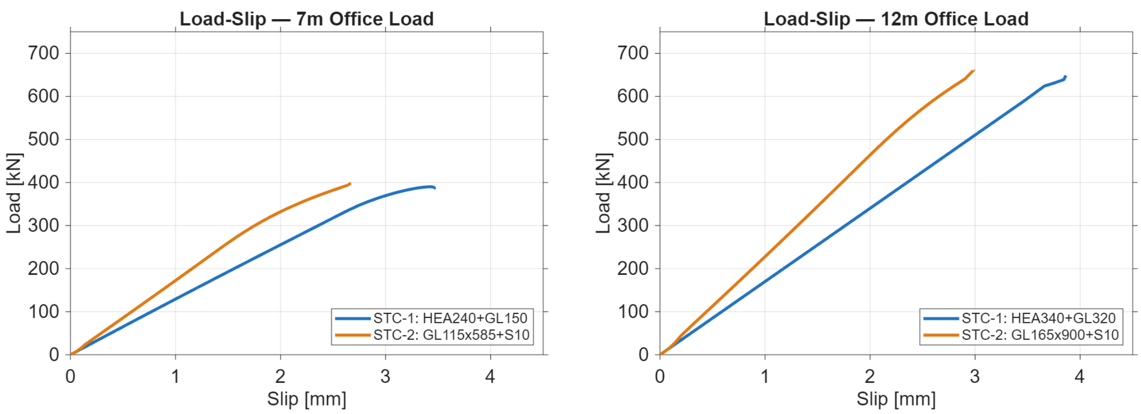

(a) 7 m span **(b)** 12 m span

Figure 4.12: Load-slip response of STC-1 and STC-2 under office load, at (a) 7 m and (b) 12 m span.

4.5.2 7m and 12m Span: Shopping Mall Load

Figure 4.13 presents the load-slip behavior of both composite beams at 7 m and 12 m span under shopping mall loading. At 7 m, the response follows the same stiffness trend observed under office loading, though the disparity between the two configurations is more pronounced: STC-2 reaches an ultimate load of approximately 700 kN at a slip of 2.3 mm, while STC-1 reaches approximately 550 kN at 3.8 mm, reflecting a greater gap in both strength and ductility than in the office load case. At 12 m, STC-2 again shows the higher initial stiffness, and here the two configurations reach a similar ultimate load of approximately 1200 kN; however, STC-1 still demonstrates greater ductility, with a slip at failure of approximately 4.2 mm compared to approximately 2.5 mm for STC-2. The connectors in both configurations, 12 mm bolts in STC-1 and 8 mm screws in STC-2, are modeled in Abaqus as Cartesian point-based fasteners with linear-elastic stiffness, assigned from the K_{ser} and K_u slip modulus values per Eurocode 5. As no connection failure criterion is defined, the post-peak response in both configurations is governed entirely by material failure in the timber or steel, rather than by the connectors themselves.

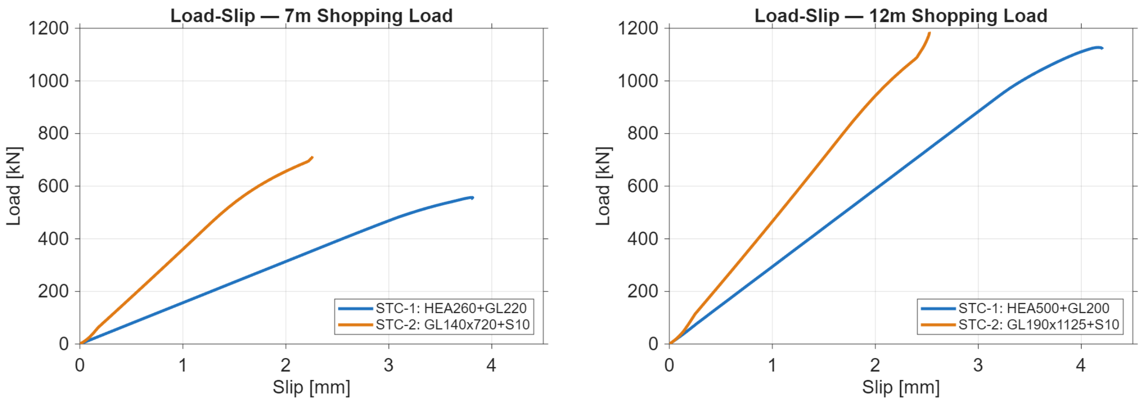

(a) 7 m span **(b)** 12 m span

Figure 4.13: Load-slip response of STC-1 and STC-2 under shopping mall load, at (a) 7 m and (b) 12 m span.

4.6 Stress Distribution

This section presents the stress distribution along the beam depth at mid-span for the composite beam configurations STC-1 and STC-2, obtained from the numerical analysis phase as described in Section 3.4, and evaluated at span lengths of 7 m and 12 m. The reference beams are excluded from this analysis, as homogeneous single-material beams exhibit a linear stress distribution. The stress distributions are evaluated at three loading stages: pre-yield, post-yield, and peak load. The results indicate that all composite beams exhibit a stress discontinuity at the interface between the two materials, and that this discontinuity becomes more pronounced with increasing load.

4.6.1 Stress Distribution of STC-1

The stress distribution of STC-1 follows a consistent pattern across all investigated span lengths and load cases. Figure 4.14 is presented as a representative example for the 7 m span under office loading. At the pre-yield stage, the section behaves elastically, with a clear stress discontinuity at the interface. As the load increases, yielding initiates in the steel, and the glulam approaches its compressive strength. At peak load, the steel has fully yielded, with a trapezoidal stress distribution indicating the formation of a of a fully developed plastic zone, while the compressive stress in the glulam remains essentially unchanged, reflecting compressive crushing. The remaining stress distributions are presented in Appendix C for completeness, and the corresponding stress values across all span lengths and load cases are summarized in Section 4.6.3 below.

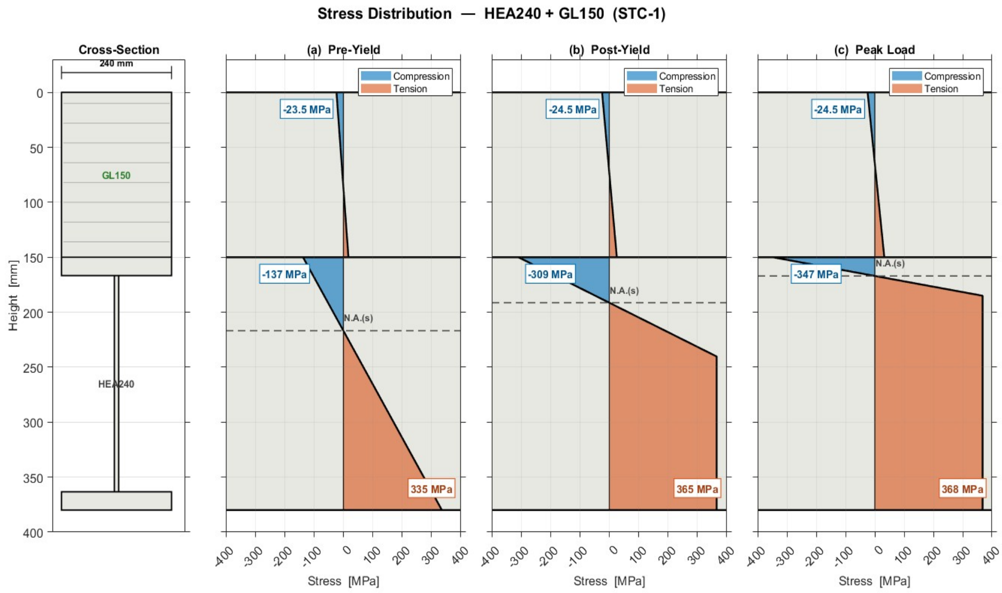

Figure 4.14: Stress distribution of STC-1 at 7 m span under office load.

4.6.2 Stress Distribution of STC-2

The stress distribution of STC-2 also follows a consistent pattern across all investigated span lengths and load cases. Figure 4.15 is presented as a representative example for the 7 m span under office loading. At the pre-yield stage, the section behaves elastically, with a distinct stress discontinuity at the interface. As the load increases, the glulam reaches both its compressive and tensile strength limits, whereas the steel plate remains in the elastic range. At peak load, the compressive stress in the glulam stabilizes at its compressive capacity, while the tensile stress distribution in the timber remains linear, reflecting the brittle tensile behavior of glulam up to its tensile strength. By this stage, the steel plate has fully yielded, developing a fully plastic stress distribution. The remaining stress distributions are presented in Appendix C for completeness, and the corresponding stress values across all span lengths and load cases are summarized in Section 4.6.3 below.

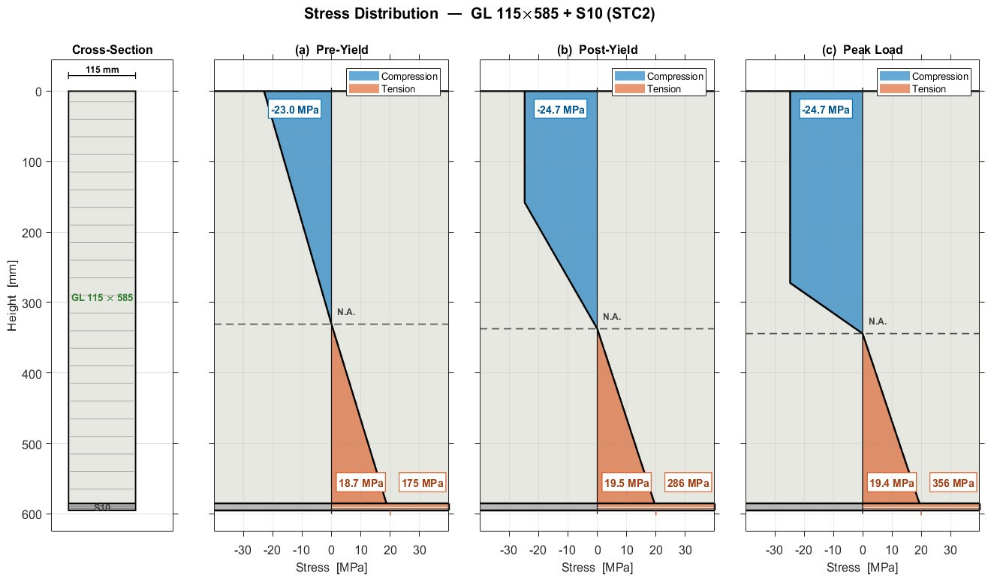

Figure 4.15: Stress distribution of STC-2 at 7 m span under office load.

4.6.3 Stress Distribution Summary

This section evaluates the degree of material utilization in the two materials immediately prior to yielding for each STC configuration. Figure 4.16 presents the material utilization of STC-1, where both the timber and steel are utilized to a high extent across all span lengths and load combinations. The timber achieves a minimum utilization ratio of 88.2%, while the steel reaches a minimum utilization ratio of 83.1%. In average, the timber and steel attain utilization ratios of approximately 95.1% and 93.7%, respectively, demonstrating efficient use of both materials throughout the investigated cases.

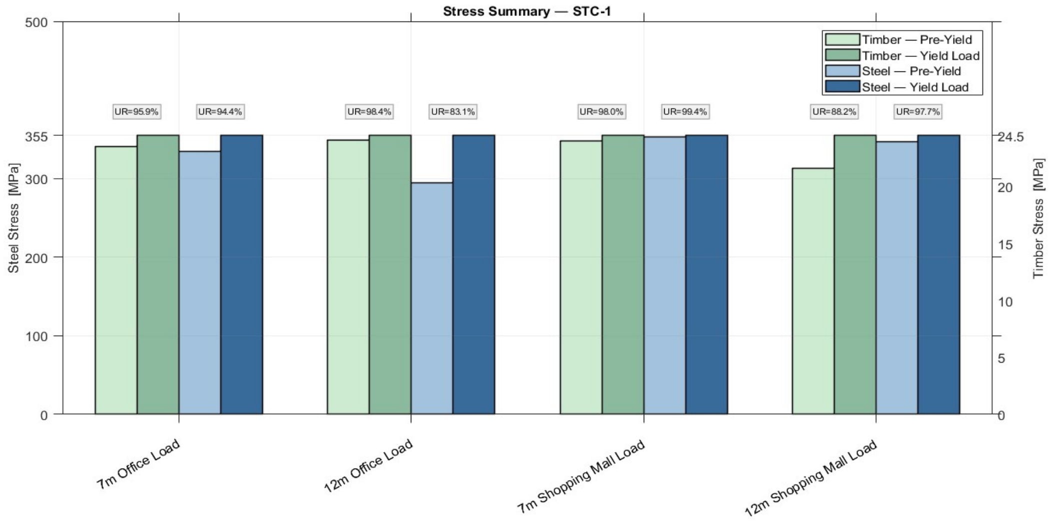

Figure 4.16: Summary of bending stress prior to yielding vs corresponding yield load of STC-1.

Figure 4.17 illustrates the material utilization of STC-2 for the different span lengths and load cases. In contrast to STC-1, the two materials are not utilized to a similar extent. The timber exhibits a minimum utilization ratio of 93.9% and an average utilization of 95.7% across all investigated cases, indicating that it is used efficiently. However, the steel shows considerably lower utilization, with a minimum value of 49.3% and an average utilization ratio of 56.2%. These results suggest that the full strength potential of both materials is not being exploited in the most efficient manner.

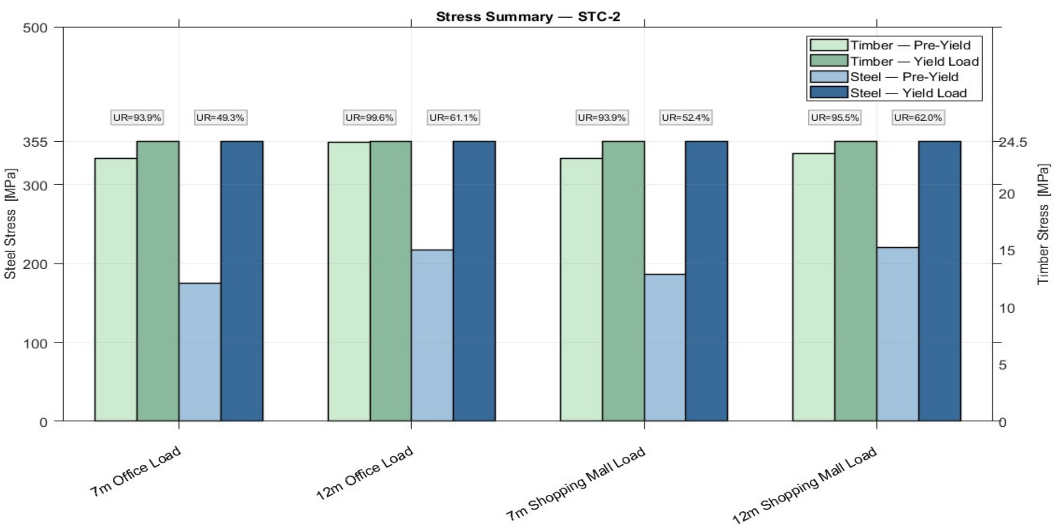

Figure 4.17: Summary of bending stress prior to yielding vs corresponding yield load of STC-2.

4.7 Failure Modes

The stress distributions presented in Section 4.6 identified which material approaches its capacity first under increasing load. The failure modes presented in this section, obtained from the same nonlinear finite element analysis described in Section 3.4, illustrate how each configuration ultimately fails as a physical consequence of that stress state. The results are presented separately to allow direct comparison between the two configurations STC-1 and STC-2. Depending on the governing failure mechanism, the figures display either the equivalent plastic strain (PEEQ) or the logarithmic strain (LE), in order to better illustrate the location and extent to which each beam has reached its ultimate capacity.

4.7.1 Failure Modes of STC-1

The failure mode of STC-1 remains consistent across all investigated span lengths and load cases. Figure 4.18 illustrates this for the 7 m span under office loading. Consistent with the stress distributions presented in Section 4.6, failure is governed by compressive crushing of the glulam above the top flange, where compressive capacity is reached. This is followed by progressive yielding of the HEA steel section, resulting in a ductile post-peak response as observed in the load-displacement curve. The localized plastic strain concentration at mid-span, visible in the PEEQ contour, confirms that failure initiates and remains concentrated at the point of maximum bending moment. The failure modes of the remaining STC-1 configurations are presented in Appendix C.

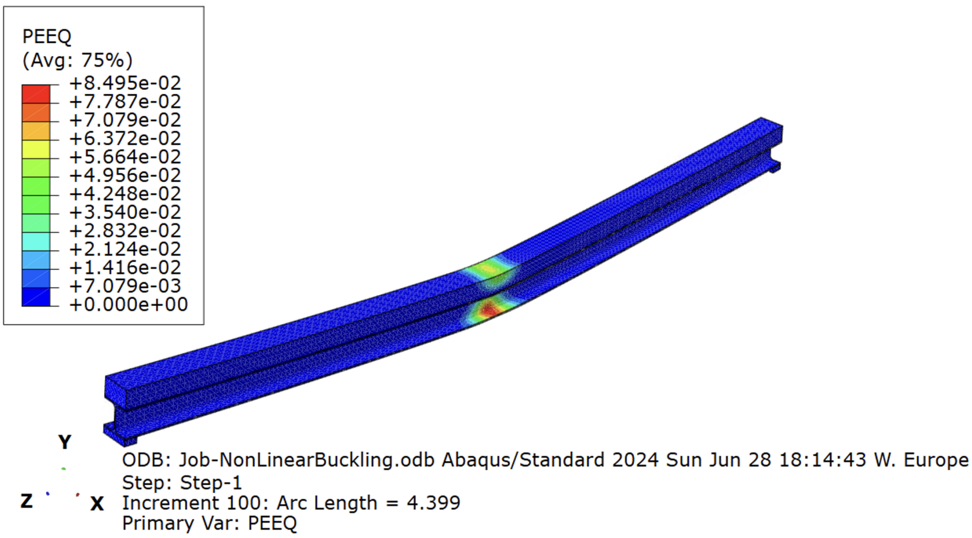

Figure 4.18: Failure mode of STC-1 at 7 m span under office load.

4.7.2 Failure Modes of STC-2

The failure mode of STC-2 is largely consistent across the investigated configurations. Figure 4.19 is presented as a representative example for the 7 m span under office loading. Failure is governed by brittle tensile rupture of the glulam at the bottom face, where the tensile capacity is reached. The steel plate, operating significantly below its yield stress at failure initiation, contributes stiffness to the system but does not prevent the timber-governed failure, resulting in the abrupt post-peak response observed in the load-displacement curve. This fundamental difference in failure character between STC-1 and STC-2 reflects the contrasting roles of the steel component in each configuration, as the primary load-carrying element in STC-1, and as a stiffness contributor in STC-2 where timber governs both strength and failure mode.

An exception to this pattern is observed at the 12 m span under office loading, shown in Figure 4.20. Here, failure is characterized by longitudinal splitting of the glulam along its mid-height, rather than tensile rupture at the bottom face. This is reflected in the LE Max. Principal contour, which shows a broad horizontal strain concentration running along the grain direction at mid-height, indicative of timber splitting. This failure mode is attributed to the longer span, where the distribution of shear stresses along the beam length becomes more critical relative to the bending-induced tensile stresses at the bottom face. The failure modes for the remaining STC-2 configurations are presented in Appendix C.

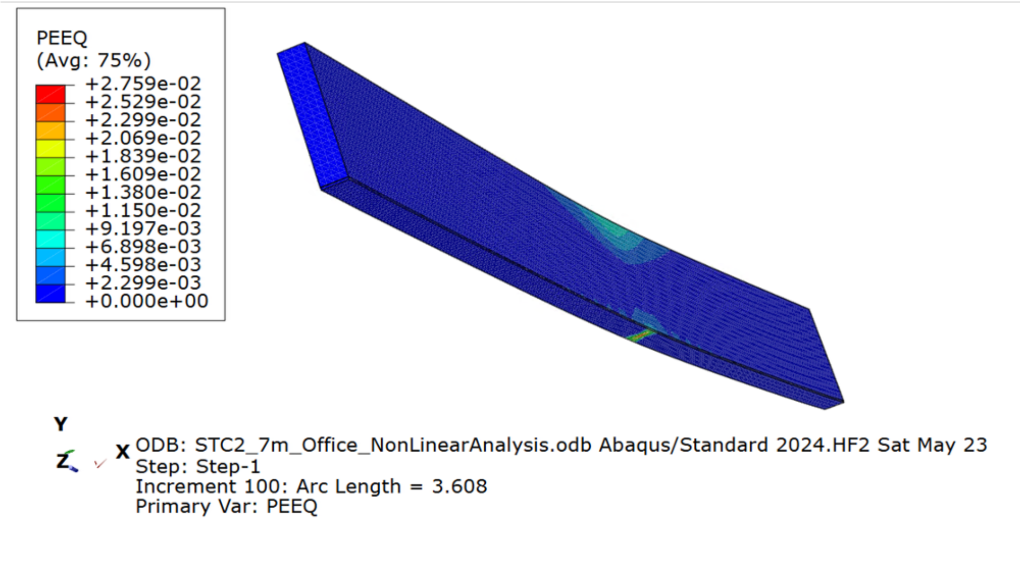

Figure 4.19: Failure mode of STC-2 at 7 m span under office load.

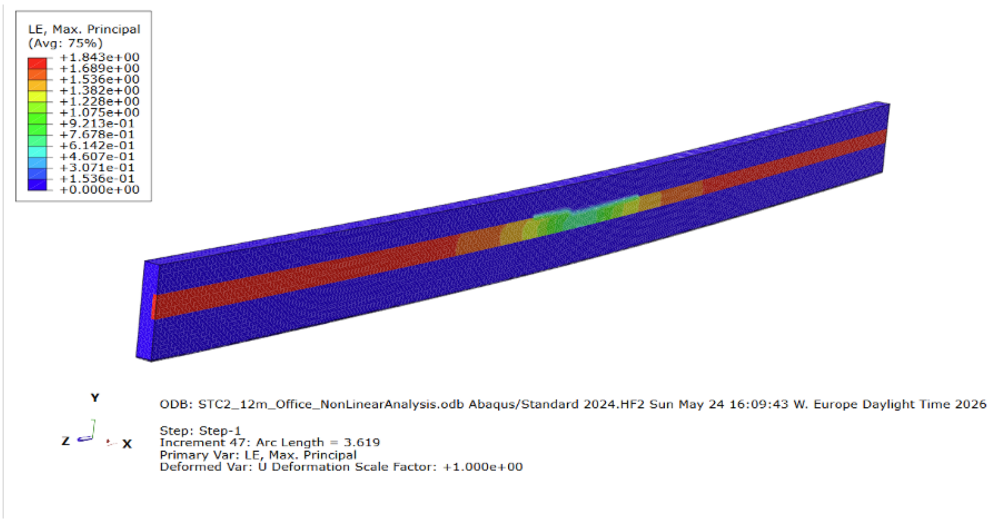

Figure 4.20: Failure mode of STC-2 at 12 m span under office load.

5

Discussion

5.1 Summary of Findings

This study evaluated two steel–timber composite systems: STC-1, consisting of an HEA beam with a glulam member on top, and STC-2, consisting of a glulam beam reinforced with a steel plate on its bottom. The steel and timber components were connected using shear connectors, with bolts used in STC-1 and screws used in STC-2.

The study developed an analytical model based on Newmark's linear-elastic composite beam theory. Since the theory was originally formulated for steel–concrete composite beams, its applicability to steel–timber composite (STC) beams was verified due to the lack of dedicated Eurocode provisions.

Validation was performed using finite element simulations in Abaqus on STC beams with spans of 7 m and 12 m under office and shopping mall loading conditions. Predicted deflections and axial stresses were compared with FE results. Overall, good agreement was observed, although notable deviations occurred for the STC-2 configuration under the 7 m office load case, indicating that while the theory is generally reliable, its accuracy may be limited by connection complexity.

The design step in the genetic algorithm included STC-1 and STC-2 configurations for spans ranging from 3 m to 12 m, and their performance was compared to reference HEA steel and glulam beams to evaluate environmental and economic benefits. These benefits were found to emerge only beyond certain threshold spans: In general STC-1 reduced CO_2 emissions by up to 20% compared to steel beyond approximately 5 m, while STC-2 reduced costs by up to 30% compared to glulam for spans above approximately 9 m, without a significant increase in CO_2 emissions.

A non-linear FEM analysis was performed to capture the realistic behavior of the structural systems. The results showed that both STC configurations with spans of 7 m and 12 m satisfied the design load requirements for office and shopping mall load cases. Compared to the reference glulam beam, STC-2 exhibited a more ductile failure mode, thereby reducing the brittle failure behavior associated with glulam. This indicates that even though the steel plate does not reach its yield strength before system yielding, it imparts slight ductile behavior to STC-2 system. STC-1 showed a slightly lower load-carrying capacity than the reference HEA beam, but exhibited a similar response up to failure.

The stress distribution revealed a clear contrast between the two systems. In STC-1, both the HEA steel section and the glulam were highly utilized, reaching average utilization ratios of 93.7% and 95.1%, respectively, indicating a well-balanced composite section in which both materials contribute comparably to the bending resistance. In STC-2, however, the timber remained efficiently utilized (95.7% on average) while the steel plate was substantially under-utilized, averaging only 56.2%. This reflects the fact that STC-2 is derived from a timber beam that is already deflection-governed: failure consistently initiates through tensile rupture of the glulam before the steel plate approaches yield, and the steel plate's cross-sectional area is governed by the serviceability deflection criterion rather than by strength requirements. As a result, the steel plate contributes primarily to stiffness rather than load-carrying capacity, and may be over-designed from a pure strength perspective. This suggests that thinner or wider plate geometries, sized explicitly for stiffness demands rather than inheriting excess strength margin, could improve material efficiency in future designs.

This pattern also reflects a limitation of the optimization methodology: since the genetic algorithm selects designs based on deflection, strength, and the MAC ranking, it does not explicitly minimize excess steel capacity once stiffness requirements are met. As a result, the steel plate in STC-2 is not refined for strength efficiency, and its under-utilization is a by-product of the optimization setup rather than a targeted outcome. Another possible source of error lies in the numerical model itself: the neutral axis used to partition the glulam's material properties was determined assuming full composite action, since the actual partial-interaction stress distribution was not known beforehand. This simplification may introduce some inaccuracy in the predicted stress distribution, and therefore in the resulting steel utilization values.

5.2 Answers to Research Questions

5.2.1 Applicability of Newmark's Partial-Interaction Beam Theory

The differences in deflection and axial stress between Newmark's partial-interaction theory and the FEM results are presented in Figures 4.1 (STC-1) and 4.2 (STC-2). STC-1 showed generally good agreement in deflection, with differences ranging from 0.8% to 6.9%, where the 12 m shopping mall beam exhibited the largest deviation. The axial stress differences were higher, ranging from 4.6% to 9.2% for the STC-1 configurations.

STC-2, on the other hand, showed overall larger deviations compared to STC-1, with deflection differences ranging from 6.5% to 15.2% and axial stress differences from 2.4% to 10.2%. The maximum deviation of 15.2% in deflection for the 7 m shopping mall beam (Figure 4.2) is notably higher than the remaining results. The corresponding axial stress difference of 8.3% for the same case may indicate a potential modeling inconsistency in the FEM analysis that could not be conclusively identified. This configuration uses an inclined screw layout, necessitated by the large glulam depth. In the numerical model, this inclination was accounted for only through a reduced connector stiffness rather than by explicitly modeling the inclined geometry, which likely contributes to the elevated deviation.

These divergences are expected and can be attributed to the simplifying assumptions of Newmark's theory. As discussed in Section 2.4.4, the theory assumes uniformly distributed connection stiffness, one-dimensional Euler–Bernoulli behavior, and no transverse separation at the interface. In contrast, the Abaqus model captures discrete connector behavior, local stress concentrations near connection points, and three-dimensional stress states in the cross-section, none of which are represented in the analytical formulation.

Despite these differences, the overall agreement is considered acceptable for an emerging design method in the absence of standardized Eurocode provisions for steel–timber composite beams. Consequently, Newmark's partial-interaction theory is deemed sufficiently accurate for the purposes of this study, for all selected spans and load cases. This is comparable to similar transformed-section elastic models reported in the literature: Jurkiewiez et al. [15] found discrepancies of approximately 10% between analytical and experimental results using an equivalent homogenized-section approach. STC-1's deviations fall within this range for all cases, while the 15.2% deviation for STC-2 under the 7 m shopping load exceeds it, reinforcing that this case warrants closer scrutiny.

5.2.2 Comparative Environmental and Economic Performance for Varying Span

Comparing the two configurations directly, a trade-off emerges between environmental and economic performance. STC-1 offers a clearer environmental benefit, achieving CO_2 reductions of up to 20% relative to its steel reference at longer spans, but at a persistent cost premium that only approaches parity at 12 m. STC-2 shows the opposite pattern, consistent cost savings of up to 30% relative to its glulam reference, but limited and inconsistent CO_2 reduction, never exceeding 15%. This reflects their different roles. STC-1 is more suitable where reducing embodied carbon is the priority, typically replacing steel beams, while STC-2 is more suitable where cost efficiency is the priority, typically replacing glulam beams. However, it should be noted that STC-1 and STC-2 are evaluated against different reference beams, so the reported percentages are not directly comparable in absolute terms but rather indicate each configuration's relative performance against its respective baseline.

5.2.2.1 LCA Results

The LCA result in Figure 4.4 shows that below approximately 5m span, the LCA results show no clear trend for either configuration. In these short spans, normalized CO_2 emissions are significantly higher than the reference beams, due to the small material volumes. The variability is further influenced by the MAC selection method, which balances cost and CO_2 rather than minimizing emissions directly. As a result, different feasible designs with similar utilization ratios can have different CO_2 outcomes, and the selected solution does not necessarily represent the lowest-carbon option. Therefore, the preferred configuration depends on the chosen objective: prioritizing lower CO_2 may result in higher cost, while minimizing cost may lead to higher emissions.

For STC-1, a clear trend appears at spans beyond approximately 5 m, where CO_2 emissions decrease and fall below the steel reference. At 12 m, reductions reach about 20% for the shopping load case and about 8% for the office case. This shows that STC-1 becomes environmentally beneficial at longer spans, where the lower embodied carbon of glulam offsets the added material and connector emissions.

For STC-2, no consistent CO_2 reduction is observed compared to the glulam reference. The shopping load case performs better than the office case and stays below the reference beyond 5 m, but the maximum reduction remains under 15%. This limited benefit is explained by the high emissions of the steel plate and the relatively small net benefit from glulam due to end-of-life carbon release. As a result, STC-2 provides limited environmental advantage and is mainly more attractive from a cost perspective than a carbon reduction perspective.

5.2.2.2 LCC Results

Unlike the LCA results, the LCC analysis shown in Figure 4.6 reveals distinct patterns that differed between the two composite configurations.

For STC-2, the office load case is consistently less expensive than the reference glulam beam across all studied spans, with cost reductions ranging from approximately 15% to 30%. Under shopping loads, STC-2 carries a cost premium of approximately 20% at short spans, which decreases steadily with increasing span length, falling below the reference beyond approximately 9 m and reaching a maximum cost reduction of approximately 30% at 11 m. This consistent cost advantage is explained by the nature of the configuration: the steel plate is a small-volume reinforcement that allows a significantly smaller glulam section to satisfy the deflection criterion compared to the pure glulam reference.

Since glulam costs approximately 29,500 SEK/ton equivalent, derived from the unit price of 11,500 SEK/m^3 and a characteristic density of 390 kg/m^3, compared to 13,500 SEK/ton for steel, timber is more than twice as expensive per unit mass. The material savings in timber volume outweigh the added steel plate cost, particularly under lower load intensities where the required glulam depth reduction is most pronounced relative to the plate size., which explains the cost variation over the span shown in Figure 4.6b.

For STC-1, the composite beam is more expensive than the HEA reference across almost all studied spans and load cases. The cost premium decreases with increasing span, from approximately 70% at 3 m to near parity at 12 m under shopping loads, where STC-1 slightly undercuts the reference. The office load case remains above the reference across the entire span range.

This persistent cost premium is mainly due to the higher unit cost of glulam compared to steel, combined with additional connector costs. As with the LCA results, the trend is also influenced by the MAC selection method, which balances cost and CO_2 rather than minimizing cost alone. As a result, the selected configuration is not necessarily the lowest-cost feasible option, and a cost-only optimization would likely yield more favorable LCC results for STC-1 at longer spans.

5.2.3 Structural Behavior (Load-Displacement,Stress, Slip, Failure Modes)

The load-displacement plots shown in Figures 4.7 - 4.10 shows that both STC configurations satisfied the design load requirements across both investigated span lengths and load combinations. STC-1 exhibited load-displacement responses closely following the steel reference beam up to yielding, after which a gradual and ductile post-peak response was observed.

STC-2 exhibited improved deformation capacity compared to the glulam reference beam across all investigated cases, with failure occurring at substantially larger displacements than the brittle termination observed in the pure glulam beams. However, the post-peak response of STC-2 remains relatively brittle compared to STC-1 and the HEA reference beams, which both exhibit gradual post-peak plateaus with significant residual load capacity.

This suggests that the steel plate in STC-2 delays and slightly softens the brittle wood failure rather than fundamentally transforming it into a ductile mechanism. STC-1, by contrast, inherits the ductile post-yield behavior of its HEA steel section, resulting in a response closely resembling that of the steel reference beam up to and beyond peak load. The clear hierarchy in ductility, HEA reference $\approx$ STC-1 $>$ STC-2 $>$ glulam reference, reflects the degree to which the steel component governs the post-peak response in each configuration.

This hierarchy is most pronounced for the 12 m span under shopping mall loading (Section 4.4.4), where STC-1 avoids the lateral-torsional buckling failure that terminates its steel reference beam at only 45 mm displacement, instead sustaining a ductile post-peak plateau to approximately 345 mm. This is a qualitatively different, rather than merely incremental, improvement: the glulam element braces the steel flange against lateral movement, changing which failure mechanism governs the design rather than simply delaying it. This is consistent with Jurkiewiez et al. [15], who observed a comparable shift away from lateral-torsional buckling toward a different failure mode in a tee-section steel-timber hybrid beam once timber was added. Chen et al. [16] similarly found that timber reinforcement substantially raises the load at which lateral-torsional buckling occurs in steel-timber composite beams, though in their tests the failure mode itself remained buckling-governed rather than being replaced entirely.

This hierarchy in ductility is further supported by the observed failure modes across all configurations. Failure in both STC-1 and STC-2 is consistently initiated in the glulam component regardless of span length or load combination, with reaching its compressive or tensile capacity before the steel approaches yielding.

Although STC-1 achieves a higher degree of composite action as indicated by the gamma coefficient, STC-2 consistently produces a higher effective bending stiffness across all configurations. This apparent contradiction reflects the distinction between composite efficiency and absolute stiffness. STC-1 makes more efficient use of the composite connection, but the inherently larger cross-section of STC-2's glulam component results in a higher absolute stiffness despite the lower degree of composite action. This suggests that for maximizing bending stiffness, cross-section geometry plays a more dominant role than the degree of composite action alone.

In STC-1, failure is governed by compressive crushing of the glulam under the top flange, followed by progressive yielding of the steel HEA section, resulting in the ductile post-peak response observed in the load-displacement curves. In STC-2, failure is governed by tensile rupture of the glulam at the bottom face, which occurs before the steel plate reaches yield, consistent with the low steel utilization ratios reported in Figure 4.17. This distinction is important: STC-1 fails in a compression-then-yielding sequence that is inherently ductile, while STC-2 fails through brittle timber tension despite the presence of the steel plate, explaining the more abrupt post-peak response.

This is consistent with the stress distribution results presented in Figures C.5–C.6, where the glulam operates near its strength limits at pre-yield while the steel stresses remain significantly below yield, particularly in STC-2, where the steel plate averages only approximately 56% utilization at the pre-yield stage as summarized in Figure 4.17, compared to approximately 94% for STC-1 in Figure 4.16.

This disparity in material utilization raises an important question regarding the efficiency of the current designs. In STC-1, the relatively balanced utilization of both materials suggests that the composite section is well-proportioned, with steel and timber contributing roughly equally to the bending resistance at the serviceability stage. In STC-2 however, the timber consistently governs failure while the steel plate carries significantly less stress, indicating that the configuration is effectively timber-governed throughout the loading history. The steel plate primarily contributes stiffness to satisfy the serviceability deflection criterion rather than strength, meaning that its cross-sectional area is determined by stiffness requirements rather than by strength utilization.

This is an inherent consequence of the STC-2 configuration being derived from a timber beam that is already deflection-governed, adding a steel plate shifts the neutral axis and increases the effective stiffness, reducing deflection, but does not necessarily engage the steel's full strength capacity in the process. This suggests that the current steel plate thickness in STC-2 may be overdesigned from a pure strength perspective.

The load-slip behavior at the steel-timber interface, presented in Figures 4.12a–4.13b, is consistent with the observed differences in ductility between the two configurations. STC-2 exhibits a higher initial connection stiffness and accumulates less total slip at failure compared to STC-1 across all investigated span lengths and load combinations. For the 7 m office load case, STC-1 reaches approximately 3.5 mm slip at failure compared to 2.7 mm for STC-2, and this pattern is maintained across all cases.

This difference reflects the connector stiffness values assigned in the numerical model. Although the bolt connectors in STC-1 have a higher per-connector slip modulus K_{ser} than the screws in STC-2, STC-2's closer connector spacing results in a higher overall connection stiffness, which governs the global load-slip response. This is consistent with the deflection-governed nature of STC-2 discussed above: the tighter connector spacing, like the steel plate itself, is driven by the need to satisfy serviceability stiffness requirements rather than to maximize strength utilization. It should be noted that in the numerical model, connector stiffness is assigned as a constant elastic value throughout the analysis, meaning no connection failure criterion is defined. The failure sequence observed in both configurations is therefore governed entirely by material failure in the timber or steel components. Consequently, the difference in post-peak response between STC-1 and STC-2 reflects the difference in which material governs failure, rather than any difference in connection behavior.

5.2.4 Methodological Constraints Affecting the Results

The genetic algorithm design process included several geometric constraints that influence the resulting LCA and LCC outcomes. The glulam width was constrained to equal the steel flange width ($b_t = b_f$) to prevent local failures at the interface, while the timber depth in STC-1 was limited by the steel section depth ($h_t \leq h_s$). These restrictions reduce the range of feasible composite configurations and may exclude solutions with lower CO_2 emissions.

In addition, the total composite depth was limited to $h_s + h_t \leq 0.8, \mathrm{m}$ and $h_s + h_t \leq 1.2, \mathrm{m}$ for the 7 m and 12 m spans, respectively, further constraining the design space. Finally, the assessment was based on a single load combination per span, meaning that results may vary under alternative loading scenarios or tributary widths.

Another important limitation is lateral-torsional buckling (LTB), which is not considered in the design of the STC-configurations, but only in the reference beams. In practice, the compression flange of the steel section in STC-1 is partially restrained by the glulam through the connector interface, which would increase the effective LTB resistance compared to a bare steel beam. Neglecting this restraint is therefore conservative for the reference HEA beams but may underestimate the structural efficiency of the composite configurations.

6
Conclusion

This study investigated two steel–timber composite (STC) beam configurations: STC-1, consisting of an HEA steel beam with an overlying glulam element, and STC-2, consisting of a glulam beam reinforced with a steel plate. Their structural, environmental, and economic performance was evaluated against steel and glulam reference beams.

Newmark's partial-interaction theory was found to predict the behavior of both configurations with acceptable accuracy, supporting its use as a preliminary design method in the absence of dedicated Eurocode provisions for STC beams.

The environmental and economic benefits of the composite systems were found to be span-dependent. STC-1 achieved CO_2 reductions of up to 20% relative to the steel reference at longer spans, whereas STC-2 provided no consistent carbon advantage over glulam. Economically, STC-2 proved advantageous, achieving cost reductions of up to 30% compared to glulam, while STC-1 remained generally more expensive than the steel reference. Consequently, neither configuration outperformed its reference beam in both cost and environmental impact, and the preferred solution depends on the project's design priorities.

Both STC configurations satisfied the structural requirements for all investigated spans and load cases. STC-1 exhibited a ductile response comparable to the steel reference beam, while STC-2 showed improved ductility relative to glulam but remained governed by timber tension failure. Material utilization indicated efficient use of both materials in STC-1, whereas the steel plate in STC-2 was primarily stiffness-governed, suggesting potential for further optimization.

Overall, STC beams represent a structurally sound and potentially beneficial alternative to conventional steel or glulam beams beyond certain threshold spans, with STC-1 favored for environmental performance and STC-2 for economic efficiency relative to glulam.

6.1 Recommendations for Future Work

- **Experimental Validation.** Physical experimental validation through push-out tests and full-scale beam tests is the most immediate next step, particularly for STC-2 with inclined screws, where the numerical model showed the largest deviations from Newmark's theory. Experimental data would allow calibration of the connector stiffness model beyond the Eurocode 5 provisions used in this study and provide a more reliable basis for the partial-interaction design approach.

- **Lateral-Torsional Buckling.** Lateral-torsional buckling was verified for the reference beams but not explicitly incorporated into the design of the STC configurations. Accounting for the lateral restraint provided by the glulam to the steel section in STC-1 could allow more efficient HEA section selection, which would in turn affect the LCA and LCC outcomes and potentially increase the span range over which STC-1 offers environmental and economic advantages.
- **Steel Plate Optimization for STC-2.** The results indicate that the steel plate in STC-2 is governed by stiffness rather than strength requirements, with an average utilization of only approximately 56% at the pre-yield stage. A dedicated geometric optimization investigating thinner but wider plates or alternative steel profiles could improve material efficiency, reduce cost, and lower embodied carbon simultaneously, addressing the main structural limitation identified in this study.

Bibliography

[1] Mosly, I. (2025) *Carbon footprint of global construction industries: A cross-country analysis of emissions, drivers, and the construction carbon sustainability index (1990–2023)*, *Sustainability*, 17, p. 9274.

[2] Naturvårdsverket (2025) *Underlag till regeringens klimatpolitiska handlingsplan.* Stockholm: Naturvårdsverket.

[3] Boverket (2025a) *Växthusgaser från bygg- och fastighetssektorn.* Available at: https://www.boverket.se/sv/byggande/hallbart-byggande-och-forvaltning/miljoindikatorer—aktuell-status/vaxthusgaser/ (Accessed: 8 June 2026).

[4] Naturskyddsföreningen (2023) *Cement, klimat och miljö – en faktabroschyr.* Available at: https://www.naturskyddsforeningen.se/faktablad/cement-klimat-och-miljo/ (Accessed: 8 June 2026).

[5] Swedish Climate Policy Council (2019) *Report of the Swedish Climate Policy Council* (Report No. 2). Klimatpolitiska rådet. ISBN 978-91-984671-2-3.

[6] González-Retamal, M., Forcael, E., Saelzer, G. and Vargas Mosqueda, M. (2022) 'From trees to skyscrapers: holistic review of the advances and limitations of multi-storey timber buildings', *Buildings*, 12(8), p. 1263. DOI: 10.3390/buildings12081263.

[7] Wimmers, G. (2017) 'Wood: a construction material for tall buildings', *Nature Reviews Materials*, 2(12), p. 17051. DOI: 10.1038/natrevmats.2017.51.

[8] Yang, L., Cao, W., Xu, K. and Fan, J. (2025) 'Study on flexural performance of stainless steel-timber composite beams with different combination forms', *Engineering Structures*, 335, p. 120377. DOI: 10.1016/j.engstruct.2025.120377.

[9] Gilbert, B.P., Guan, H., Ngo, T. and Remennikov, A. (2024) 'Shear performance of glued and screwed timber-steel composite connections for composite timber-steel beams', *Construction and Building Materials*, 450, p. 138762. DOI: 10.1016/j.conbuildmat.2024.138762.

[10] Eldeib, M., Ma, X., Zhuge, Y., Rameezdeen, R., Hassanli, R., Ellis, M. and Abd-Elaal, E. (2025) 'Structural behaviour of steel-timber composite elements: an overview', *Low-carbon Materials and Green Construction*, 3, article 4. DOI: 10.1007/s44242-025-00065-x.

[11] Ranzi, G. and Zona, A. (2007) 'A steel-concrete composite beam model with partial interaction including the shear deformability of the steel component', *Engineering Structures*, 29(11), pp. 3026–3041. DOI: 10.1016/j.engstruct.2007.02.007.

[12] Swedish Institute for Standards (2019) *SS-EN 15804:2012+A2:2019 Sustainability of construction works - Environmental product declarations - Core rules for the product category of construction products*. Stockholm: SIS.

[13] Ramage, M.H., Burridge, H., Busse-Wicher, M., Fereday, G., Reynolds, T., Shah, D.U., Wu, G., Yu, L., Fleming, P., Densley-Tingley, D., Allwood, J., Dupree, P., Linden, P.F. and Scherman, O.A. (2017) 'The wood from the trees: the use of timber in construction', *Renewable and Sustainable Energy Reviews*, 68(1), pp. 333–359. DOI: 10.1016/j.rser.2016.09.107.

[14] Zhang, A., Liu, J., Chen, Z. and Niu, X. (2026) 'Shear performance tests and theoretical analysis of self-tapping screw connection in light gauge steel-timber composite structures', *Structures*, 64, p. 111245. DOI: 10.1016/j.istruc.2026.111245.

[15] Jurkiewiez, B., Durif, S., Bouchaïr, A. and Grazide, C. (2022) 'Experimental and analytical study of hybrid steel-timber beams in bending', *Structures*, 39, pp. 1231–1248. DOI: 10.1016/j.istruc.2022.03.055.

[16] Chen, L., Yang, L. and Xu, K. (2025) 'Experimental and numerical research on overall stability of stainless steel-timber composite beams', *Engineering Structures*, [volume], p. 119982. DOI: 10.1016/j.engstruct.2025.119982.

[17] Patowary, M.Z., Al-Deen, S. and Ashraf, M. (2024) 'Significance of end connection rigidity on the economic design of long-span timber beams', in Chouw, N. and Zhang, C. (eds.) *Proceedings of the 26th Australasian Conference on the Mechanics of Structures and Materials*. Lecture Notes in Civil Engineering, vol. 513. Singapore: Springer, pp. 323–332. DOI: 10.1007/978-981-97-3397-2_29.

[18] Saad, K. and Lengyel, A. (2022) 'Strengthening timber structural members with CFRP and GFRP: a state-of-the-art review', *Polymers*, 14(12), p. 2381. DOI: 10.3390/polym14122381.

[19] Harrach, D., Habashneh, M. and Movahedi Rad, M. (2022) 'Reliability-based numerical analysis of glulam beams reinforced by CFRP plate', *Scientific Reports*, 12(1). DOI: 10.1038/s41598-022-17751-6.

[20] Gunasekaran, P., Ghanbari-Ghazijahani, T., Valipour, H. and Makki Alamdari, M. (2026) 'Timber beams and columns reinforced with steel and FRP – techniques and performance: A state-of-the-art review', *Structures*, 86, p. 111029. DOI: 10.1016/j.istruc.2025.111029.

[21] Aghayere, A., Vigil, J. et al. (2025) *Structural Steel Design*. 4th edn. DOI: 10.1515/9781501520594.

[22] Hassan, O. and Christopher, J. (2018) 'Glued laminated timber and steel beams: A comparative study of structural design, economic and environmental consequences', *Journal of Engineering, Design and Technology*, 16(3), pp. 398–417.

[23] Luo, L., Zhang, Y., Pan, C., Zheng, N. and Xu, C. (2024) 'Lateral torsional buckling in H-shaped steel beams considering the combined action of bending and torsion', *Structures*, 66, p. 106935. DOI: 10.1016/j.istruc.2024.106935.

[24] Hassanieh, A., Valipour, H.R. and Bradford, M.A. (2016) 'Experimental and numerical study of steel-timber composite (STC) beams', *Journal of Constructional Steel Research*, 122, pp. 367–378. DOI: 10.1016/j.jcsr.2016.04.005.

[25] Safarik, D., Miranda, W. and Anthony, S. (2024) *Steel-Timber Hybrid Buildings: Case Studies*. Chicago: Council on Tall Buildings and Urban Habitat.

[26] Nabati, A., Ghanbari-Ghazijahani, T. and Valipour, H.R. (2021) 'Innovative flitch sandwich beams with steel core under four-point bending', *Engineering Structures*, 233, p. 111724. DOI: 10.1016/j.engstruct.2020.111724.

[27] Gouveia Henriques, J., Turgut, A., Demonceau, J.-F. and Degee, H. (2024) 'Semi-rigid STC beam-to-column joints: review, future perspectives and needs', in *Proceedings of the 10th International Conference on Steel and Aluminium Structures (ICSAS24)*, pp. 624–635.

[28] Haase, P., Boretzki, J., Aurand, S., Sandhaas, C., Ummenhofer, T. and Albiez, M. (2024) 'Influence of the joining technique on the structural behaviour of hybrid timber-steel cross-sections', *The Journal of Adhesion*, pp. 1–28. DOI: 10.1080/00218464.2024.2360498.

[29] Tsai, M.-T. and Le, T.D.H. (2018) 'Determination of initial stiffness of timber-steel composite (TSC) beams based on experiment and simulation modeling', *Sustainability*, 10(4), p. 1220. DOI: 10.3390/su10041220.

[30] Robatmili, R., Du, Y. and Doudak, G. (2025) 'Elastic lateral-torsional buckling of wooden built-up beams with mechanical fasteners', *Structures*, 80, p. 109720. DOI: 10.1016/j.istruc.2025.109720.

[31] Shahin, A., Cowled, C.J.L., Bailleres, H. and Fawzia, S. (2024) 'Experimental study on shear performance of nail and screw-laminated timber-steel composite and timber-timber systems using low-grade timber and mechanical fasteners', *Construction and Building Materials*, 418, p. 135403. DOI: 10.1016/j.conbuildmat.2024.135403.

[32] Hu, W., Liu, Y. and Konukcu, A.C. (2022) 'Study on withdrawal load resistance of screw in wood-based materials: experimental and numerical', [Journal Name], pp. 334–343. DOI: 10.1080/17480272.2022.2084699.

[33] Zhao, Y., Yuan, Y., Wang, C.-L. and Meng, S. (2023) 'Experimental and finite element analysis of flexural performance of steel-timber composite beams connected by hybrid-anchored screws', *Engineering Structures*, 292, p. 116503. DOI: 10.1016/j.engstruct.2023.116503.

[34] Liu, Y., Wang, Y., Zhang, Y., Chen, M. and Nie, X. (2020) 'Force-displacement relations of bolted timber joints with slotted-in steel plates parallel to the grain', *Journal of Wood Science*, 66, article 83.

[35] Moritani, F.Y., Santos, P., Carneiro, L. and Dias, A.M.P.G. (2025) 'Experimental assessment of bolt-based connections for cold-formed steel and cross-laminated timber composite floor systems', *Construction and Building Materials*, 492, p. 143004. DOI: 10.1016/j.conbuildmat.2025.143004.

[36] Abdulmalik, A., Gilbert, B.P., Guan, H., Ngo, T. and Remennikov, A. (2025) 'Advancements in timber-steel hybridisation: a review on techniques, applications, and structural performances', *Buildings*, 15(13), p. 2252. DOI: 10.3390/buildings15132252.

[37] Hassanieh, A., Valipour, H.R. and Bradford, M.A. (2016) 'Load-slip behaviour of steel-cross laminated timber (CLT) composite connections', *Journal of Constructional Steel Research*, 122, pp. 110–121. DOI: 10.1016/j.jcsr.2016.03.008.

[38] Lin, J.-P., Qiao, N., Zhang, L., Tang, J., Zhou, L., Huo, J. and Wang, G. (2024) 'Study on the mechanical properties of hybrid bonding shear connec-

tions with shear studs and epoxy mortar layer', *Structures*, 70, p. 107642. DOI: 10.1016/j.istruc.2024.107642.

[39] Kyvelou, P., Gardner, L. and Nethercot, D.A. (2017) 'Design of composite cold-formed steel flooring systems', *Structures*, 12, pp. [pages]. DOI: 10.1016/j.istruc.2017.09.006.

[40] Mascia, N.T. and de Oliveira Santana, C.L. (2009) 'Remarks on the slip modulus of nailed connections for linear analysis of plywood timber beams', *Construction and Building Materials*, 23(8), pp. 2731–2737. DOI: 10.1016/j.conbuildmat.2009.02.037.

[41] Hassanieh, A., Valipour, H.R. and Bradford, M.A. (2016) 'Experimental and analytical behaviour of steel-timber composite connections', *Construction and Building Materials*, 118, pp. 63–75. DOI: 10.1016/j.conbuildmat.2016.05.052.

[42] Shather, L.M. and Al-Shuwaili, M.A.H. (2025) 'A novel one-sided push-out test for shear connectors in composite beams', *Civil Engineering Journal*, 11(7). DOI: 10.28991/CEJ-2025-011-07-05.

[43] Yossef, M. and Chen, A. (2018) 'A solution considering partial degree of composite action for insulated sandwich panels with general configuration flexible shear connectors', *Engineering Structures*, 162, pp. 135–150. DOI: 10.1016/j.engstruct.2018.02.019.

[44] Strzelecka, J., Polus, Ł. and Chybiński, M. (2023) 'Theoretical and numerical analyses of steel-timber composite beams with LVL slabs', *Civil and Environmental Engineering Reports*, 33(2), pp. 64–84. DOI: 10.59440/ceer/172510.

[45] Wu, Y.F., Oehlers, D.J. and Griffith, M.C. (2002) 'Partial-interaction analysis of composite beam/column members', *Mechanics of Structures and Machines*, 30(3), pp. 309–332. DOI: 10.1081/SME-120004420.

[46] CEN (2004) *EN 1995-1-1: Eurocode 5 – Design of timber structures – Part 1-1: General – Common rules and rules for buildings*. Brussels: European Committee for Standardization.

[47] Xu, R.Q. and Wu, Y.F. (2007) 'Static, dynamic, and buckling analysis of partial interaction composite members using Timoshenko's beam theory', *International Journal of Mechanical Sciences*, 49(10), pp. 1139–1155. DOI: 10.1016/j.ijmecsci.2007.02.006.

[48] Wang, Z. and Sobey, A. (2020) 'A comparative review between Genetic Algorithm use in composite optimisation and the state-of-the-art in evolutionary computation', *Composite Structures*, 233, p. 111739. DOI: 10.1016/j.compstruct.2019.111739.

[49] Whitley, D. (1994) 'A genetic algorithm tutorial', *Statistics and Computing*, 4, pp. 65–85. DOI: 10.1007/BF00175354.

[50] Singh, R.K., Panchal, V.K. and Singh, B.K. (2018) 'A review on Genetic Algorithm and its applications', in *2018 Second International Conference on Green Computing and Internet of Things (ICGCIoT)*. IEEE, pp. 376–380. DOI: 10.1109/ICGCIoT.2018.8753030.

[51] Mohamed, K.S. (2018) 'Bio-inspired machine learning algorithm: genetic algorithm', in *Machine Learning for Model Order Reduction*. Cham: Springer, pp. 19–34.

[52] Zhang, R., Xu, X., Liu, K., Kong, L., Wang, X., Zhao, L. and Abuduwayiti, A. (2024) 'Does architectural design require single-objective or multi-objective optimisation? A critical choice with a comparative study between model-based algorithms and genetic algorithms', *Frontiers of Architectural Research*, 13(5), pp. 1079–1094. DOI: 10.1016/j.foar.2024.03.010.

[53] Kramer, O. (2017) *Genetic Algorithm Essentials*. Cham: Springer.

[54] Boverket (2025b) *Introduktion till livscykelanalys (LCA)*. Available at: https://www.boverket.se/sv/byggande/hallbart-byggande-och-forvaltning/livscykelanalys/introduktion-till-livscykelanalys-lca/ (Accessed: 8 June 2026).

[55] Hauschild, M.Z., Rosenbaum, R.K. and Olsen, S.I. (eds.) (2018) *Life Cycle Assessment: Theory and Practice*. Cham: Springer.

[56] Boverket (2025c) *Klimatdata till beräkningen – Klimatdeklaration*. Available at: https://www.boverket.se/sv/klimatdeklaration/gor-sa-har/underlag/klimatdata-till-berakningen/ (Accessed: 8 June 2026).

[57] Salokangas, L. (2013) *ETSI project: Bridge Life Cycle Optimisation – stage 3*. Esbo: Aalto University, School of Engineering.

[58] Luthin, A., Backes, J.G. and Traverso, M. (2021) *A framework to identify environmental-economic trade-offs by combining life cycle assessment and life cycle costing – A case study of aluminium production*, *Journal of Cleaner Production*, 321, p. 128902. DOI: 10.1016/j.jclepro.2021.128902.

[59] Dunant, C.F., Skelton, A.C.H., Drewniok, M.P., Cullen, J.M. and Allwood, J.M. (2019) 'A marginal abatement cost curve for material efficiency accounting for uncertainty', *Resources, Conservation and Recycling*, 144, pp. 39–47. DOI: 10.1016/j.resconrec.2019.01.020.

[60] McKinsey & Company (2009) *Pathways to a Low-Carbon Economy: Version 2 of the Global Greenhouse Gas Abatement Cost Curve*. Available at: https://www.mckinsey.com/business-functions/sustainability/our-insights/pathways-to-a-low-carbon-economy.

[61] CEN (2002) *EN 1991-1-1: Eurocode 1 – Actions on structures – Part 1-1: General actions – Densities, self-weight, imposed loads for buildings*. Brussels: European Committee for Standardization.

[62] CEN (2005) *EN 1993-1-1: Eurocode 3 – Design of steel structures – Part 1-1: General rules and rules for buildings*. Brussels: European Committee for Standardization.

[63] CEN (2004) *EN 1994-1-1: Eurocode 4 – Design of composite steel and concrete structures – Part 1-1: General rules and rules for buildings*. Brussels: European Committee for Standardization.

A
Appendix: Calculations of Beam

7m Office Beam HEA 280

$h := 270\ mm$

$f_y := 355\ MPa$

$b_f := 260\ mm$

$\gamma_{M0} := 1$

$t_f := 13\ mm$

$l_{beam} := 7\ m$

$g := 9.81\ \frac{m}{s^2}$

$h_w := h - 2\ t_f = 0.244\ m$

$E := 200\ GPa$

$t_w := 8\ mm$

$\rho := 7850\ \frac{kg}{m^3}$

$I_{0.1} := b_f \cdot \frac{{t_f}^3}{12} = \left(4.76 \cdot 10^{-8}\right)\ m^4$

$A_{flange} := b_f \cdot t_f = 0.003\ m^2$

$A_{web} := t_w \cdot h_w = 0.002\ m^2$

$I_{0.2} := t_w \cdot \frac{{h_w}^3}{12} = \left(9.685 \cdot 10^{-6}\right)\ m^4$

$y := \frac{h}{2} - \frac{t_f}{2} = 0.129\ m$

$I_{0.3} := b_f \cdot \frac{{t_f}^3}{12} = \left(4.76 \cdot 10^{-8}\right)\ m^4$

$y_{top} := \frac{h}{2} = 0.135\ m$

$I_{tot} := \left(I_{0.1} + A_{flange} \cdot y^2\right) + I_{0.2} + \left(I_{0.3} + A_{flange} \cdot y^2\right) = \left(1.214 \cdot 10^{-4}\right)\ m^4$

Imposed load

$q_{k.imp} := 3\ \frac{kN}{m^2}$

$q_k := q_{k.imp} \cdot 6\ m = 18\ \frac{kN}{m}$

Self weight

$A_{beam} := 2 \cdot A_{flange} + A_{web} = 0.009\ m^2$

$g_k := \rho \cdot A_{beam} \cdot g = 0.671\ \frac{kN}{m}$

Total load

$q_{d.SLS} := 1 \cdot g_k + 1 \cdot q_k = 18.671\ \frac{kN}{m}$

$q_{d.ULS} := 1.35 \cdot g_k + 1.5 \cdot q_k = 27.906\ \frac{kN}{m}$

Check of bending moment capacity:

Outstanding flange

$e := 0.81$

$c_F := \frac{b_f}{2} - \frac{t_w}{2} = 126\ mm$

$CSC1 := 9 \cdot e = 7.29$

$t_F := t_f = 13\ mm$

$CSC2 := 10 \cdot e = 8.1$

$\frac{c_F}{t_F} = 9.692$

$CSC3 := 14 \cdot e = 11.34$

$M_{Ed} := \frac{q_{d.ULS} \cdot l_{beam}^{\ 2}}{8} = 170.922\ kN \cdot m$

$W_{el} := \frac{I_{tot}}{y_{top}} = 0.0009\ m^3$

$M_{Rd} := \frac{W_{el} \cdot f_y}{\gamma_{M0}} = 319.244\ kN \cdot m$

Utilization ratio

$\frac{M_{Ed}}{M_{Rd}} = 53.54\%$

Check of deflection limit:

$$w := \frac{5 \cdot q_{d.SLS} \cdot l_{beam}^{4}}{384 \cdot E \cdot I_{tot}} = 24.04\ mm$$

$$w_{lim} := \frac{l_{beam}}{250} = 28\ mm$$

Utilization ratio

$$\frac{w}{w_{lim}} = 85.858\%$$

Check of lateral torsional buckling:

$C_1 := 1.127$

$I_z := 4763 \cdot 10^4 \ mm^4$ $\quad I_w := 785 \cdot 10^6 \ mm^6$ $\quad I_t := 0.624 \cdot 10^6 \ mm^4$

$k_w := 1$

$k := 1$

$$G := \frac{E}{2\ (1+0.3)} = 76.923 \ GPa$$

$$M_{cr} := C_1 \cdot \frac{\pi^2 \cdot E \cdot I_z}{(k \cdot l_{beam})^2} \cdot \sqrt{\left(\frac{k}{k_w}\right)^2 \cdot \frac{I_w}{I_z} + \frac{(k \cdot l_{beam})^2 \cdot G \cdot I_t}{\pi^2 \cdot E \cdot I_z}} = 342.133 \ kN \cdot m$$

$W_{el} := 1010 \cdot 10^3 \ mm^3$

$\alpha_{LT} := 0.34$

$\gamma_{M1} := 1$

$$\lambda_{LT} := \sqrt{\frac{W_{el} \cdot f_y}{M_{cr}}} = 1.024$$

$$\phi_{LT} := 0.5 \cdot \left(1 + \alpha_{LT} \cdot (\lambda_{LT} - 0.2) + {\lambda_{LT}}^2\right) = 1.164$$

$$\chi_{LT} := \frac{1}{\phi_{LT} + \sqrt{{\phi_{LT}}^2 - {\lambda_{LT}}^2}} = 0.582$$

$$M_{bRd} := \chi_{LT} \cdot W_{el} \cdot \frac{f_y}{\gamma_{M1}} = 208.694 \ kN \cdot m$$

Utilization ratio

$$\frac{M_{Ed}}{M_{bRd}} = 81.901\%$$

Check of shear capacity:

Assume all shear is taken in the web, i.e. minimal flange contribution

$\eta := 1.2$ $\varepsilon := 0.81$ $\nu := 0.3$

$\gamma_{M1} := 1$

$a_{shear} := \dfrac{l_{beam}}{6} = 1.167\ m$

$\dfrac{a_{shear}}{h_w} = 4.781$ Larger than 1

$\kappa_\tau := 5.34 + 4 \cdot \left(\dfrac{h_w}{a_{shear}}\right)^2 = 5.515$

Check of slenderness limit

$\dfrac{72}{\eta} \cdot \varepsilon = 48.6$

$\dfrac{h_w}{t_w} = 30.5$

$\tau_{cr} := \kappa_\tau \cdot \dfrac{\pi^2 \cdot E \cdot t_w^{\ 2}}{12 \cdot \left(1 - \nu^2\right) \cdot h_w^{\ 2}} = \left(1.072 \cdot 10^3\right)\ MPa$

$\lambda_{bar.w} := 0.76 \cdot \sqrt{\dfrac{f_y}{\tau_{cr}}} = 0.437$

$\chi_w := \eta = 1.2$

$V_{bw.Rd} := \dfrac{\chi_w \cdot f_y \cdot h_w \cdot t_w}{\sqrt{3} \cdot \gamma_{M1}} = 480\ kN$ $V_{Ed} := \dfrac{q_{d.ULS} \cdot l_{beam}}{2} = 97.67\ kN$

Utilization Ratio

$\dfrac{V_{Ed}}{V_{bw.Rd}} = 20.344\%$

12m Office Beam HEA 500

$h := 490\ mm$

$b_f := 300\ mm$

$t_f := 23\ mm$

$h_w := h - 2\ t_f = 0.444\ m$

$t_w := 12\ mm$

$f_y := 355\ MPa$

$\gamma_{M0} := 1$

$l_{beam} := 12\ m \qquad g := 9.81\ \frac{m}{s^2}$

$E := 200\ GPa$

$\rho := 7850\ \frac{kg}{m^3}$

$I_{0.1} := b_f \cdot \frac{{t_f}^3}{12} = \left(3.042 \cdot 10^{-7}\right)\ m^4$

$I_{0.2} := t_w \cdot \frac{{h_w}^3}{12} = \left(8.753 \cdot 10^{-5}\right)\ m^4$

$I_{0.3} := b_f \cdot \frac{{t_f}^3}{12} = \left(3.042 \cdot 10^{-7}\right)\ m^4$

$A_{flange} := b_f \cdot t_f = 0.007\ m^2$

$A_{web} := t_w \cdot h_w = 0.005\ m^2$

$y := \frac{h}{2} - \frac{t_f}{2} = 0.234\ m$

$y_{top} := \frac{h}{2} = 0.245\ m$

$I_{tot} := \left(I_{0.1} + A_{flange} \cdot y^2\right) + I_{0.2} + \left(I_{0.3} + A_{flange} \cdot y^2\right) = \left(8.405 \cdot 10^{-4}\right)\ m^4$

Imposed load

$q_{k.imp} := 3\ \frac{kN}{m^2}$

$q_k := q_{k.imp} \cdot 6\ m = 18\ \frac{kN}{m}$

Self weight

$A_{beam} := 2 \cdot A_{flange} + A_{web} = 0.019\ m^2$

$g_k := \rho \cdot A_{beam} \cdot g = 1.473\ \frac{kN}{m}$

Total load

$q_{d.SLS} := 1 \cdot g_k + 1 \cdot q_k = 19.473\ \frac{kN}{m}$

$q_{d.ULS} := 1.35 \cdot g_k + 1.5 \cdot q_k = 28.989\ \frac{kN}{m}$

Check of bending moment capacity:

Outstanding flange

$e := 0.81$

$c_F := \frac{b_f}{2} - \frac{t_w}{2} = 144\ mm$ $\qquad CSC1 := 9 \cdot e = 7.29$

$t_F := t_f = 23\ mm$ $\qquad CSC2 := 10 \cdot e = 8.1$

$\frac{c_F}{t_F} = 6.261$ $\qquad CSC3 := 14 \cdot e = 11.34$

$M_{Ed} := \frac{q_{d.ULS} \cdot {l_{beam}}^2}{8} = 521.794\ kN \cdot m$

$W_{el} := \frac{I_{tot}}{y_{top}} = 0.00343\ m^3$ $\qquad W_{pl} := 3950 \cdot 10^3\ mm^3$

$M_{Rd} := \frac{W_{pl} \cdot f_y}{\gamma_{M0}} = \left(1.402 \cdot 10^3\right)\ kN \cdot m$

Utilization ratio

$\frac{M_{Ed}}{M_{Rd}} = 37.211\%$

Check of deflection limit:

$$w := \frac{5 \cdot q_{d.SLS} \cdot l_{beam}{}^{4}}{384 \cdot E \cdot I_{tot}} = 31.276\ mm$$

$$w_{lim} := \frac{l_{beam}}{250} = 48\ mm$$

Utilization ratio

$$\frac{w}{w_{lim}} = 65.158\%$$

Check of lateral torsional buckling:

$C_1 := 1.127$

$I_z := 10370 \cdot 10^4 \ mm^4 \quad I_w := 5640 \cdot 10^6 \ mm^6 \quad I_t := 3.1 \cdot 10^6 \ mm^4$

$k_w := 1$

$k := 1$

$$G := \frac{E}{2\ (1+0.3)} = 76.923 \ GPa$$

$$M_{cr} := C_1 \cdot \frac{\pi^2 \cdot E \cdot I_z}{\left(k \cdot l_{beam}\right)^2} \cdot \sqrt{\left(\frac{k}{k_w}\right)^2 \cdot \frac{I_w}{I_z} + \frac{\left(k \cdot l_{beam}\right)^2 \cdot G \cdot I_t}{\pi^2 \cdot E \cdot I_z}} = 656.261 \ kN \cdot m$$

$\alpha_{LT} := 0.21$

$\gamma_{M1} := 1$

$$\lambda_{LT} := \sqrt{\frac{W_{pl} \cdot f_y}{M_{cr}}} = 1.462$$

$$\phi_{LT} := 0.5 \cdot \left(1 + \alpha_{LT} \cdot \left(\lambda_{LT} - 0.2\right) + {\lambda_{LT}}^2\right) = 1.701$$

$$\chi_{LT} := \frac{1}{\phi_{LT} + \sqrt{{\phi_{LT}}^2 - {\lambda_{LT}}^2}} = 0.389$$

$$M_{bRd} := \chi_{LT} \cdot W_{pl} \cdot \frac{f_y}{\gamma_{M1}} = 545.533 \ kN \cdot m$$

Utilization ratio

$$\frac{M_{Ed}}{M_{bRd}} = 95.648\%$$

Check of shear capacity:

Assume all shear is taken in the web, i.e. minimal flange contribution

$\eta := 1.2$ $\varepsilon := 0.81$ $\nu := 0.3$

$\gamma_{M1} := 1$

$a_{shear} := \frac{l_{beam}}{6} = 2\ m$

$\frac{a_{shear}}{h_w} = 4.505$ Larger than 1

$\kappa_\tau := 5.34 + 4 \cdot \left(\frac{h_w}{a_{shear}}\right)^2 = 5.537$

Check of slenderness limit

$\frac{72}{\eta} \cdot \varepsilon = 48.6$

$\frac{h_w}{t_w} = 37$

$\tau_{cr} := \kappa_\tau \cdot \frac{\pi^2 \cdot E \cdot t_w^{\ 2}}{12 \cdot (1 - \nu^2) \cdot h_w^{\ 2}} = 731.12\ MPa$

$\lambda_{bar.w} := 0.76 \cdot \sqrt{\frac{f_y}{\tau_{cr}}} = 0.53$

$\chi_w := \eta = 1.2$

$V_{bw.Rd} := \frac{\chi_w \cdot f_y \cdot h_w \cdot t_w}{\sqrt{3} \cdot \gamma_{M1}} = 1310\ kN$ $V_{Ed} := \frac{q_{d.ULS} \cdot l_{beam}}{2} = 173.931\ kN$

Utilization ratio

$\frac{V_{Ed}}{V_{bw.Rd}} = 13.273\%$

7m Shopping Mall Beam HEA 320

$h := 310\ mm$

$b_f := 300\ mm$

$t_f := 15.5\ mm$

$h_w := h - 2\ t_f = 0.279\ m$

$t_w := 9\ mm$

$f_y := 355\ MPa$

$\gamma_{M0} := 1$

$l_{beam} := 7\ m$ $\quad g := 9.81\ \frac{m}{s^2}$

$E := 210\ GPa$

$\rho := 7850\ \frac{kg}{m^3}$

$I_{0.1} := b_f \cdot \frac{t_f^{\ 3}}{12} = \left(9.31 \cdot 10^{-8}\right)\ m^4$

$I_{0.2} := t_w \cdot \frac{h_w^{\ 3}}{12} = \left(1.629 \cdot 10^{-5}\right)\ m^4$

$I_{0.3} := b_f \cdot \frac{t_f^{\ 3}}{12} = \left(9.31 \cdot 10^{-8}\right)\ m^4$

$A_{flange} := b_f \cdot t_f = 0.005\ m^2$

$A_{web} := t_w \cdot h_w = 0.003\ m^2$

$y := \frac{h}{2} - \frac{t_f}{2} = 0.147\ m$

$y_{top} := \frac{h}{2} = 0.155\ m$

$I_{tot} := \left(I_{0.1} + A_{flange} \cdot y^2\right) + I_{0.2} + \left(I_{0.3} + A_{flange} \cdot y^2\right) = \left(2.181 \cdot 10^{-4}\right)\ m^4$

Imposed load

$q_{k.imp} := 5\ \frac{kN}{m^2}$

$q_k := q_{k.imp} \cdot 6\ m = 30\ \frac{kN}{m}$

Self weight

$A_{beam} := 2 \cdot A_{flange} + A_{web} = 0.012\ m^2$

$g_k := \rho \cdot A_{beam} \cdot g = 0.91\ \frac{kN}{m}$

Total load

$q_{d.SLS} := 1 \cdot g_k + 1 \cdot q_k = 30.91\ \frac{kN}{m}$

$q_{d.ULS} := 1.35 \cdot g_k + 1.5 \cdot q_k = 46.228\ \frac{kN}{m}$

$Q_{SLS} := q_{d.SLS} \cdot l_{beam} = 216.367\ kN$

Check of bending moment capacity:

Outstanding flange

$e := 0.81$

$c_F := \frac{b_f}{2} - \frac{t_w}{2} = 145.5\ mm$

$CSC1 := 9 \cdot e = 7.29$

$t_F := t_f = 15.5\ mm$

$CSC2 := 10 \cdot e = 8.1$

$\frac{c_F}{t_F} = 9.387$

$CSC3 := 14 \cdot e = 11.34$

$M_{Ed} := \frac{q_{d.ULS} \cdot {l_{beam}}^2}{8} = 283.146\ kN \cdot m$

$W_{el} := \frac{I_{tot}}{y_{top}} = 0.00141\ m^3$

$M_{Rd} := \frac{W_{el} \cdot f_y}{\gamma_{M0}} = 499.57\ kN \cdot m$

Utilization ratio

$\frac{M_{Ed}}{M_{Rd}} = 56.678\%$

Check of deflection limit:

$$w := \frac{5 \cdot q_{d.SLS} \cdot l_{beam}^{4}}{384 \cdot E \cdot I_{tot}} = 21.096\ mm$$

$$w_{lim} := \frac{l_{beam}}{250} = 28\ mm$$

Utilization ratio

$$\frac{w}{w_{lim}} = 75.344\%$$

Check of lateral torsional buckling:

$$C_1 := 1.127$$

$$I_z := 6985 \cdot 10^4 \ mm^4 \qquad I_w := 1510 \cdot 10^6 \ mm^6 \qquad I_t := 1.08 \cdot 10^6 \ mm^4$$

$$k_w := 1$$

$$k := 1$$

$$G := \frac{E}{2\ (1+0.3)} = 80.769\ GPa$$

$$M_{cr} := C_1 \cdot \frac{\pi^2 \cdot E \cdot I_z}{(k \cdot l_{beam})^2} \cdot \sqrt{\left(\frac{k}{k_w}\right)^2 \cdot \frac{I_w}{I_z} + \frac{(k \cdot l_{beam})^2 \cdot G \cdot I_t}{\pi^2 \cdot E \cdot I_z}} = 572.351\ kN \cdot m$$

$$W_{el} := 1480 \cdot 10^3 \ mm^3$$

$$\alpha_{LT} := 0.34$$

$$\gamma_{M1} := 1$$

$$\lambda_{LT} := \sqrt{\frac{W_{el} \cdot f_y}{M_{cr}}} = 0.958$$

$$\phi_{LT} := 0.5 \cdot \left(1 + \alpha_{LT} \cdot (\lambda_{LT} - 0.2) + \lambda_{LT}^2\right) = 1.088$$

$$\chi_{LT} := \frac{1}{\phi_{LT} + \sqrt{\phi_{LT}^2 - \lambda_{LT}^2}} = 0.624$$

$$M_{bRd} := \chi_{LT} \cdot W_{el} \cdot \frac{f_y}{\gamma_{M1}} = 327.739\ kN \cdot m$$

Utilization ratio

$$\frac{M_{Ed}}{M_{bRd}} = 86.394\%$$

Check of shear capacity:

Assume all shear is taken in the web, i.e. minimal flange contribution

$\eta := 1.2$ $\varepsilon := 0.81$ $\nu := 0.3$

$\gamma_{M1} := 1$

$a_{shear} := \dfrac{l_{beam}}{6} = 1.167\ m$

$\dfrac{a_{shear}}{h_w} = 4.182$ Larger than 1

$\kappa_\tau := 5.34 + 4 \cdot \left(\dfrac{h_w}{a_{shear}}\right)^2 = 5.569$

Check of slenderness limit

$\dfrac{72}{\eta} \cdot \varepsilon = 48.6$

$\dfrac{h_w}{t_w} = 31$

$\tau_{cr} := \kappa_\tau \cdot \dfrac{\pi^2 \cdot E \cdot {t_w}^2}{12 \cdot \left(1 - \nu^2\right) \cdot {h_w}^2} = \left(1.1 \cdot 10^3\right)\ MPa$

$\lambda_{bar.w} := 0.76 \cdot \sqrt{\dfrac{f_y}{\tau_{cr}}} = 0.432$

$\chi_w := \eta = 1.2$

$V_{bw.Rd} := \dfrac{\chi_w \cdot f_y \cdot h_w \cdot t_w}{\sqrt{3} \cdot \gamma_{M1}} = 618\ kN$ $V_{Ed} := \dfrac{q_{d.ULS} \cdot l_{beam}}{2} = 161.798\ kN$

Utilization Ratio

$\dfrac{V_{Ed}}{V_{bw.Rd}} = 26.198\%$

12m Shopping Mall Beam HEA 800

$h := 790\ mm$

$b_f := 300\ mm$

$t_f := 28\ mm$

$h_w := h - 2\ t_f = 0.734\ m$

$t_w := 15\ mm$

$f_y := 355\ MPa$

$\gamma_{M0} := 1$

$l_{beam} := 12\ m$ $\quad g := 9.81\ \frac{m}{s^2}$

$E := 200\ GPa$

$\rho := 7850\ \frac{kg}{m^3}$

$I_{0.1} := b_f \cdot \frac{t_f^{\ 3}}{12} = \left(5.488 \cdot 10^{-7}\right)\ m^4$

$I_{0.2} := t_w \cdot \frac{h_w^{\ 3}}{12} = \left(4.943 \cdot 10^{-4}\right)\ m^4$

$I_{0.3} := b_f \cdot \frac{t_f^{\ 3}}{12} = \left(5.488 \cdot 10^{-7}\right)\ m^4$

$A_{flange} := b_f \cdot t_f = 0.008\ m^2$

$A_{web} := t_w \cdot h_w = 0.011\ m^2$

$y := \frac{h}{2} - \frac{t_f}{2} = 0.381\ m$

$y_{top} := \frac{h}{2} = 0.395\ m$

$I_{tot} := \left(I_{0.1} + A_{flange} \cdot y^2\right) + I_{0.2} + \left(I_{0.3} + A_{flange} \cdot y^2\right) = 0.003\ m^4$

Imposed load

$q_{k.imp} := 5\ \frac{kN}{m^2}$

$q_k := q_{k.imp} \cdot 6\ m = 30\ \frac{kN}{m}$

Self weight

$A_{beam} := 2 \cdot A_{flange} + A_{web} = 0.028\ m^2$

$g_k := \rho \cdot A_{beam} \cdot g = 2.142\ \frac{kN}{m}$

Total load

$q_{d.SLS} := 1 \cdot g_k + 1 \cdot q_k = 32.142\ \frac{kN}{m}$

$q_{d.ULS} := 1.35 \cdot g_k + 1.5 \cdot q_k = 47.891\ \frac{kN}{m}$

Check of bending moment capacity:

Outstanding flange

$e := 0.81$

$c_F := \frac{b_f}{2} - \frac{t_w}{2} = 142.5\ mm$

$CSC1 := 9 \cdot e = 7.29$

$t_F := t_f = 28\ mm$

$CSC2 := 10 \cdot e = 8.1$

$\frac{c_F}{t_F} = 5.089$

$CSC3 := 14 \cdot e = 11.34$

If CF/TF is CSC1 or CSC2: use Wpl

If CF/TF is CSC3 or CSC4: use Wel

$M_{Ed} := \frac{q_{d.ULS} \cdot {l_{beam}}^2}{8} = 862.041\ kN \cdot m$

$W_{el} := 7680 \cdot 10^3\ mm^3$

$W_{pl} := 8700 \cdot 10^3\ mm^3$

$M_{Rd} := \frac{W_{pl} \cdot f_y}{\gamma_{M0}} = \left(3.089 \cdot 10^3\right)\ kN \cdot m$

Utilization ratio

$\frac{M_{Ed}}{M_{Rd}} = 27.911\%$

Check of deflection limit:

$$w := \frac{5 \cdot q_{d.SLS} \cdot {l_{beam}}^4}{384 \cdot E \cdot I_{tot}} = 14.789\ mm$$

$$w_{lim} := \frac{l_{beam}}{250} = 48\ mm$$

Utilization ratio

$$\frac{w}{w_{lim}} = 30.809\%$$

Check of lateral torsional buckling:

$C_1 := 1.127$

$I_z := 12640 \cdot 10^4 \ mm^4 \quad I_w := 18300 \cdot 10^6 \ mm^6 \quad I_t := 5.99 \cdot 10^6 \ mm^4$

$k_w := 1$

$k := 1$

$$G := \frac{E}{2\,(1+0.3)} = 76.923 \ GPa$$

$$M_{cr} := C_1 \cdot \frac{\pi^2 \cdot E \cdot I_z}{\left(k \cdot l_{beam}\right)^2} \cdot \sqrt{\left(\frac{k}{k_w}\right)^2 \cdot \frac{I_w}{I_z} + \frac{\left(k \cdot l_{beam}\right)^2 \cdot G \cdot I_t}{\pi^2 \cdot E \cdot I_z}} = \left(1.007 \cdot 10^3\right) \ kN \cdot m$$

$\alpha_{LT} := 0.21$

$\gamma_{M1} := 1$

$$\lambda_{LT} := \sqrt{\frac{W_{pl} \cdot f_y}{M_{cr}}} = 1.751$$

$$\phi_{LT} := 0.5 \cdot \left(1 + \alpha_{LT} \cdot \left(\lambda_{LT} - 0.2\right) + {\lambda_{LT}}^2\right) = 2.196$$

$$\chi_{LT} := \frac{1}{\phi_{LT} + \sqrt{{\phi_{LT}}^2 - {\lambda_{LT}}^2}} = 0.284$$

$$M_{bRd} := \chi_{LT} \cdot W_{pl} \cdot \frac{f_y}{\gamma_{M1}} = 877.125 \ kN \cdot m$$

Utilization ratio

$$\frac{M_{Ed}}{M_{bRd}} = 98.28\%$$

Check of shear capacity:

Assume all shear is taken in the web, i.e. minimal flange contribution

$\eta := 1.2$ $\varepsilon := 0.81$ $\nu := 0.3$

$\gamma_{M1} := 1$

$a_{shear} := \dfrac{l_{beam}}{6} = 2\ m$

$\dfrac{a_{shear}}{h_w} = 2.725$ Larger than 1

$\kappa_\tau := 5.34 + 4 \cdot \left(\dfrac{h_w}{a_{shear}}\right)^2 = 5.879$

Check of slenderness limit

$\dfrac{72}{\eta} \cdot \varepsilon = 48.6$

$\dfrac{h_w}{t_w} = 48.933$

$\tau_{cr} := \kappa_\tau \cdot \dfrac{\pi^2 \cdot E \cdot t_w^{\ 2}}{12 \cdot (1 - \nu^2) \cdot h_w^{\ 2}} = 443.796\ MPa$

$\lambda_{bar.w} := 0.76 \cdot \sqrt{\dfrac{f_y}{\tau_{cr}}} = 0.68$

$\chi_w := \eta = 1.2$

$V_{bw.Rd} := \dfrac{\chi_w \cdot f_y \cdot h_w \cdot t_w}{\sqrt{3} \cdot \gamma_{M1}} = 2708\ kN$ $V_{Ed} := \dfrac{q_{d.ULS} \cdot l_{beam}}{2} = 287.347\ kN$

Utilization ratio

$\dfrac{V_{Ed}}{V_{bw.Rd}} = 10.611\%$

Beam dimensions:

$b := 140\ mm$ Width of beam

$h := 720\ mm$ Height of beam

$l_{beam} := 7\ m$

$A_{beam} := b \cdot h = 0.101\ m^2$ $\rho := 390\ \frac{kg}{m^3}$ $g := 9.81\ \frac{m}{s^2}$

$V_{beam} := A_{beam} \cdot l_{beam} = 0.706\ m^3$

Imposed load

$q_{k.imp} := 3\ \frac{kN}{m^2}$

$q_k := q_{k.imp} \cdot 6\ m = 18\ \frac{kN}{m}$

Self weight

$g_k := \rho \cdot A_{beam} \cdot g = 0.386\ \frac{kN}{m}$

Total load:

$q_{d.SLS} := 1 \cdot g_k + 1 \cdot q_k = 18.386\ \frac{kN}{m}$

$q_{d.ULS} := 1.35 \cdot g_k + 1.5 \cdot q_k = 27.521\ \frac{kN}{m}$

$M_d := \frac{q_{d.ULS} \cdot {l_{beam}}^2}{8} = 168.564\ kN \cdot m$ Moment for simply supported beam

Check of bending stress in ULS

The bending stress shall satisfy: $\sigma_{m.y.d} \le f_{m.d}$

Service class 1. Load duration class medium

$$M_d := \frac{q_{d.ULS} \cdot {l_{beam}}^2}{8} = 168.564\ kN \cdot m$$

$$W_y := \frac{b \cdot h^2}{6} = 0.012\ m^3$$ Section modulus

$$\sigma_{m.y.d} := \frac{M_d}{W_y} = 13.936\ MPa$$

$$k_{mod} := 0.8$$ Modification factor

$$k_h := \left(\frac{600}{\frac{h}{mm}}\right)^{0.1} = 0.982$$ Size effect

$$f_{m.k} := 30\ MPa$$ GL30c

$$\gamma_M := 1.25$$ Partial coefficient

$$f_{m.d} := \frac{k_{mod} \cdot k_h \cdot f_{m.k}}{\gamma_M} = 18.853\ MPa$$

$\sigma_{m.y.d} \le f_{m.d}$ OK!

Utilization rate:

$$\frac{\sigma_{m.y.d}}{f_{m.d}} = 73.916\%$$

Check of shear capacity in ULS:

The shear capacity shall satisfy: $\tau_d \le f_{v.d}$

Service class 1. Load duration class medium

$V_d := \frac{q_{d.ULS} \cdot l_{beam}}{2} = 96.322\ kN$ Shear force for simply supported beam

$k_{cr} := 0.857$ For glulam

$b_{ef} := b \cdot k_{cr} = 0.12\ m$ Effective width

$\tau_d := \frac{1.5 \cdot V_d}{b_{ef} \cdot h} = 1.673\ MPa$

$f_{v.k} := 3.5\ MPa$

$k_{mod} := 0.8$ Modification factor

$k_h := \left(\frac{600}{\frac{h}{mm}}\right)^{0.1} = 0.982$ Size effect

$\gamma_M := 1.25$ Partial coefficient

$f_{v.d} := \frac{\left(k_{mod} \cdot k_h \cdot f_{v.k}\right)}{\gamma_M} = 2.2\ MPa$

$\tau_d \le f_{v.d}$ OK!

Utilization rate:

$\frac{\tau_d}{f_{v.d}} = 76\%$

Check of deflection in SLS:

$E_{0.mean} := 13000\ MPa$

$G := 650\ MPa$ $k_{def} := 0.8$

$I := \dfrac{b \cdot h^3}{12} = 0.004\ m^4$

$w_{inst.bend} := \dfrac{5 \cdot q_{d.SLS} \cdot {l_{beam}}^4}{384 \cdot E_{0.mean} \cdot I} = 10.154\ mm$

$w_{inst.shear} := \dfrac{1.2 \cdot q_{d.SLS} \cdot {l_{beam}}^2}{8 \cdot G \cdot A_{beam}} = 2.062\ mm$

$w_{inst} := w_{inst.bend} + w_{inst.shear} = 12.216\ mm$

$w_{fin} := w_{inst} \cdot \left(1 + k_{def}\right) = 21.989\ mm$

$w_{lim} := \dfrac{l_{beam}}{300} = 23.333\ mm$

Utilization rate:

$\dfrac{w_{fin}}{w_{lim}} = 94.239\%$

Check for lateral torsional buckling:

$l_{ef} := l_{beam} \cdot 0.9 = 6.3 \; m$

$E_{0.05} := 10800 \; MPa$

$\sigma_{m.crit} := \frac{\left(0.78 \cdot b^2\right)}{h \cdot l_{ef}} \cdot E_{0.05} = 36.4 \; MPa$

$\lambda_{rel.m} := \sqrt{\frac{f_{m.k}}{\sigma_{m.crit}}} = 0.908$

$k_{crit} := 1.56 - 0.75 \cdot \lambda_{rel.m} = 0.879$

Utilization rate:

$\frac{\sigma_{m.y.d}}{k_{crit} \cdot f_{m.d}} = 84.08\%$

Beam dimensions:

$b := 190\ mm$ Width of beam

$h := 1125\ mm$ Height of beam

$l_{beam} := 12\ m$

$A_{beam} := b \cdot h = 0.214\ m^2$ $\rho := 390\ \frac{kg}{m^3}$ $g := 9.81\ \frac{m}{s^2}$

$V_{beam} := A_{beam} \cdot l_{beam} = 2.565\ m^3$

Imposed load

$q_{k.imp} := 3\ \frac{kN}{m^2}$

$q_k := q_{k.imp} \cdot 6\ m = 18\ \frac{kN}{m}$

Self weight

$g_k := \rho \cdot A_{beam} \cdot g = 0.818\ \frac{kN}{m}$

Total load:

$q_{d.SLS} := 1 \cdot g_k + 1 \cdot q_k = 18.818\ \frac{kN}{m}$

$q_{d.ULS} := 1.35 \cdot g_k + 1.5 \cdot q_k = 28.104\ \frac{kN}{m}$

$M_d := \frac{q_{d.ULS} \cdot {l_{beam}}^2}{8} = 505.872\ kN \cdot m$ Moment for simply supported beam

Check of bending stress in ULS

The bending stress shall satisfy: $\sigma_{m.y.d} \le f_{m.d}$

Service class 1. Load duration class medium

$$M_d := \frac{q_{d.ULS} \cdot l_{beam}^{\ 2}}{8} = 505.872\ kN \cdot m$$

$$W_y := \frac{b \cdot h^2}{6} = 0.04\ m^3$$ Section modulus

$$\sigma_{m.y.d} := \frac{M_d}{W_y} = 12.622\ MPa$$

$$k_{mod} := 0.8$$ Modification factor

$$k_h := \left(\frac{600}{\frac{h}{mm}} \right)^{0.1} = 0.939$$ Size effect

$$f_{m.k} := 30\ MPa$$ GL30c

$$\gamma_M := 1.25$$ Partial coefficient

$$f_{m.d} := \frac{k_{mod} \cdot k_h \cdot f_{m.k}}{\gamma_M} = 18.03\ MPa$$

$\sigma_{m.y.d} \le f_{m.d}$ OK!

Utilization rate:

$$\frac{\sigma_{m.y.d}}{f_{m.d}} = 70.006\%$$

Check of shear capacity in ULS:

The shear capacity shall satisfy: $\tau_d \le f_{v.d}$

Service class 1. Load duration class medium

$V_d := \dfrac{q_{d.ULS} \cdot l_{beam}}{2} = 168.624\ kN$ — Shear force for simply supported beam

$k_{cr} := 0.67$ — For glulam

$b_{ef} := b \cdot k_{cr} = 0.127\ m$ — Effective width

$\tau_d := \dfrac{1.5 \cdot V_d}{b_{ef} \cdot h} = 1.766\ MPa$

$f_{v.k} := 3.5\ MPa$

$k_{mod} := 0.8$ — Modification factor

$k_h := \left(\dfrac{600}{\dfrac{h}{mm}}\right)^{0.1} = 0.939$ — Size effect

$\gamma_M := 1.25$ — Partial coefficient

$f_{v.d} := \dfrac{\left(k_{mod} \cdot k_h \cdot f_{v.k}\right)}{\gamma_M} = 2.104\ MPa$

$\tau_d \le f_{v.d}$ OK!

Utilization rate:

$\dfrac{\tau_d}{f_{v.d}} = 84\%$

Check of deflection in SLS:

$E_{0.mean} := 13000\ MPa$

$G := 650\ MPa$ $k_{def} := 0.8$

$$I := \frac{b \cdot h^3}{12} = 0.023\ m^4$$

$$w_{inst.bend} := \frac{5 \cdot q_{d.SLS} \cdot l_{beam}{}^4}{384 \cdot E_{0.mean} \cdot I} = 17.336\ mm$$

$$w_{inst.shear} := \frac{1.2 \cdot q_{d.SLS} \cdot l_{beam}{}^2}{8 \cdot G \cdot A_{beam}} = 2.926\ mm$$

$$w_{inst} := w_{inst.bend} + w_{inst.shear} = 20.262\ mm$$

$$w_{fin} := w_{inst} \cdot \left(1 + k_{def}\right) = 36.471\ mm$$

$$w_{lim} := \frac{l_{beam}}{300} = 40\ mm$$

Utilization rate:

$$\frac{w_{fin}}{w_{lim}} = 91.179\%$$

Check of lateral torsional buckling:

$$l_{ef} := l_{beam} \cdot 0.9 = 10.8\ m$$

$$E_{0.05} := 10800\ MPa$$

$$\sigma_{m.crit} := \frac{\left(0.78 \cdot b^2\right)}{h \cdot l_{ef}} \cdot E_{0.05} = 25.029\ MPa$$

$$\lambda_{rel.m} := \sqrt{\frac{f_{m.k}}{\sigma_{m.crit}}} = 1.095$$

$$k_{crit} := 1.56 - 0.75 \cdot \lambda_{rel.m} = 0.739$$

Utilization rate:

$$\frac{\sigma_{m.y.d}}{k_{crit} \cdot f_{m.d}} = 94.743\%$$

Beam dimensions:

$b := 190\ mm$ Width of beam

$h := 990\ mm$ Height of beam

$l_{beam} := 7\ m$

$A_{beam} := b \cdot h = 0.188\ m^2$ $\rho := 390\ \frac{kg}{m^3}$ $g := 9.81\ \frac{m}{s^2}$

$V_{beam} := A_{beam} \cdot l_{beam} = 1.317\ m^3$

Imposed load

$q_{k.imp} := 5\ \frac{kN}{m^2}$

$q_k := q_{k.imp} \cdot 6\ m = 30\ \frac{kN}{m}$

Self weight

$g_k := \rho \cdot A_{beam} \cdot g = 0.72\ \frac{kN}{m}$

Total load:

$q_{d.SLS} := 1 \cdot g_k + 1 \cdot q_k = 30.72\ \frac{kN}{m}$

$q_{d.ULS} := 1.35 \cdot g_k + 1.5 \cdot q_k = 45.972\ \frac{kN}{m}$

$M_d := \frac{q_{d.ULS} \cdot {l_{beam}}^2}{8} = 281.576\ kN \cdot m$ Moment for simply supported beam

Check of bending stress in ULS

The bending stress shall satisfy: $\sigma_{m.y.d} \le f_{m.d}$

Service class 1. Load duration class medium

$$M_d := \frac{q_{d.ULS} \cdot l_{beam}^{\ 2}}{8} = 281.576\ kN \cdot m$$

$$W_y := \frac{b \cdot h^2}{6} = 0.031\ m^3$$ Section modulus

$$\sigma_{m.y.d} := \frac{M_d}{W_y} = 9.072\ MPa$$

$$k_{mod} := 0.8$$ Modification factor

$$k_h := \left(\frac{600}{\frac{h}{mm}}\right)^{0.1} = 0.951$$ Size effect

$$f_{m.k} := 30\ MPa$$ GL30c

$$\gamma_M := 1.25$$ Partial coefficient

$$f_{m.d} := \frac{k_{mod} \cdot k_h \cdot f_{m.k}}{\gamma_M} = 18.262\ MPa$$

$\sigma_{m.y.d} \le f_{m.d}$ OK!

Utilization rate:

$$\frac{\sigma_{m.y.d}}{f_{m.d}} = 49.679\%$$

Check of shear capacity in ULS:

The shear capacity shall satisfy: $\tau_d \le f_{v.d}$

Service class 1. Load duration class medium

$$V_d := \frac{q_{d.ULS} \cdot l_{beam}}{2} = 160.9\ kN$$

Shear force for simply supported beam

$$k_{cr} := 0.67$$

For glulam

$$b_{ef} := b \cdot k_{cr} = 0.127\ m$$

Effective width

$$\tau_d := \frac{1.5 \cdot V_d}{b_{ef} \cdot h} = 1.915\ MPa$$

$$f_{v.k} := 3.5\ MPa$$

$$k_{mod} := 0.8$$

Modification factor

$$k_h := \left(\frac{600}{\frac{h}{mm}} \right)^{0.1} = 0.951$$

Size effect

$$\gamma_M := 1.25$$

Partial coefficient

$$f_{v.d} := \frac{\left(k_{mod} \cdot k_h \cdot f_{v.k}\right)}{\gamma_M} = 2.131\ MPa$$

$\tau_d \le f_{v.d}$ OK!

Utilization rate:

$$\frac{\tau_d}{f_{v.d}} = 89.9\%$$

Check of deflection in SLS:

$E_{0.mean} := 13000\ MPa$

$G := 650\ MPa$ $\quad k_{def} := 0.8$

$I := \dfrac{b \cdot h^3}{12} = 0.015\ m^4$

$w_{inst.bend} := \dfrac{5 \cdot q_{d.SLS} \cdot l_{beam}{}^4}{384 \cdot E_{0.mean} \cdot I} = 4.809\ mm$

$w_{inst.shear} := \dfrac{1.2 \cdot q_{d.SLS} \cdot l_{beam}{}^2}{8 \cdot G \cdot A_{beam}} = 1.847\ mm$

$w_{inst} := w_{inst.bend} + w_{inst.shear} = 6.655\ mm$

$w_{fin} := w_{inst} \cdot \left(1 + k_{def}\right) = 11.98\ mm$

$w_{lim} := \dfrac{l_{beam}}{300} = 23.333\ mm$

Utilization rate:

$\dfrac{w_{fin}}{w_{lim}} = 51.342\%$

Check for lateral torsional buckling:

$$l_{ef} := l_{beam} \cdot 0.9 = 6.3\ m$$

$$E_{0.05} := 10800\ MPa$$

$$\sigma_{m.crit} := \frac{\left(0.78 \cdot b^2\right)}{h \cdot l_{ef}} \cdot E_{0.05} = 48.758\ MPa$$

$$\lambda_{rel.m} := \sqrt{\frac{f_{m.k}}{\sigma_{m.crit}}} = 0.784$$

$$k_{crit} := 1.56 - 0.75 \cdot \lambda_{rel.m} = 0.972$$

Utilization rate:

$$\frac{\sigma_{m.y.d}}{k_{crit} \cdot f_{m.d}} = 51.125\%$$

Beam dimensions:

$b := 215\ mm$ Width of beam

$h := 1440\ mm$ Height of beam

$l_{beam} := 12\ m$

$A_{beam} := b \cdot h = 0.31\ m^2$ $\rho := 390\ \frac{kg}{m^3}$ $g := 9.81\ \frac{m}{s^2}$

$V_{beam} := A_{beam} \cdot l_{beam} = 3.715\ m^3$

Imposed load

$q_{k.imp} := 5\ \frac{kN}{m^2}$

$q_k := q_{k.imp} \cdot 6\ m = 30\ \frac{kN}{m}$

Self weight

$g_k := \rho \cdot A_{beam} \cdot g = 1.184\ \frac{kN}{m}$

Total load:

$q_{d.SLS} := 1 \cdot g_k + 1 \cdot q_k = 31.184\ \frac{kN}{m}$

$q_{d.ULS} := 1.35 \cdot g_k + 1.5 \cdot q_k = 46.599\ \frac{kN}{m}$

$M_d := \frac{q_{d.ULS} \cdot {l_{beam}}^2}{8} = 838.783\ kN \cdot m$ Moment for simply supported beam

Check of bending stress in ULS

The bending stress shall satisfy: $\sigma_{m.y.d} \le f_{m.d}$

Service class 1. Load duration class medium

$$M_d := \frac{q_{d.ULS} \cdot l_{beam}^{\ 2}}{8} = 838.783 \ kN \cdot m$$

$$W_y := \frac{b \cdot h^2}{6} = 0.074 \ m^3$$ Section modulus

$$\sigma_{m.y.d} := \frac{M_d}{W_y} = 11.289 \ MPa$$

$k_{mod} := 0.8$ Modification factor

$$k_h := \left(\frac{600}{\frac{h}{mm}} \right)^{0.1} = 0.916$$ Size effect

$f_{m.k} := 30 \ MPa$ GL30c

$\gamma_M := 1.25$ Partial coefficient

$$f_{m.d} := \frac{k_{mod} \cdot k_h \cdot f_{m.k}}{\gamma_M} = 17.591 \ MPa$$

$\sigma_{m.y.d} \le f_{m.d}$ OK!

Utilization rate:

$$\frac{\sigma_{m.y.d}}{f_{m.d}} = 64.174\%$$

Check of shear capacity in ULS:

The shear capacity shall satisfy: $\tau_d \le f_{v.d}$

Service class 1. Load duration class medium

$V_d := \frac{q_{d.ULS} \cdot l_{beam}}{2} = 279.594\ kN$ Shear force for simply supported beam

$k_{cr} := 0.67$ For glulam

$b_{ef} := b \cdot k_{cr} = 0.144\ m$ Effective width

$\tau_d := \frac{1.5 \cdot V_d}{b_{ef} \cdot h} = 2.022\ MPa$

$f_{v.k} := 3.5\ MPa$

$k_{mod} := 0.8$ Modification factor

$k_h := \left(\frac{600}{\frac{h}{mm}} \right)^{0.1} = 0.916$ Size effect

$\gamma_M := 1.25$ Partial coefficient

$f_{v.d} := \frac{\left(k_{mod} \cdot k_h \cdot f_{v.k}\right)}{\gamma_M} = 2.052\ MPa$

$\tau_d \le f_{v.d}$ OK!

Utilization rate:

$\frac{\tau_d}{f_{v.d}} = 98.5\%$

Check of deflection in SLS:

$E_{0.mean} := 13000\ MPa$

$G := 650\ MPa$ $\quad$ $k_{def} := 0.8$

$I := \frac{b \cdot h^3}{12} = 0.053\ m^4$

$w_{inst.bend} := \frac{5 \cdot q_{d.SLS} \cdot l_{beam}{}^4}{384 \cdot E_{0.mean} \cdot I} = 12.106\ mm$

$w_{inst.shear} := \frac{1.2 \cdot q_{d.SLS} \cdot l_{beam}{}^2}{8 \cdot G \cdot A_{beam}} = 3.347\ mm$

$w_{inst} := w_{inst.bend} + w_{inst.shear} = 15.454\ mm$

$w_{fin} := w_{inst} \cdot \left(1 + k_{def}\right) = 27.816\ mm$

$w_{lim} := \frac{l_{beam}}{300} = 40\ mm$

Utilization rate:

$\frac{w_{fin}}{w_{lim}} = 69.541\%$

Check for lateral torsional buckling:

$$l_{ef} := l_{beam} \cdot 0.9 = 10.8\ m$$

$$E_{0.05} := 10800\ MPa$$

$$\sigma_{m.crit} := \frac{\left(0.78 \cdot b^2\right)}{h \cdot l_{ef}} \cdot E_{0.05} = 25.039\ MPa$$

$$\lambda_{rel.m} := \sqrt{\frac{f_{m.k}}{\sigma_{m.crit}}} = 1.095$$

$$k_{crit} := 1.56 - 0.75 \cdot \lambda_{rel.m} = 0.739$$

Utilization rate:

$$\frac{\sigma_{m.y.d}}{k_{crit} \cdot f_{m.d}} = 86.833\%$$

B

Appendix: Calculations of Connection

DOWEL 12MM

$d := 12$ $\quad t_{timber} := 100$ $\quad t_f := 13$

$f_{u.k} := 800$ $\quad \rho_k := 390$ $\quad t_1 := 100$ $\quad k_{mod} := 0.8$ $\quad \gamma_M := 1.3$

$k_{90} := 1.35 + 0.015 \cdot d = 1.53$

$\alpha := 90\ deg$

$$f_{h.0.k} := 0.082 \cdot (1 - 0.01 \cdot d) \cdot \rho_k \cdot \frac{N}{mm^2} = 28.142\ \frac{N}{mm^2}$$

$$f_{h.\alpha.k} := \frac{f_{h.0.k}}{k_{90} \cdot \left((\sin(\alpha))^2 + (\cos(\alpha))^2\right)} = 18.394\ \frac{N}{mm^2}$$

$f_{h.k} := f_{h.\alpha.k}$

$$M_{y.Rk} := 0.3 \cdot f_{u.k} \cdot d^{2.6} \cdot N \cdot mm = \left(1.535 \cdot 10^5\right)\ N \cdot mm$$

$$F_{v.Rk1} := f_{h.k} \cdot d \cdot t_1 \cdot mm^2 = 22.072\ kN \qquad \text{(c)}$$

$$F_{v.Rk2} := f_{h.k} \cdot d \cdot t_1 \cdot mm^2 \cdot \left(\sqrt{2 + \frac{4 \cdot M_{y.Rk}}{f_{h.k} \cdot d \cdot {t_1}^2 \cdot mm^3}} - 1\right) = 11.243\ kN \qquad \text{(d)}$$

$$F_{v.Rk3} := 2.3 \cdot \sqrt{\frac{M_{y.Rk}}{N \cdot mm} \cdot \frac{f_{h.k}}{\frac{N}{mm^2}} \cdot d} \cdot N = 13.387\ kN \qquad \text{(e)}$$

$$F_{v.Rk} := min\left(F_{v.Rk1}, F_{v.Rk2}, F_{v.Rk3}\right) = 11.243\ kN$$

$$F_{v.Rd} := k_{mod} \cdot \frac{F_{v.Rk}}{\gamma_M} = 6.919\ kN$$

$\rho_{mean} := 430$

$$K_{ser} := 2 \cdot \left(\frac{{\rho_{mean}}^{1.5}\ d}{23} \right) \frac{N}{mm} = \left(9.304 \cdot 10^{3}\right) \frac{N}{mm}$$

$a_1 := 3 \cdot d \cdot mm = 36\ mm$

$a_2 := 3 \cdot d \cdot mm = 36\ mm$

$a_3 := \max\left(7 \cdot d, 80\right) \cdot mm = 84\ mm$

$a_4 := 4 \cdot d \cdot mm = 48\ mm$

DOWEL 16MM

$d := 16$

$f_{u.k} := 800$ $\rho_k := 390$ $t_1 := 100$ $k_{mod} := 0.8$ $\gamma_M := 1.3$

$k_{90} := 1.35 + 0.015 \cdot d = 1.59$

$\alpha := 90$

$$f_{h.0.k} := 0.082 \cdot (1 - 0.01 \cdot d) \cdot \rho_k \cdot \frac{N}{mm^2} = 26.863 \ \frac{N}{mm^2}$$

$$f_{h.\alpha.k} := \frac{f_{h.0.k}}{k_{90} \cdot \left((\sin(\alpha))^2 + (\cos(\alpha))^2 \right)} = 16.895 \ \frac{N}{mm^2}$$

$f_{h.k} := f_{h.\alpha.k}$

$$M_{y.Rk} := 0.3 \cdot f_{u.k} \cdot d^{2.6} \cdot N \cdot mm = \left(3.243 \cdot 10^5\right) \ N \cdot mm$$

$$F_{v.Rk1} := f_{h.k} \cdot d \cdot t_1 \cdot mm^2 = 27.032 \ kN \qquad \text{(c)}$$

$$F_{v.Rk2} := f_{h.k} \cdot d \cdot t_1 \cdot mm^2 \cdot \left(\sqrt{2 + \frac{4 \cdot M_{y.Rk}}{f_{h.k} \cdot d \cdot {t_1}^2 \cdot mm^3}} - 1 \right) = 15.537 \ kN \qquad \text{(d)}$$

$$F_{v.Rk3} := 2.3 \cdot \sqrt{\frac{M_{y.Rk}}{N \cdot mm} \cdot \frac{f_{h.k}}{\frac{N}{mm^2}} \cdot d} \cdot N = 21.534 \ kN \qquad \text{(e)}$$

$$F_{v.Rk} := min\left(F_{v.Rk1}, F_{v.Rk2}, F_{v.Rk3}\right) = 15.537 \ kN$$

$$F_{v.Rd} := k_{mod} \cdot \frac{F_{v.Rk}}{\gamma_M} = 9.561 \ kN$$

$\rho_{mean} := 430$

$K_{ser} := 2 \cdot \left(\frac{\rho_{mean}^{1.5} \ d}{23} \right) \frac{N}{mm} = \left(1.2406 \cdot 10^{4}\right) \frac{N}{mm}$

$a_1 := 3 \cdot d \cdot mm = 48 \ mm$

$a_2 := 3 \cdot d \cdot mm = 48 \ mm$

$a_3 := \max\left(7 \cdot d, 80\right) \cdot mm = 112 \ mm$

$a_4 := 4 \cdot d \cdot mm = 64 \ mm$

DOWEL 20MM

$d := 20$

$f_{u.k} := 800 \qquad \rho_k := 390 \qquad t_1 := 100 \qquad k_{mod} := 0.8 \qquad \gamma_M := 1.3$

$k_{90} := 1.35 + 0.015 \cdot d = 1.65$

$\alpha := 90\ deg$

$$f_{h.0.k} := 0.082 \cdot (1 - 0.01 \cdot d) \cdot \rho_k \cdot \frac{N}{mm^2} = 25.584\ \frac{N}{mm^2}$$

$$f_{h.\alpha.k} := \frac{f_{h.0.k}}{k_{90} \cdot \left((\sin(\alpha))^2 + (\cos(\alpha))^2\right)} = 15.505\ \frac{N}{mm^2}$$

$f_{h.k} := f_{h.\alpha.k}$

$$M_{y.Rk} := 0.3 \cdot f_{u.k} \cdot d^{2.6} \cdot N \cdot mm = \left(5.793 \cdot 10^5\right)\ N \cdot mm$$

$$F_{v.Rk1} := f_{h.k} \cdot d \cdot t_1 \cdot mm^2 = 31.011\ kN \qquad \text{(c)}$$

$$F_{v.Rk2} := f_{h.k} \cdot d \cdot t_1 \cdot mm^2 \cdot \left(\sqrt{2 + \frac{4 \cdot M_{y.Rk}}{f_{h.k} \cdot d \cdot {t_1}^2 \cdot mm^3}} - 1\right) = 20.389\ kN \qquad \text{(d)}$$

$$F_{v.Rk3} := 2.3 \cdot \sqrt{\frac{M_{y.Rk}}{N \cdot mm} \cdot \frac{f_{h.k}}{\frac{N}{mm^2}} \cdot d} \cdot N = 30.827\ kN \qquad \text{(e)}$$

$$F_{v.Rk} := min\left(F_{v.Rk1}, F_{v.Rk2}, F_{v.Rk3}\right) = 20.389\ kN$$

$$F_{v.Rd} := k_{mod} \cdot \frac{F_{v.Rk}}{\gamma_M} = 12.547\ kN$$

$$\rho_{mean} := 430$$

$$K_{ser} := 2 \cdot \left(\frac{\rho_{mean}^{\ 1.5}\ d}{23} \right) \frac{N}{mm} = \left(1.5507 \cdot 10^{4}\right) \frac{N}{mm}$$

$$a_1 := 3 \cdot d \cdot mm = 60\ mm$$

$$a_2 := 3 \cdot d \cdot mm = 60\ mm$$

$$a_3 := \max\left(7 \cdot d, 80\right) \cdot mm = 140\ mm$$

$$a_4 := 4 \cdot d \cdot mm = 80\ mm$$

DOWEL 24MM

$d := 24$

$f_{u.k} := 800$ $\rho_k := 390$ $t_1 := 100$ $k_{mod} := 0.8$ $\gamma_M := 1.3$

$k_{90} := 1.35 + 0.015 \cdot d = 1.71$

$\alpha := 90 \ deg$

$$f_{h.0.k} := 0.082 \cdot (1 - 0.01 \cdot d) \cdot \rho_k \cdot \frac{N}{mm^2} = 24.305 \ \frac{N}{mm^2}$$

$$f_{h.\alpha.k} := \frac{f_{h.0.k}}{k_{90} \cdot \left((\sin(\alpha))^2 + (\cos(\alpha))^2\right)} = 14.213 \ \frac{N}{mm^2}$$

$f_{h.k} := f_{h.\alpha.k}$

$$M_{y.Rk} := 0.3 \cdot f_{u.k} \cdot d^{2.6} \cdot N \cdot mm = \left(9.306 \cdot 10^5\right) \ N \cdot mm$$

$$F_{v.Rk1} := f_{h.k} \cdot d \cdot t_1 \cdot mm^2 = 34.112 \ kN \qquad \text{(c)}$$

$$F_{v.Rk2} := f_{h.k} \cdot d \cdot t_1 \cdot mm^2 \cdot \left(\sqrt{2 + \frac{4 \cdot M_{y.Rk}}{f_{h.k} \cdot d \cdot {t_1}^2 \cdot mm^3}} - 1\right) = 25.863 \ kN \qquad \text{(d)}$$

$$F_{v.Rk3} := 2.3 \cdot \sqrt{\frac{M_{y.Rk}}{N \cdot mm} \cdot \frac{f_{h.k}}{\frac{N}{mm^2}} \cdot d} \cdot N = 40.979 \ kN \qquad \text{(e)}$$

$$F_{v.Rk} := min\left(F_{v.Rk1}, F_{v.Rk2}, F_{v.Rk3}\right) = 25.863 \ kN$$

$$F_{v.Rd} := k_{mod} \cdot \frac{F_{v.Rk}}{\gamma_M} = 15.916 \ kN$$

$$\rho_{mean} := 430$$

$$K_{ser} := 2 \cdot \left(\frac{{\rho_{mean}}^{1.5}\ d}{23} \right) \frac{N}{mm} = \left(1.8609 \cdot 10^{4}\right) \frac{N}{mm}$$

$$a_1 := 3 \cdot d \cdot mm = 72\ mm$$

$$a_2 := 3 \cdot d \cdot mm = 72\ mm$$

$$a_3 := \max\left(7 \cdot d, 80\right) \cdot mm = 168\ mm$$

$$a_4 := 4 \cdot d \cdot mm = 96\ mm$$

SCREW 6MM

$d := 6$

$f_{u.k} := 800$ $\rho_k := 390$ $t_{pen} := 50$ $t_f := 13$ $L_{screw} := 100$

$d_{ef} := d \cdot 0.75 = 4.5$ $k_{mod} := 0.8$ $\gamma_M := 1.3$ $t_1 := L_{screw} - t_f = 87$

Lateral capacity of the screw

$k_{90} := 1.35 + 0.015 \cdot d = 1.44$

$\alpha := 45\ deg$

$$f_{h.0.k} := 0.082 \cdot (1 - 0.01 \cdot d) \cdot \rho_k \cdot \frac{N}{mm^2} = 30.061\ \frac{N}{mm^2}$$

$$f_{h.\alpha.k} := \frac{f_{h.0.k}}{k_{90} \cdot \left((\sin(\alpha))^2 + (\cos(\alpha))^2\right)} = 20.876\ \frac{N}{mm^2}$$

$f_{h.k} := f_{h.\alpha.k}$

$M_{y.Rk} := 0.3 \cdot f_{u.k} \cdot d^{2.6} \cdot N \cdot mm = \left(2.532 \cdot 10^4\right)\ N \cdot mm$

Axial resistance of the screw

$f_{ax.k} := 0.52 \cdot d^{-0.5} \cdot t_{pen}{}^{-0.1} \cdot \rho_k{}^{0.8} = 16.978$

$$k_d := min\left(1, \frac{d}{8}\right) = 0.75$$

$$F_{ax.Rk} := \frac{f_{ax.k} \cdot d \cdot t_{pen} \cdot k_d \cdot N}{1.2 \cdot (\cos(\alpha))^2 + (\sin(\alpha))^2} = 3.473\ kN$$

$$F_{v.Rk1} := f_{h.k} \cdot d_{ef} \cdot t_1 \cdot mm^2 = 8.173\ kN \tag{c}$$

$$F_{v.Rk2} := f_{h.k} \cdot d_{ef} \cdot t_1 \cdot mm^2 \cdot \left(\sqrt{2 + \frac{4 \cdot M_{y.Rk}}{f_{h.k} \cdot d \cdot t_1^{\ 2} \cdot mm^3}} - 1 \right) + \frac{F_{ax.Rk}}{4} = 4.558\ kN \tag{d}$$

$$F_{v.Rk3} := 2.3 \cdot \sqrt{\frac{M_{y.Rk}}{N \cdot mm} \cdot \frac{f_{h.k}}{\frac{N}{mm^2}} \cdot d_{ef}} \cdot N + \frac{F_{ax.Rk}}{4} = 4.415\ kN \tag{e}$$

$$F_{v.Rk} := min\left(F_{v.Rk1}, F_{v.Rk2}, F_{v.Rk3}\right) = 4.415\ kN$$

$$F_{v.Rd} := k_{mod} \cdot \frac{F_{v.Rk}}{\gamma_M} = 2.717\ kN$$

$$\rho_{mean} := 430$$

$$K_{ser} := 2 \cdot \left(\frac{\rho_{mean}^{\ 1.5}\ d}{23} \right) \frac{N}{mm} = \left(4.652 \cdot 10^3\right) \frac{N}{mm}$$

$$a_1 := 7 \cdot d \cdot mm = 42\ mm$$

$$a_2 := 5 \cdot d \cdot mm = 30\ mm$$

$$a_3 := 10 \cdot d \cdot mm = 60\ mm$$

$$a_4 := 4 \cdot d \cdot mm = 24\ mm$$

SCREW 8MM

$d := 8$

$f_{u.k} := 800$ $\rho_k := 390$ $t_{pen} := 52$ $t_f := 13$ $L_{screw} := 100$

$d_{ef} := d \cdot 0.75 = 6$ $k_{mod} := 0.8$ $\gamma_M := 1.3$ $t_1 := L_{screw} - t_f = 87$

Lateral capacity of the screw

$k_{90} := 1.35 + 0.015 \cdot d = 1.47$

$\alpha := 45\ deg$

$$f_{h.0.k} := 0.082 \cdot (1 - 0.01 \cdot d) \cdot \rho_k \cdot \frac{N}{mm^2} = 29.422\ \frac{N}{mm^2}$$

$$f_{h.\alpha.k} := \frac{f_{h.0.k}}{k_{90} \cdot \left((\sin(\alpha))^2 + (\cos(\alpha))^2\right)} = 20.015\ \frac{N}{mm^2}$$

$f_{h.k} := f_{h.\alpha.k}$

$M_{y.Rk} := 0.3 \cdot f_{u.k} \cdot d^{2.6} \cdot N \cdot mm = \left(5.349 \cdot 10^4\right)\ N \cdot mm$

Axial resistance of the screw

$f_{ax.k} := 0.52 \cdot d^{-0.5} \cdot t_{pen}{}^{-0.1} \cdot \rho_k{}^{0.8} = 14.646$

$$k_d := min\left(1, \frac{d}{8}\right) = 1$$

$$F_{ax.Rk} := \frac{f_{ax.k} \cdot d \cdot t_{pen} \cdot k_d \cdot N}{1.2 \cdot (\cos(\alpha))^2 + (\sin(\alpha))^2} = 5.539\ kN$$

$$F_{v.Rk1} := f_{h.k} \cdot d_{ef} \cdot t_1 \cdot mm^2 = 10.448\ kN \qquad \text{(c)}$$

$$F_{v.Rk2} := f_{h.k} \cdot d_{ef} \cdot t_1 \cdot mm^2 \cdot \left(\sqrt{2 + \frac{4 \cdot M_{y.Rk}}{f_{h.k} \cdot d \cdot t_1^{\,2} \cdot mm^3}} - 1 \right) + \frac{F_{ax.Rk}}{4} = 6.351\ kN \qquad \text{(d)}$$

$$F_{v.Rk3} := 2.3 \cdot \sqrt{\frac{M_{y.Rk}}{N \cdot mm} \cdot \frac{f_{h.k}}{\frac{N}{mm^2}} \cdot d_{ef}} \cdot N + \frac{F_{ax.Rk}}{4} = 7.214\ kN \qquad \text{(e)}$$

$$F_{v.Rk} := min\left(F_{v.Rk1}, F_{v.Rk2}, F_{v.Rk3}\right) = 6.351\ kN$$

$$F_{v.Rd} := k_{mod} \cdot \frac{F_{v.Rk}}{\gamma_M} = 3.908\ kN$$

$$\rho_{mean} := 430$$

$$K_{ser} := 2 \cdot \left(\frac{\rho_{mean}^{\ 1.5}\ d}{23} \right) \frac{N}{mm} = \left(6.203 \cdot 10^3\right) \frac{N}{mm}$$

$$a_1 := 7 \cdot d \cdot mm = 56\ mm$$

$$a_2 := 5 \cdot d \cdot mm = 40\ mm$$

$$a_3 := 10 \cdot d \cdot mm = 80\ mm$$

$$a_4 := 4 \cdot d \cdot mm = 32\ mm$$

SCREW 10MM

$d := 10$

$f_{u.k} := 800 \qquad \rho_k := 390 \qquad t_{pen} := 52 \qquad t_f := 13 \qquad L_{screw} := 100$

$d_{ef} := d \cdot 0.75 = 7.5 \qquad k_{mod} := 0.8 \qquad \gamma_M := 1.3 \qquad t_1 := L_{screw} - t_f = 87$

Lateral capacity of the screw

$k_{90} := 1.35 + 0.015 \cdot d = 1.5$

$\alpha := 45 \ \boldsymbol{deg}$

$$f_{h.0.k} := 0.082 \cdot (1 - 0.01 \cdot d) \cdot \rho_k \cdot \frac{\boldsymbol{N}}{\boldsymbol{mm}^2} = 28.782 \ \frac{\boldsymbol{N}}{\boldsymbol{mm}^2}$$

$$f_{h.\alpha.k} := \frac{f_{h.0.k}}{k_{90} \cdot \left((\sin(\alpha))^2 + (\cos(\alpha))^2\right)} = 19.188 \ \frac{\boldsymbol{N}}{\boldsymbol{mm}^2}$$

$f_{h.k} := f_{h.\alpha.k}$

$M_{y.Rk} := 0.3 \cdot f_{u.k} \cdot d^{2.6} \cdot \boldsymbol{N} \cdot \boldsymbol{mm} = \left(9.555 \cdot 10^4\right) \ \boldsymbol{N} \cdot \boldsymbol{mm}$

Axial resistance of the screw

$f_{ax.k} := 0.52 \cdot d^{-0.5} \cdot t_{pen}^{\ -0.1} \cdot \rho_k^{\ 0.8} = 13.099$

$$k_d := min\left(1, \frac{d}{8}\right) = 1$$

$$F_{ax.Rk} := \frac{f_{ax.k} \cdot d \cdot t_{pen} \cdot k_d \cdot \boldsymbol{N}}{1.2 \cdot (\cos(\alpha))^2 + (\sin(\alpha))^2} = 6.192 \ \boldsymbol{kN}$$

$$F_{v.Rk1} := f_{h.k} \cdot d_{ef} \cdot t_1 \cdot mm^2 = 12.52\ kN$$ (c)

$$F_{v.Rk2} := f_{h.k} \cdot d_{ef} \cdot t_1 \cdot mm^2 \cdot \left(\sqrt{2 + \frac{4 \cdot M_{y.Rk}}{f_{h.k} \cdot d \cdot t_1^{\ 2} \cdot mm^3}} - 1\right) + \frac{F_{ax.Rk}}{4} = 7.863\ kN$$ (d)

$$F_{v.Rk3} := 2.3 \cdot \sqrt{\frac{M_{y.Rk}}{N \cdot mm} \cdot \frac{f_{h.k}}{\frac{N}{mm^2}} \cdot d_{ef}} \cdot N + \frac{F_{ax.Rk}}{4} = 10.077\ kN$$ (e)

$$F_{v.Rk} := min\left(F_{v.Rk1}, F_{v.Rk2}, F_{v.Rk3}\right) = 7.863\ kN$$

$$F_{v.Rd} := k_{mod} \cdot \frac{F_{v.Rk}}{\gamma_M} = 4.839\ kN$$

$$\rho_{mean} := 430$$

$$K_{ser} := 2 \cdot \left(\frac{\rho_{mean}^{\ 1.5}\ d}{23}\right) \frac{N}{mm} = \left(7.754 \cdot 10^3\right) \frac{N}{mm}$$

$$a_1 := 7 \cdot d \cdot mm = 70\ mm$$

$$a_2 := 5 \cdot d \cdot mm = 50\ mm$$

$$a_3 := 10 \cdot d \cdot mm = 100\ mm$$

$$a_4 := 4 \cdot d \cdot mm = 40\ mm$$

SCREW 12MM

$d := 12$

$f_{u.k} := 800$ $\rho_k := 390$ $t_{pen} := 80$ $t_f := 13$ $L_{screw} := 120$

$d_{ef} := d \cdot 0.75 = 9$ $k_{mod} := 0.8$ $\gamma_M := 1.3$ $t_1 := L_{screw} - t_f = 107$

Lateral capacity of the screw

$k_{90} := 1.35 + 0.015 \cdot d = 1.53$

$\alpha := 45\ deg$

$$f_{h.0.k} := 0.082 \cdot (1 - 0.01 \cdot d) \cdot \rho_k \cdot \frac{N}{mm^2} = 28.142\ \frac{N}{mm^2}$$

$$f_{h.\alpha.k} := \frac{f_{h.0.k}}{k_{90} \cdot \left((\sin(\alpha))^2 + (\cos(\alpha))^2\right)} = 18.394\ \frac{N}{mm^2}$$

$f_{h.k} := f_{h.\alpha.k}$

$M_{y.Rk} := 0.3 \cdot f_{u.k} \cdot d^{2.6} \cdot N \cdot mm = \left(1.535 \cdot 10^5\right)\ N \cdot mm$

Axial resistance of the screw

$f_{ax.k} := 0.52 \cdot d^{-0.5} \cdot t_{pen}{}^{-0.1} \cdot \rho_k{}^{0.8} = 11.454$

$$k_d := min\left(1, \frac{d}{8}\right) = 1$$

$$F_{ax.Rk} := \frac{f_{ax.k} \cdot d \cdot t_{pen} \cdot k_d \cdot N}{1.2 \cdot (\cos(\alpha))^2 + (\sin(\alpha))^2} = 9.996\ kN$$

$$F_{v.Rk1} := f_{h.k} \cdot d_{ef} \cdot t_1 \cdot mm^2 = 17.713\ kN \qquad \text{(c)}$$

$$F_{v.Rk2} := f_{h.k} \cdot d_{ef} \cdot t_1 \cdot mm^2 \cdot \left(\sqrt{2 + \frac{4 \cdot M_{y.Rk}}{f_{h.k} \cdot d \cdot {t_1}^2 \cdot mm^3}} - 1\right) + \frac{F_{ax.Rk}}{4} = 11.314\ kN \qquad \text{(d)}$$

$$F_{v.Rk3} := 2.3 \cdot \sqrt{\frac{M_{y.Rk}}{N \cdot mm} \cdot \frac{f_{h.k}}{\frac{N}{mm^2}} \cdot d_{ef}} \cdot N + \frac{F_{ax.Rk}}{4} = 14.093\ kN \qquad \text{(e)}$$

$$F_{v.Rk} := min\left(F_{v.Rk1}, F_{v.Rk2}, F_{v.Rk3}\right) = 11.314\ kN$$

$$F_{v.Rd} := k_{mod} \cdot \frac{F_{v.Rk}}{\gamma_M} = 6.962\ kN$$

$$\rho_{mean} := 430$$

$$K_{ser} := 2 \cdot \left(\frac{{\rho_{mean}}^{1.5}\ d}{23}\right) \frac{N}{mm} = \left(9.304 \cdot 10^3\right) \frac{N}{mm}$$

$$a_1 := 7 \cdot d \cdot mm = 84\ mm$$

$$a_2 := 5 \cdot d \cdot mm = 60\ mm$$

$$a_3 := 10 \cdot d \cdot mm = 120\ mm$$

$$a_4 := 4 \cdot d \cdot mm = 48\ mm$$

C

Appendix: Figures of Results

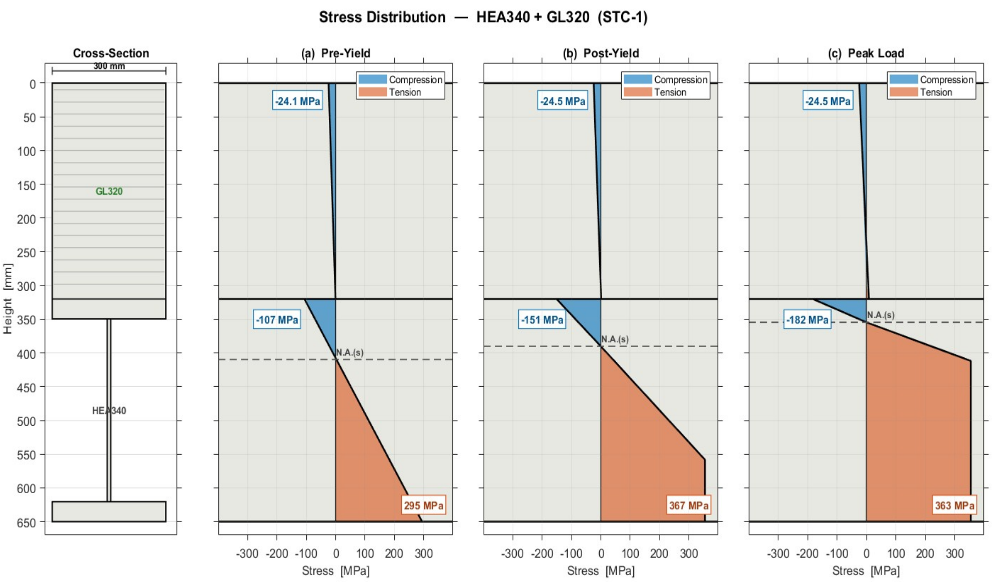

Figure C.1: Stress distribution of STC-1 at 12 m span under office load.

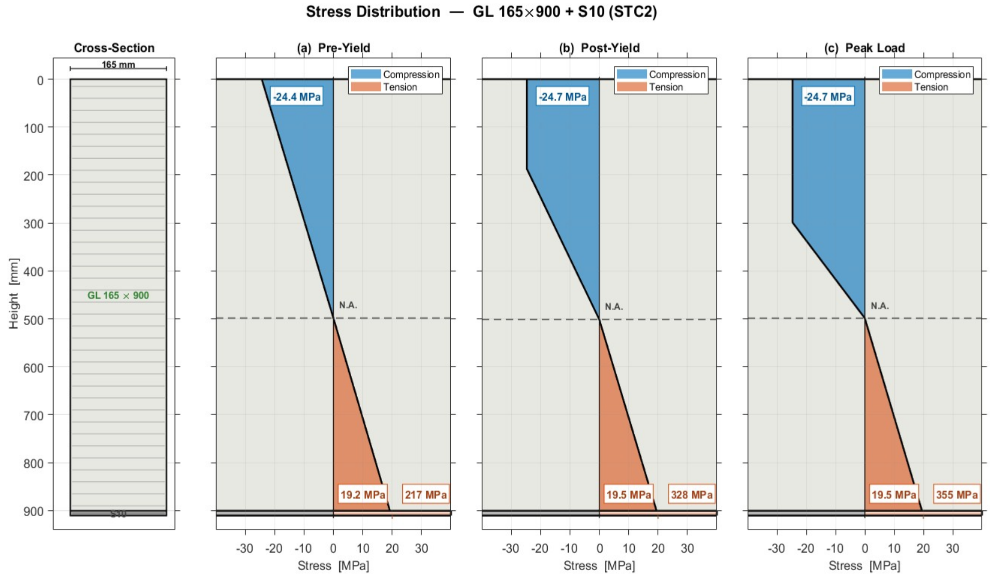

Figure C.2: Stress distribution of STC-2 at 12 m span under office load.

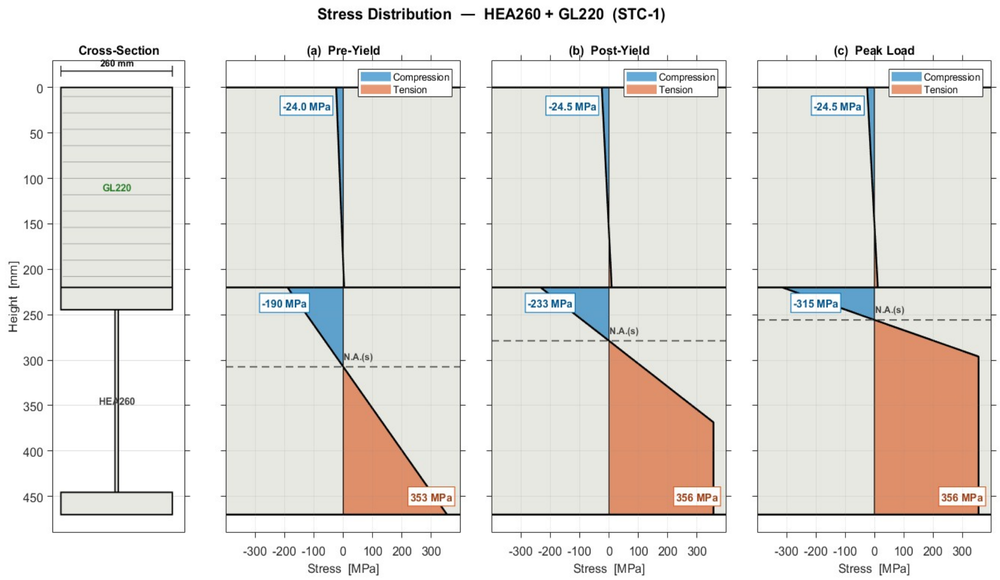

Figure C.3: Stress distribution of STC-1 at 7 m span under shopping mall load.

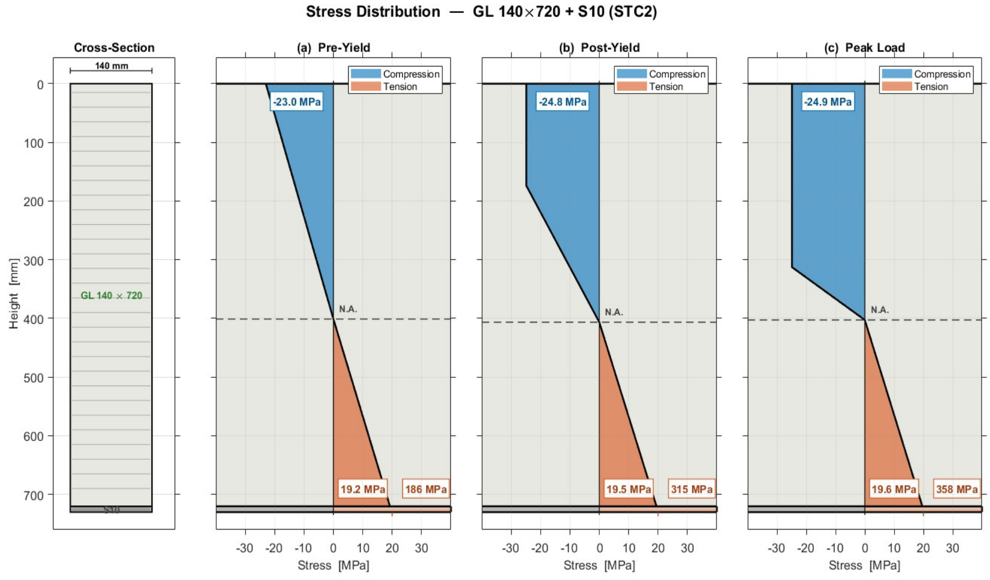

Figure C.4: Stress distribution of STC-2 at 7 m span under shopping mall load.

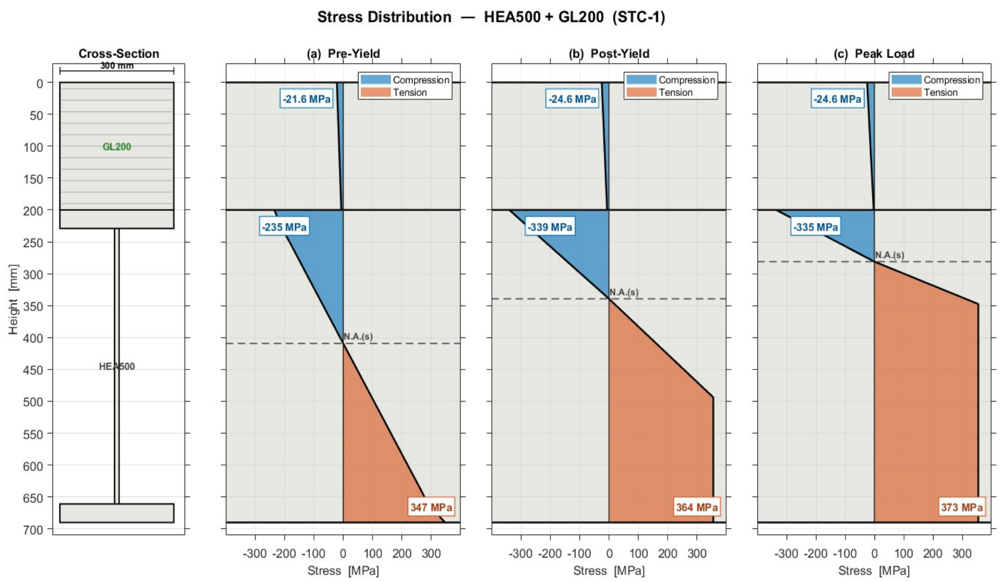

Figure C.5: Stress distribution of STC-1 at 12 m span under shopping mall load.

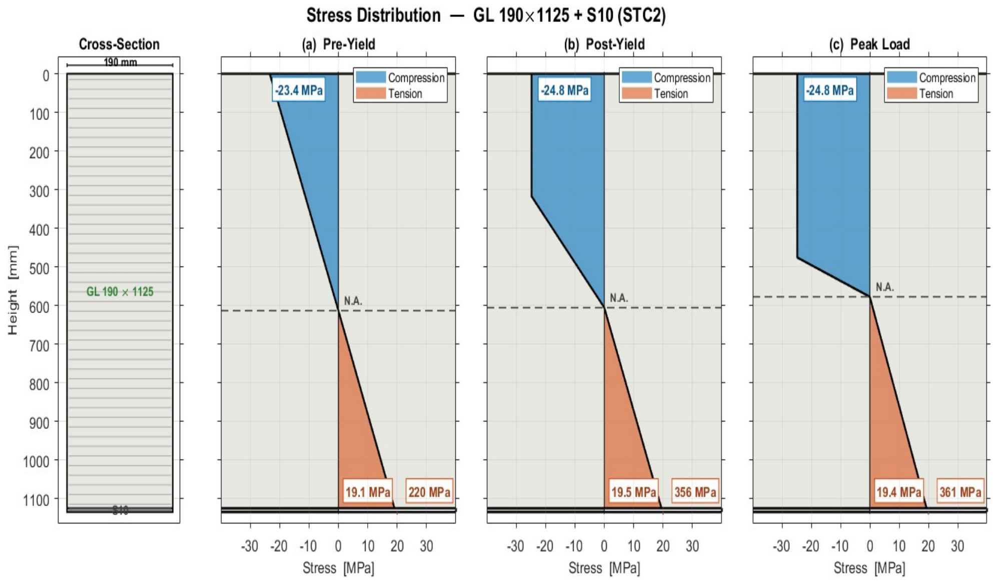

Figure C.6: Stress distribution of STC-2 at 12 m span under shopping mall load.

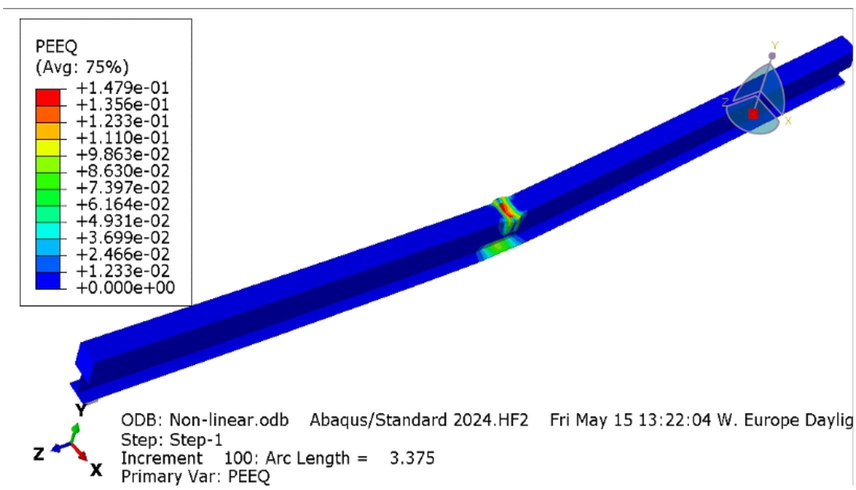

Figure C.7: Failure mode of STC-1 at 12 m span under office load.

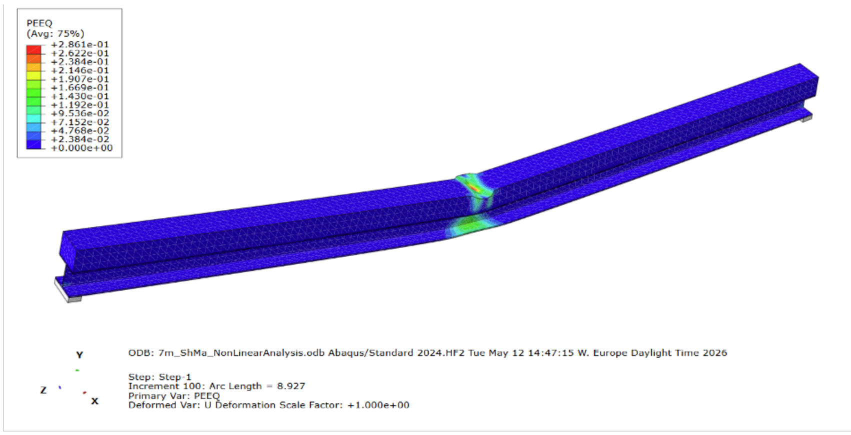

Figure C.8: Failure mode of STC-1 at 7 m span under shopping mall load.

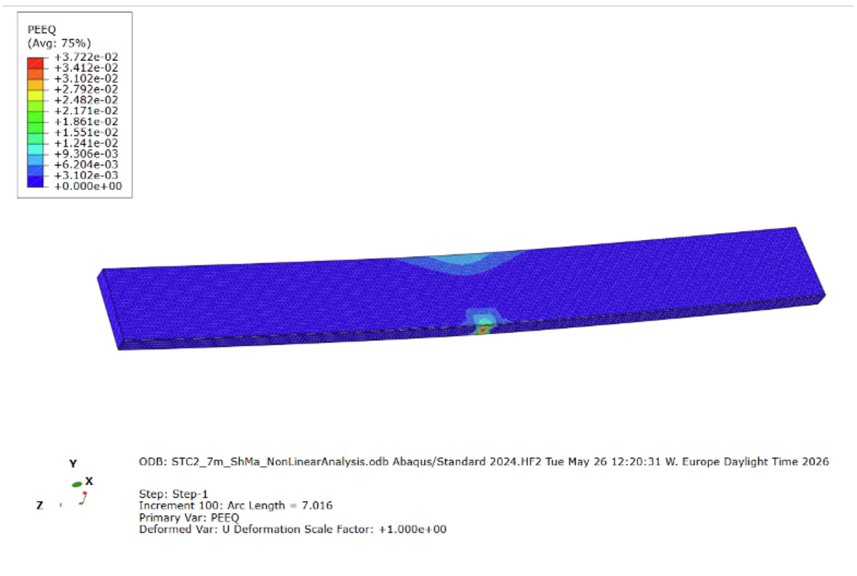

Figure C.9: Failure mode of STC-2 at 7 m span under shopping mall load.

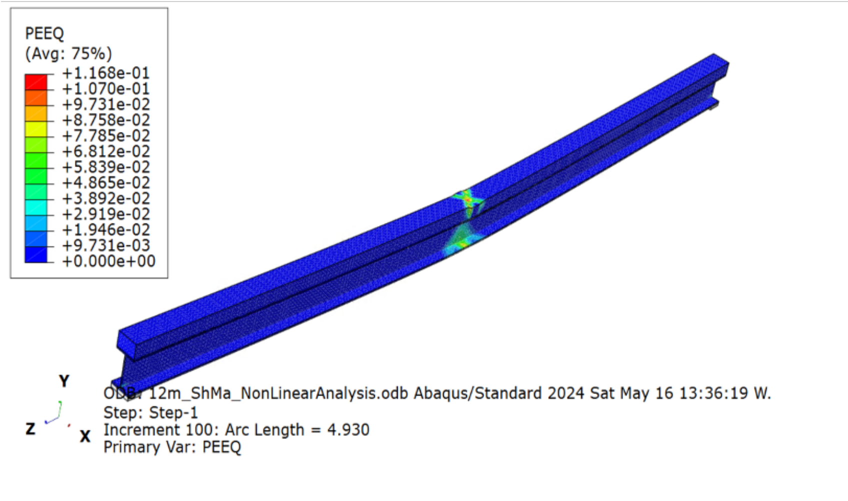

Figure C.10: Failure mode of STC-1 at 12 m span under shopping mall load.

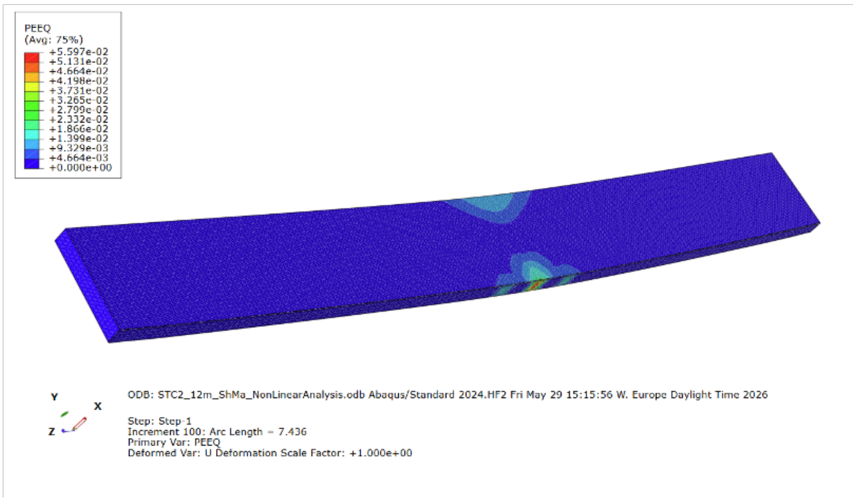

Figure C.11: Failure mode of STC-2 at 12 m span under shopping mall load.

DEPARTMENT OF SOME SUBJECT OR TECHNOLOGY
CHALMERS UNIVERSITY OF TECHNOLOGY
Gothenburg, Sweden
www.chalmers.se

AVANCEZ
1829

CHALMERS
UNIVERSITY OF TECHNOLOGY